Aquisition of temporally and spatially highly resolved data sets of relevant trace substances for model development and model evaluation purposes using a mobile measuring laboratory

D. Klemp, R. Wegener, R. Dubus, U. Javed

Energie & Umwelt / Energy & Environment
Band / Volume 497
ISBN 978-3-95806-465-2

Mitglied der Helmholtz-Gemeinschaft

JÜLICH
Forschungszentrum

Schriften des Forschungszentrums Jülich
Reihe Energie & Umwelt / Energy & Environment Band / Volume 497

Forschungszentrum Jülich GmbH
Institut für Energie- und Klimaforschung
Troposphäre (IEK-8)

Aquisition of temporally and spatially highly resolved data sets of relevant trace substances for model development and model evaluation purposes using a mobile measuring laboratory

D. Klemp, R. Wegener, R. Dubus, U. Javed

Schriften des Forschungszentrums Jülich
Reihe Energie & Umwelt / Energy & Environment Band / Volume 497

ISSN 1866-1793 ISBN 978-3-95806-465-2

Bibliografische Information der Deutschen Nationalbibliothek.
Die Deutsche Nationalbibliothek verzeichnet diese Publikation in der
Deutschen Nationalbibliografie; detaillierte Bibliografische Daten
sind im Internet über http://dnb.d-nb.de abrufbar.

This book is based on our work for the BMBF joint project Urban Climate under Change (Part 1): Evaluation of Urban Climate Models (Module B), 3D0, Subproject 6; Funding reference: 01LP1602F. The authors would like to thank Dr. Christian Ehlers for his work at the beginning of the urban climate project. The authors also thank Prof. A. Wahner and Dr. Franz Rohrer for discussions and critical reviewing of the manuscript.

Herausgeber und Vertrieb: Forschungszentrum Jülich GmbH
Zentralbibliothek, Verlag
52425 Jülich
Tel.: +49 2461 61-5368
Fax: +49 2461 61-6103
zb-publikation@fz-juelich.de
www.fz-juelich.de/zb

Umschlaggestaltung: Grafische Medien, Forschungszentrum Jülich GmbH

Titelbild: Sascha Kreklau

Druck: Grafische Medien, Forschungszentrum Jülich GmbH

Schriften des Forschungszentrums Jülich
Reihe Energie & Umwelt / Energy & Environment, Band / Volume 497

ISSN 1866-1793
ISBN 978-3-95806-465-2

Vollständig frei verfügbar über das Publikationsportal des Forschungszentrums Jülich (JuSER) unter www.fz-juelich.de/zb/openaccess.

Contents

Task definition 3

1 Task definition

The aim of the BMBF project "Stadtklima im Wandel" is the development, validation and application of a high-resolution urban climate model for entire cities. The research tasks assigned to Module-B consist of processing existing observation data and developing measurement strategies for new measurements. For this purpose, long-term observations as well as intensive measurement campaigns were carried out with a high-precision and high-resolution instrumentation, which not only allows a model evaluation of PALM-4U, but can also be used directly for applications such as air-quality control. Especially for the determination of spatial distributions of relevant trace substances, a newly equipped mobile measuring laboratory was used in subproject 6 (TP6) in Module-B. With this task, time-resolved measurements of several atmospheric trace gases including NO, NO_2 O_3, CO, CO_2 and NH_3, a comprehensive characterization of the particle phase (size and number distribution) as well as radiation measurements were performed in all four intensive measurement campaigns in Berlin and Stuttgart.

2 Conditions for project implementation

The concept for Module-B was developed on the basis of the call of the Federal Ministry of Education and Research (BMBF) published on 4 March 2015 for participation in the BMBF research programme "Stadtklima im Wandel" (onward referred as urban climate project). Within the framework of this joint project exsisting and new observation data-sets were to be compiled for three selected German cities, namely Berlin, Hamburg, and Stuttgart as well as their surrounding areas. These sets should include weather and climate data, data on turbulence and wind, energy and water balance components, impulse and mass flows, as well as data on air quality, especially aerosols and gas-phase air pollutants.

The aim was to obtain comprehensive three-dimensional data sets on atmospheric processes of entire cities with very high temporal and spatial resolution over sufficiently long periods of time. This approach was to be achieved both by long-term observations (LTOs) and by measurements during intensive observation periods (IOPs).

The data sets collected in the three selected cities represent an ideal test field for the validation of an urban climate model, as they highlight different aspects of urban atmospheric processes. Berlin (890 km^2, 3,400,000 inhabitants) is a large inland city with a flat topography. Hamburg (760 km^2, 1,750,000 inhabitants) represents a large city with coastal influence. Stuttgart (210 km^2, 604,000 inhabitants) is an example of a typical large city in topographically structured terrain with special air quality problems, which are largely caused by the complex orographic environment.

The central goal of the data sets compiled and obtained by the partners of Module-B is used for the validation of the high-resolution urban climate model PALM-4U developed by Module-A. Table 2.1 lists the 14 participating institutions of Module-B.

2.1 Institution

Forschungszentrum Jülich GmbH (FZJ) conducts interdisciplinary research in the fields of health, energy, environment as well as information based on the key competencies of physics, and supercomputing. The Institute of Energy and Climate Research (IEK) investigates modern energy conversion technologies within the framework of energy and environmental protection, taking into account the energy transition, and therefore deals comprehensively with the consequences of energy consumption and the associated emissions.

The IEK-8:Troposphere sub-institute investigates the physical and chemical processes of the troposphere, which have a significant influence on the chemical composition of the atmosphere. These include (1) the release (emission) of trace substances from soil sources, transport, and industry, (2) the chemical transformation of trace substances in the atmosphere, and (3) the distribution of pollutants through transport. The IEK-8 has been working in the field of air chemistry for more than three decades and quantifies the composition of the atmosphere and the reaction processes taking place in it under different atmospheric conditions. The chemistry and dynamics of anthropogenic and natural trace substances in the atmosphere is monitored and simulated.

Table 2.1: Overview of the sub-projects (TPs) of Module-B, the project managers (PIs) and the participating research institutions.

Subproject (TP)	Project manager (PIs)	Institution
TP1	Prof. Dr. Dieter Scherer, Jörn Welsch	TU Berlin
TP2	Prof. Dr. Christoph Schneider	HU Berlin
TP3	Prof. Dr. Sahar Sodoudi	FU Berlin
TP4	Prof. Dr. Stephan Weber	TU Braunschweig
TP5	Dr. Erika von Schneidemesser	IASS
TP6	**Dr. Dieter Klemp, Dr. Robert Wegener**	**FZ Juelich**
TP7	Prof. Dr. Stefan Emeis, Dr. Norbert Kalthoff	KIT
TP8	Dr. Ulrich Vogt, Dr. Ulrich Reuter	Uni Stuttgart
TP9	Dr. Valeri Goldberg	TU Dresden
TP10	Prof. Dr. Bernd Leitl, Prof. Dr. Felix Ament	Uni Hamburg
TP11	Dr. Meinolf Koßmann	DWD
TP12	Prof. Dr. Günter Groß	Uni Hannover
TP13	Peter Trute	GEO-NET
TP14	Thilo Erbertseder, Dr. Anke Roiger	DLR

Subproject TP6 was jointly led by Dr. Robert Wegener and Dr. Dieter Klemp (formally acting as PI). Dr. Umar Javed was hired as project scientist in subproject TP6 and financed by the project.

2.2 Mobile measuring laboratory (MobiLab)

In recent years, a number of studies [Bukowiecki, 2002; Pirjola 2004; Kittelson, 2004; Weijers, 2004; Westerdahl, 2004; Urban, 2010; Ehlers, 2013] have shown that mobile measuring systems are particularly suitable for detecting and investigating concentration fields in anthropogenically contaminated environments. Therefore, IEK-8 has carried out extensive investigations in this field of research within the framework of two doctoral theses and has acquired special expertise in the field of high-resolution measurements of pollutants.

The development of MobiLab-I based on a Mercedes VITO was the result of a dissertation which was successfully completed in 2010 [Urban, 2010]. The main starting point of this work was the determination of ambient air concentrations of relevant trace substances in urban and rural areas. The aims of the investigations were the characterisation of these scenarios and zero-dimensional box model based studies of their photochemistry. In the context of a further dissertation, the mobile measuring laboratory [Ehlers, 2013] was further optimised and expanded so that mobile measurements with measuring times of up to several hours were now possible. The results of these investigations were presented and published at conferences [Ehlers et al., 2014; Ehlers et al., 2016].

The intended extension of the investigations to further trace gases (NH_3, SO_2 and N_2O) could not be realized with the MobiLab-I without expensive reconstruction measures. For this reason, it was decided in 2015 to purchase a larger vehicle from the FZJ's own funds. The successor model to MobiLab-I has a higher payload along fulfilment of a higher energy requirements[1]. Fig. 1 shows the structure of the MobiLab-II (onward reffered as MobiLab) with a schematic representation of the trace analytics used (for equipment see Table 2.2). The MobiLab is based on a Mercedes Sprinter with a thermally insulated and air-conditioned box body. An impression of the dimensions of MobiLab-II is given by a photo taken during the IOP 4 in Berlin (Fig. 2). The photo shows the positioning of the MobiLab and DLR's Cessna during the preparation of the outdoor air comparison (17.07.2018) on the grounds of Schönhagen Airport in the southwest of Berlin.

[1] MobiLab-II now (as of autumn 2018) has sufficient battery capacity (1200 Ah) to enable measurements to be carried out for up to two hours at one location without generator support and without self-contamination by the generator's own exhaust gases.

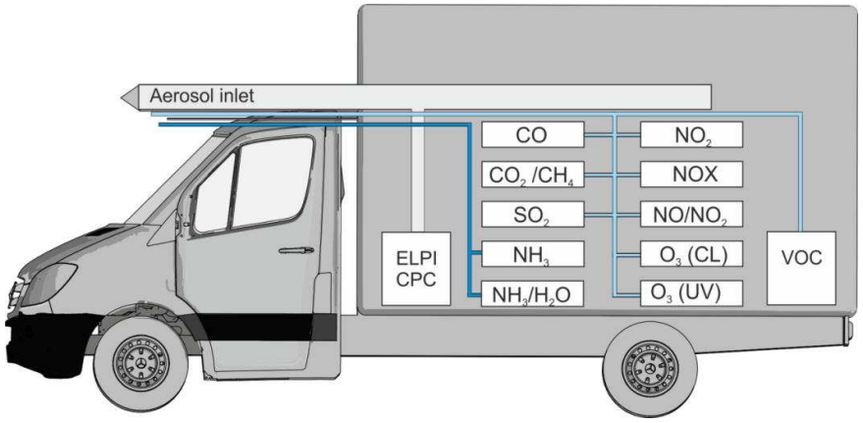

Fig. 1: MobiLab with schematic representation of the built-in trace analysis: Aerosol inlet: isokinetic inlet of the particle phase to avoid loss processes due to high velocity differences between the MobiLab's own motion and the velocity at the entry point into the aerosol inlet. Gas phase analysis: CO, CO_2 and CH_4, SO_2, NH_3, NH_3 and H_2O, NO_2, NO_x, NO and NO_2, N_2O, O_3 (chemiluminescence), O_3 (UV absorption), VOC canister samples, aerosol analysis: ELPI, CPC, filter samples: gravimetric analysis, EC/OC distribution [Ehlers et al., 2017].

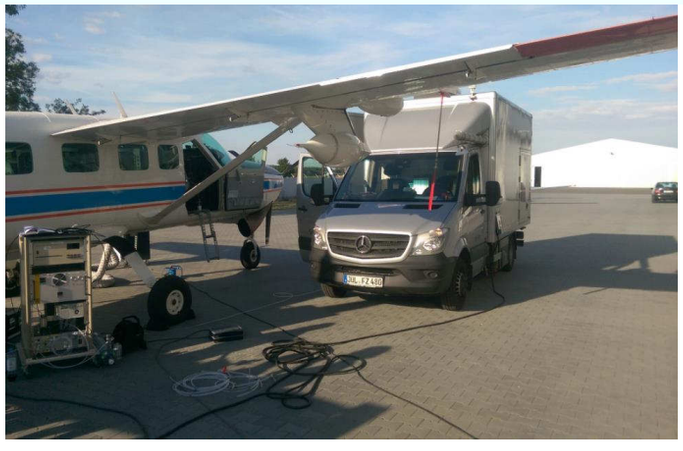

Fig. 2: Preparation for the outdoor air comparison at Schönhagen Airport (17.07.2018). Both air intake systems are positioned in close proximity to each other (Cessna: AIRPOD directly under the right wing; MobiLab: air intake at the head of the aerosol inlet). Appropriate positioning of the two systems ensured that contamination due to inherent emissions from the measuring platforms is avoided (wind-flow from the right).

Table 2.2: Measuring devices of MobiLab (available from autumn 2016) are listed. The total required power (approx. 7 kW) is achieved by a 380 V three-phase generator driven by the vehicle engine (max. 5 kW; engine speed dependent; MobiE) and an underfloor generator (3 kW output; Dometic TEC40 D[2]) as well as battery buffering by lead gel accumulators (200 Ah).

Gasphase		
CO_2, CH_4, H_2O, N_2O, NH_3	0.1s/1s 3 s	Cavity Ringdown Spectroscopy (*Picarro*)
NH_3	1s	Off-axis integrated cavity output spectrometer *(LosGatos)*
CO	1s	Vacuum UV-Resonance Fluorescence (*AeroLaser)*
O_3	10s	UV-Absorption *(Environnement S. A)*
NO_2	1s	Cavity Attenuated Phase Shift (CAPS) *(Aerodyne)*
SO_2	1s	Pulsed Fluorescence Analyzer *(Thermo-Fisher)*
NO_x, NO, O_3	2s	Chemoluminescence *(EcoPhysics)*
VOCs canister samples	10min-average	Canister samples/Offline GC/MS Agilent 6890 + MS5975 C

continues

[2] In autumn 2018 the power supply of the MobiLab-II was replaced by two diesel underfloor generators (nominal output 4 kW each) and a powerful Li-Ion battery pack. In this way, it was possible to effectively counteract the measurement time limitation that had previously often occurred in inner city measurements due to insufficient battery buffering.

Particle-phase		
Particle size distribution (7 nm-10 µm), 12-Steps	1s	ELPI (Electrical Low Pressure Impactor) *(Dekati)*
Particle counter (2 nm -3 µm)	1s	CPC-3788 *(TSI)*
Meteorology		
Temperature, Air pressure, wind velocity, and wind direction	1s	WXT 520 *(Vaisala)*
Metadata		
GPS, Camera		

2.3 The gas chromatography system

C_2 - C_{12} hydrocarbons are detected and measured by high-performance gas chromatography with flame ionization detection (HRGC-FID) and MSD (Agilent 5975) and a specially developed cryogenic enrichment unit [Schmitz et al. 1997; Schmitz et al. 2000; Mittermaier and Klemp, 2004].

The analysis system is based on a commercial gas chromatograph (GC 6890, Agilent) with flame ionization detector (FID) and MSD unit (Fig. 3). In addition, the instrument has several programmable valves and heating zones. All timing of the system necessary for fully automatic operation is done by an external control unit. The gas flows during the analysis are controlled by a valve system consisting of three multi-way valves (Valco). The valves are heated to 130 °C to minimize possible losses of the higher hydrocarbons due to interactions with the metal surface of the valve and to increase the reproducibility of the measurements.

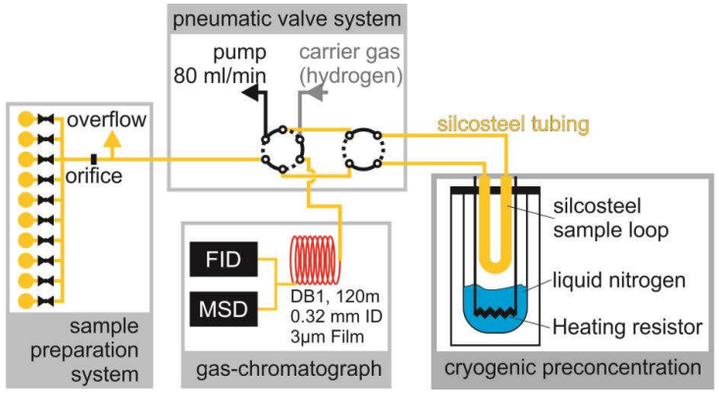

Fig. 3: Flow diagram of the GC-MS system used. Sample preparation system: A set of 10 Silco-steel cylinders previously filled with sample air can be connected to the system for analysis. Cryogenic preconcentration: Serves to concentrate the air samples by a factor of about 1000. Gas-chromatograph equipped with FID and MSD, column 120 m DB1, 0.32 mm ID.

The heat output is controlled by the programmable control loop of the GC 6890. The sample gas flow and the carrier gas (H_2) are guided via the central valve, a 6/2-way valve. The valve V2, a 4/2-way valve, separates the sample loop from the carrier gas or sample air. A 4/2 directional control valve allows the separation column to be backwashed. The suction line and all lines in contact with the sample gas are made

of silanized stainless steel. This material shows no interaction with aromatic compounds, as is observed, for example, when stainless steel pipes are used. The necessary concentration of hydrocarbons is achieved by condensation of the trace gases contained in the sample at the temperature of liquid nitrogen. This cryogenic enrichment is carried out in a U-shaped, silanized stainless steel tube (1/8 inch, Silcosteel, Restek). The enrichment loop is located in the flange of a Dewar (TRI 11, Air Liquide) partially filled with liquid-nitrogen and is located above the liquid level in the gas chamber. The temperature in the flange is about -160 °C to -170 °C, due to the evaporation of the liquid nitrogen, independent of the filling level of the Dewar. This temperature is still too high for an enrichment of the low boiling C_2-hydrocarbons, so that the temperature in the flange has to be lowered to approx. -190 °C by additional evaporation of the liquid nitrogen. This is done with a heating resistor placed directly above the bottom of the Dewar. About 10 minutes before the beginning of the enrichment of the air sample the heating resistor is switched on. In this way, a stream of cold nitrogen gas develops, which evenly flows around the enrichment loop. During the enrichment interval of 10 minutes, the flow through the collection loop is kept constant at 80 mL/min by a mass flow controller (MFC). The enrichment loop is filled with fine glass beads (80/100 mesh; Alltech). This increases the cold surface available for condensation of the VOCs and reduces the volume in which the substances are frozen out at about 1 ml. The increase in flow resistance results in a pressure gradient in the loop, which means that the nitrogen present in the sample cannot condense at all and the oxygen can only partially condense. The remaining oxygen and other low-boiling trace substances with boiling points[3] significantly lower than those of ethene are separated from the sample by evacuating the loop after the enrichment process is complete. The tube is wrapped from the outside with a sheathed heating conductor (15 Ω/m; Philips). Appropriate variation of the winding density[4] of the heating conductor ensures uniform heating inside of the sample. The sample is injected at a temperature of 130 °C. After injection, the loop is rewound with nitrogen (N_2 5.0) and heated at a temperature of 150 °C. The heating temperatures are controlled by a measuring controller (Digitemp). The measuring sensor for this control is located at the lowest and therefore coldest point of the enrichment loop to ensure complete emptying. In addition, the enrichment

[3] Ethene has the lowest boiling point of the substances analysed, bp = -104 °C

[4] Number of windings of the heating wire.

temperature is monitored and recorded by a resistance thermometer (PT100). In this way it can be checked later on whether the temperature during the enrichment process was sufficiently low to retain the low-boiling components.

A DB1 capillary column (J&W) with a length of 120 m, an inner diameter of 0.32 mm and a film thickness of 3 µm is used to separate the hydrocarbons. Since the stationary phase consists of a non-polar material, the retention times correlate essentially with the boiling points of the hydrocarbons to be separated. The separation performance of the column is optimized by a suitable temperature program: After injection, the column is first operated isothermally at -60°C for 8 min and then heated at a rate of 4 °/min to 180 °C and then at 20° /min to 220 °C. The column is then heated for 10 min at 220 °C. At the end of the analysis, the GC oven is cooled down again to the starting temperature of -60°C and a new gas chromatographic analysis is started. The separated substances are detected with a flame ionization detector (FID) and an MSD. An overview of the separation performance achievable with the system and lists the retention times for the most common organic trace gases in an air sample is shown in next section (Fig. 4).

Calibration

The sensitivity of the GC system was regularly checked using the experimentally determined mass response factors (MRF) of a 74-component pure hydrocarbon (HC) calibration standard (Apel-Riemer Environmental, Inc., Denver CO, USA). The mass response factor MRF_i of a substance i is given as

$$MRF_i = \frac{FE_i}{\mu_{HCi} \cdot MW_{HCi}},$$

Where FE_i is the integral of the peak area in the chromatogram, μ_{HCi} is the known mixing ratio of the hydrocarbon HC_i in the calibration standard and MW_{HCi} describes the molecular weight of HC_i in [g/mol]. The regression analysis of the measured peak areas against $\mu_{HCi} \times MW_{HCi}$ provides a mean mass response factor which was used to calculate the mixing ratios of all hydrocarbons detected in the canisters. Exceptions are Ethyne and a number of oxygenated compounds, as they occur in particular in

diesel exhaust gas, for which separate mass response factors were determined in each case. The retention times of the individual substances were determined by injecting the pure substances, comparing them with the corresponding retention times (Fig. 4) of the 74-component standard (Apel-Riemer Inc., Boulder, CO) and using a self-made diffusion source [Konrad and Volz, 2000].

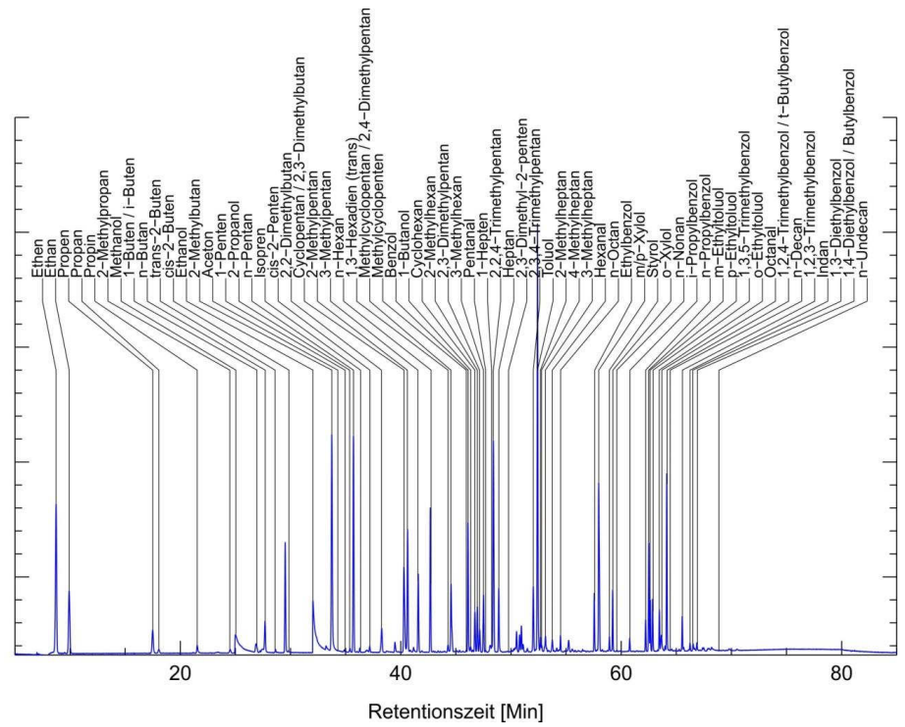

Fig. 4: Overview of the separation performance achievable with the system. Listing of retention times for the most common organic trace gases of an air sample (diluted diesel exhaust sample).

Error estimation

Experimental uncertainties in the analysis of the canister samples can result from different reasons. The influence of transport and storage on the quality of the results was investigated by parallel measurements on wet and dry samples with different storage times. Using the results of a test series of different VOCs, it was found that

alkanes, alkenes, aromatics and terpenes differed in their mixing ratios by less than 10 % from the results of directly analysed samples after a storage time of 4[5] days. For alcohols, the differences found in the time interval considered were less than 20 %. In addition, care was taken to ensure that ozone-free collection of the VOCs was carried out in the canister samples. This was ensured by using a capillary (Silco-steel, 0.15 mm diameter) heated to 120 °C for the collection process. Laboratory tests on VOCs calibration standards ensured that at this temperature of the capillary all VOCs contained in the calibration mixture were collected without loss. By specific admixtures of O_3 (maximum 160 ppb) it could be demonstrated that the O_3 degradable alkenes can also be collected, stored and enriched in the loop without any noticeable loss. The accuracy of the measurements additionally depends on the quality of the calibration standard (deviations between true and specified mixing ratios < 5 %, Apel-Riemer Environmental Inc.) Further errors are caused by uncertainties of the mass flow meters (MKS Instruments, < 2 %) and by errors in the integration of the peak areas (< 7 %). The overall uncertainty for alkanes, alkenes, aromtics, and terpenes is about 13 %, while for alkohols it is 21 %.

3 Planning and execution of the project

The chronological sequence of the Module-B work packages and related tasks are described in Table 3.1. It also describes the integration of subproject TP6 into the overall concept of 3DO (Module-B) as well as the interactions with the other modules of the overall programm [Scherer et al, 2019; Scherer et al. 2019a]. In addition, the distribution of the 36 person-months (PM) for TP6 to the individual work packages is listed.

[5] Within the scope of the campaigns carried out, care was taken to ensure that the storage and transport time of the collected canister samples never exceeded a period of 4 days until the measurement in Juelich.

Table 3.1: Timeline and work packages (AP) for urban climate module B (3DO) along contribution of subproject TP6 and allocation of the PM of TP6 to the individual work packages. The contribution of permanent-staff[6] is not listed in the table.

AP	Description	2016 I	2016 II	2016 III	2017 I	2017 II	2017 III	2017 IV	2018 I	2018 II	2018 III	2018 IV	2019 I	PM
210	Preparation of IOPs and intercalibrations			■		■		■		■				6
220	IOPs winter campaigns I and III				■				■					5
230	IOPs summer campaigns II und IV						■				■	■		5
310	Development and testing of measurement concepts	■	■	■	■	■	■	■						4
320	Development and testing of analysis concepts		■	■	■	■	■	■	■					5
330	Development and testing of the data integration platform			■	■	■	■	■	■	■				1
410	Application of numerical models for analysis				■	■	■	■	■	■	■			3
420	Model validation (in connection with module A)										■	■		4
430	Applications (in connection with module C)								■	■	■	■	■	3
													Total person months (PM)	36

3.1 Work-package 210: Preparation of IOPs and intercalibrations

Development of a suitable measurement strategy was required for the optimal use of the mobile measurement laboratory in interaction with other subprojects in Berlin and Stuttgart and the existing fixed measurement stations. The tasks within this workpackage were:

- Acquisition of temporally and spatially high-resolution data sets with the MobiLab analysis to describe the spatial representativeness of a fixed measuring station for the investigated area.

[6] FZJ contributed to the sub-project TP6 in the form of a second person with its own funds. This concerns work packages 210, 220 and 230 (the implementation of intercalibrations and intensive phases (IOPs) with MobiLab required the assignment of a second trained person). The same applies to work package 430, (for instance the use of MobiLab for chasing experiments to verify existing emission models of road traffic (HBEFA)).

- Investigation of the coherence length[7] of the data set recorded by the fixed measuring station as a function of meteorological conditions.
- Intercalibrations of the gas and particle phase measurements in the preparatory phase and the intensive phases (IOP I - IOP IV in Berlin and Stuttgart) with the MobiLab analysis as reference system.
- Comparison of the semiconductor sensors used by TP5 and TP2 with the MobiLab reference analysis under real outdoor air conditions.

3.2 Work-package 220 and 230: IOPs in Berlin and Stuttgart

The features are summarized as follows

- Participation of MobiLab in all four IOPs with temporally and spatially resolved trace gas measurements (NO, NO_2, O_3, CO, NH_3, and CO_2) as well as particle (particle size distribution, particle counter) and radiation measurements. Additional episodic measurements for detailed VOCs composition were performed.
- Characterization of the photochemical O_3 formation by detailed photochemical box model (MCM 3.3) [Jenkin et al., 1997] studies.

3.3 Work-package 310: Development and testing of measurement concepts

In connection with the development of evaluation concepts for the data sets obtained, we dealt with a whole range of following areas:

- Quantification of regional background concentrations of NO, NO_2, NH_3, O_3, CO, CO_2, and particulate matter in the windward region of the cities under investigation.

[7] Measured concentration is valid for a certain distance.

- Description of the trace substance concentration gradients on the main roads and related neighbouring residential areas.
- Development of suitable measurement strategies and route plans for MobiLab to determine the spatial coverage and accuracy of the existing fixed measuring stations.
- Quantification of the urban (local) background concentrations of the above-mentioned trace substances to distinguish between regional background, local background and the local emission source terms (QT's) of the species under consideration and to determine the mean source terms for different seasons, indicating experimental and statistical errors.

Measurements were repeated several times in different seasons in Berlin and Stuttgart to obtain a representative dataset.

3.4 Work-package 320: Development and testing of analysis concepts

Within the framework of the further development of instruments for reliable differentiation between the local background of trace substances and direct emissions, the following concepts have been successfully tested for road traffic as an emission source:

- An increased N_2O to NO_x ratio as an indicator of the extent to which an air mass is affected by traffic.
- A high NO to NO_2 ratio as an indicator of the extent to which an air mass is affected by traffic.

- Composition of the VOCs mix as an indicator of the extent of traffic impact.
- The O_x-concept ($O_x = O_3 + NO_2$) as a method for determining the direct NO_2 emission fraction.

3.5 Work-package 330: Data integration platform

The data sets obtained by the mobile measuring laboratory during IOP-I - IOP-IV in Berlin and Stuttgart were stored on a common database after detailed evaluation, so that these results are available for all project partners for validation purposes of PALM-4U.

3.6 Work-package 410: Application for model analysis

The subject of the investigations is the modelling of summer photo-oxidant formation (ozone) using a detailed box model (MCM-3.3). For this approach the results of episodic VOCs measurements (C_2 - C_{11}) of the Berlin measurements from IOP-II and IOP-IV were used. In addition, the VOC/NO_x ratios derived by MobiLab from the measurements were used for these models.

3.7 Work-package 420: Model validation

A central goal of the project is to compare the results of the MobiLab test drives with the results of the PALM-4U modelling. In a first step, the agreed simulation runs VALRO1 to VALRO6 will be used for these validations. Table 3.2 gives an overview of measurement periods and measurement locations. A summary of the results of selected measurement runs of TP6 for the different validation periods (VALR01, VALR02, VALR03, VALR04 and VALR06) is given in the appendix (section 7.3).

Table 3.2: Overview is shown for the agreed evaluation periods for model simulations and reference measurements.

Reference-designation	Start	End		City
VALM01, VALR01	17.01.2017 06:00 UTC	18.01.2017 06:00 UTC	Winter 2017	Berlin
VALM02, VALR02	16.07.2018 06:00 UTC	18.07.2018 06:00 UTC	Summer 2018	Berlin
VALM03, VALR03	14.02.2017 06:00 UTC	16.02.2017 06:00 UTC	Winter 2017	Stuttgart
VALM04, VALR04	08.07.2018 04:00 UTC	09.07.2018 19:00 UTC	Summer 2018	Stuttgart
VALM05, VALR05	Ideal case*		-	Hamburg
VALM06, VALR06	30.07.2017 06:00 UTC	01.08.2017 06:00 UTC	Summer 2017	Berlin

* The ideal case of Hamburg was brought forward and already carried out.

3.8 Work-package 430: Applications: Test vehicle emission factors

The research carried out by TP6 in this context focuses on two areas:

- Determination of the emission behaviour of the current vehicle fleet by means of tunnel studies (Heslacher Tunnel, Stuttgart and Tiergarten Tunnel, Berlin), see section 6.2.1.
- Performance of chasing experiments to determine the emission behaviour of individual emitters, see section 6.2.3.

4 Scientific and technical status

History

For more than 20 years, the working group "Energy-Related Emissions" has been working on the quantification of anthropogenic trace substance emission and immission levels. In the past, we have published a number of investigations and studies on the role of anthropogenically emitted trace substances in the formation of photooxidants: [Kern et al., 1996; Schmitz et al., 1997; Schmitz, Hassel and Weber, 2000]. In process studies, the degradation of trace substances and the formation of secondary pollutants were investigated [Wegener et al. 2007; Kaminski et al. 2017; Fuchs et al. 2013]. A central task is to ensure the data quality of atmospheric measurements in the World Calibration Centre for Nitrogen Oxides (WCC-NO_x) of the Global Atmosphere Watch (GAW) programme and in measurement comparisons [Hoerger et al. 2015; Fuchs et al. 2010; Fuchs et al. 2017; Apel et al. 2008]. Our working group was and is successfully involved in a number of publicly funded projects:

- **The TOR sub-project of EUROTRAC**: 1989 - 1996 ozone production at the Schauinsland [Klemp et al., 1997; Mihelcic et al., 1993; Pätz et al., 2000]
- **BMBF project Tropospheric Research Programme (TFS):** (1998 – 2001) Evaluation of Calculated Emissions of a City (EVA, Augsburg) [Klemp et al., 2002; Mannschreck et al., 2002; Möllmann-Coers et al., 2002]
- **MOBINET:** (1998 – 2003) BMBF lead project, [Mittermaier, Klemp and Buers, 2003; Klemp et al., 2002a; Mittermaier et al., 2004; Mittermaier and Klemp, 2004]
- BMBF project: **Zeppelin-based investigation of regional photochemistry and air quality:** (2008-2009), [Urban, 2010]
- EU Project **PEGASOS:** (2011-2013), [Ehlers, 2013; Li et al., 2014; Kaiser et al., 2015]
- Measurement campaign **BAERLIN 2014:** [Bonn et al., 2016; von Schneidemesser et al., 2018; Bonn et al., 2018]
- Municipal funding: **Studies on air quality in Bad Homburg**: [Ehlers et al., 2017]

- BMWi-Projekt **ALASKA:** (2014 – 2017), "Evaluation of air pollution scenarios for designing pollutant gas filters and cathode regeneration cycles for automotive fuel cells [Klemp et al., 2020; Talke et al., 2018].
- EFRE project **Virtual Institute Electricity to Gas and Heat:** (2019-2022).
- Helmholtz project **SMARAGD** on Citizen Science (2019-2022)

Recent work includes the results of our own long-term studies on the development of VOC- and NO_x-emissions in traffic-polluted areas in Germany [Ehlers et al., 2016]. Further areas of work include the verification of existing emission inventories [Slemr et al., 2002] with detailed emission measurements of vehicles in real road traffic [Mittermaier and Klemp, 2004; Klemp et al., 2012; Ehlers et al., 2017].

5 Cooperation with other subprojects

TP6 (FZJ) participated with the MobiLab in a total of 8 intensive campaigns in Berlin and Stuttgart during the funding period. Each of the 8 measurement campaigns had duration of about 12 measurement days.

5.1 Measurement comparisons for data harmonisation

In addition to the acquisition of temporally and spatially highly resolved trace substance data by means of MobiLab measurement runs, intercalibrations with the other trace substance measurement teams were offered and carried out in all campaigns. These intercalibrations serve to harmonize the data sets so that data sets with a known uncertainty can now be made available for the validation of PALM-4U. Fig. 5 shows some exemplary photos of measurement comparisons from the IOP-II in Berlin and Stuttgart.

(a) (b)

(c) (d)

Fig. 5: (a) Ambient air comparison for NO, NO_2 and O_3 with TP8 on the premises of the IFK of the University of Stuttgart (b) Measurement comparison on the Marienplatz in Stuttgart: Mobile bicycle-analytics and stationary-analytics of the IFK with MobiLab-analytics (c) Measurement comparison between MobiLab-analytics and Zephyr probes of the IASS (TP5) (d) Measurement comparison between MobiLab-analytics and mobile analytics of the University of Braunschweig (TP4). The measurement comparisons shown here took place during IOP-II in the summer of 2017.

Fig. 6 shows the results of the comparative CO_2 measurements during the summer campaign 2017 (IOP-II) with measuring instruments of the TU Braunschweig (TP4) (see also Fig. 5(d)). Apart from the differences in the CO_2 concentration peaks, a small offset of 2.1 ppm (corresponding to about 0.5% of the mean background value for CO_2) was found between the two CO_2 analysis systems.

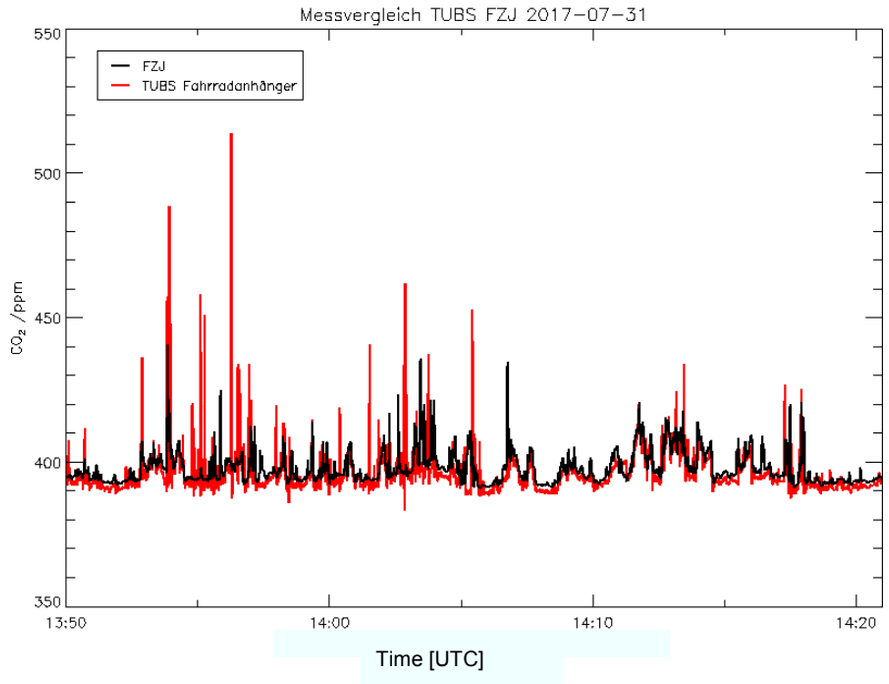

Fig. 6: Parallel measurements of CO_2 during the IOP-II in Berlin on 31.07.2017 using a cavity ringdown system from Picarro (time resolution 10 Hz, absolute calibration using the known IR absorption). The following system was used by the TU Braunschweig (TUBS): LI-COR Inc., (LI-840A).

In addition, the particle measurement systems used were also operated in a joint outdoor air comparison at the MobiLab site in front of the TU main building for a period of approx. 30 min. directly next to each other (see Fig. 7). As expected, higher particle number concentrations were observed with the FZJ CPC than with TUBS CPC, due to its lower separation limit. Larger changes in the number concentrations were observed with both systems in parallel. A clear comparability of particle measurements is much more difficult to realise than in the case of gas-phase

measurements. Nevertheless, the observable differences in the particle number concentrations, of 25 - 30 % have to be considered when creating a common validation data set for PALM-4U by indicating the respective separation limit.

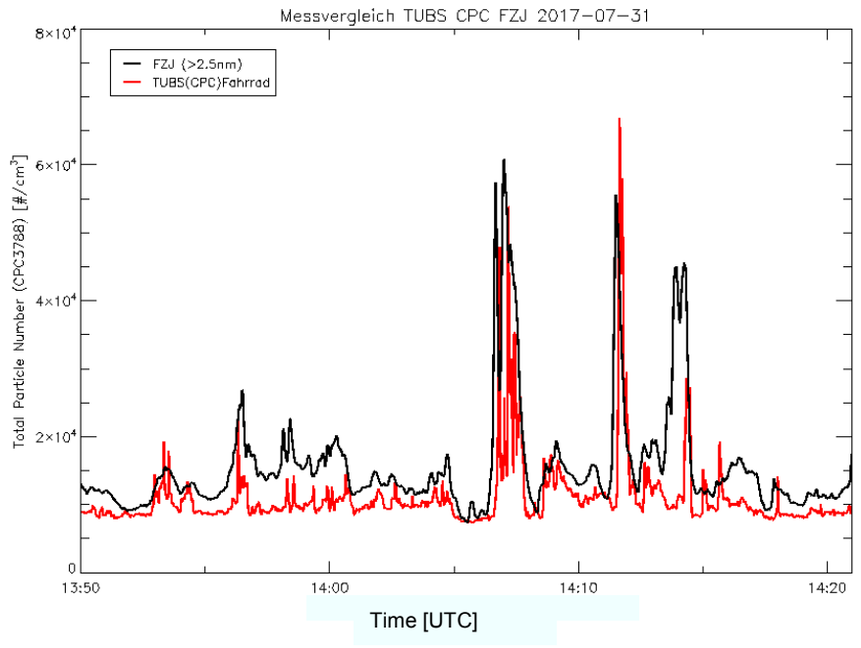

Fig. 7: Parallel measurements of particle number concentrations during the IOP-II in Berlin on 31.07.2017. FZJ used an Ultra-CPC-3788 from TSI GmbH with a deposition limit of 2.5 nm and a time resolution of 1 s. The TU Braunschweig (TUBS) used the following system to measure the particle number concentration: CPC-3007 with a deposition limit of 10 nm and a time resolution of 1 s.

Table 5.1 gives an overall overview of the type and number of measurement comparisons carried out during the first phase of the urban climate project.

Table 5.1: Listing of intercals and measurement comparisons (trace substance measurements)

Date / IOPs	**Partner**	**Devices (FZJ) / Description**
Nov. 2016	Parallel measurements with TP2: particles	Particles (ELP)
	Parallel measurements with TP5: O_3	Ansyco O_3 monitor
	Parallel measurements with TP1: CO_2 (Mast)	CO_2 (Cavity ringdown)
IOP-I		
Berlin	Parallel measurements with TP4: CO_2	CO_2 (Cavity ringdown)
	Parallel measurements with TP4: particles	Particles (ELP)
	Parallel measurements with TP5: Zephyr probes	Measuring trip MobiLab
Stuttgart	Parallel measurements TP8: Bicycle measurements	NO_x (Chemiluminescence) Particles (ELP) CO (AeroLaser)
	Additional Intercals with TP8	Concentration series measurements using standards
IOP-II		
Stuttgart	Intercals with TP8	Concentration series measurements using standards for NO, NO_2, CO, and Particles
Berlin	Parallel measurements with TP2: particles	Particles (ELP, CPC)
	Parallel measurements with TP4: CO_2	CO_2 (Cavity ringdown)
	Parallel measurements with TP5: Zephyr probes	Measuring trip MobiLab
	Additional Intercals with TP5	Concentration series measurements using standards

IOP-III		
Stuttgart	Parallel measurements TP8: Bicycle measurements	NO_x (Chemiluminescence) Particles (ELP) CO (AeroLaser)
	Additional Intercals with TP8	Concentration series measurements using standards for NO, NO_2, CO, and Particles
Berlin	Parallel measurements with TP4: CO_2	Cavity ringdown: CO_2
IOP-IV		
Stuttgart	Parallel measurements TP8: Bicycle measurements	NO_x (Chemiluminescence) Particles (ELP) CO (AeroLaser)
	Additional Intercals with TP8	Concentration series measurements using standards for NO, NO_2, CO, and Particles
Berlin	Intercal Airport, Schoenhagen near Berlin (see Fig. 2) Parallel measurements with TP14 : CO_2, NO_2, CH_4	CO_2 (Cavity ringdown) NO_2 (CAPS) CH_4 (Cavity ringdown)
	Additionally Intercals with TP14	Concentration series measurements using standards for CO_2, NO_2, and CH_4

5.2 Support for the studies carried out

5.2.1 IOPs in Berlin

TU Berlin

- Provision of a stand in front of the TU main building for MobiLab with 32-A three-phase power supply during all 4 IOPs
- Provision of a measuring station for radiation measurements on the roof of the TU main building

TU Berlin, Institute for Ecology

- Provision of a replacement site with power supply during IOP-III and in the run-up IOPs (November 2016)

IASS Potsdam

- Provision of a stand with power supply in the preparation phase of the Berlin IOPs (November 2016) for first intercals with TP5 and TP2

Senate Department for Environment, Traffic and Climate

- Logistic support

5.2.2 IOPs in Stuttgart

Administration City of Stuttgart

- Permission to use the Marienplatz for parking and loading purposes of MobiLab

VVS Stuttgart

- Provision of a 32 A power connection (subject to charge)

Uni-Stuttgart, Institute for Combustion and Power Plant Technology (IFK)

- Multiple provision of a replacement stand with power supply in case of power supply failures at Marienplatz

City of Stuttgart - Office for Environmental Protection

- Traffic censuses for various streets in Stuttgart.

We would like to thank everyone involved for their helpful support of our investigations.

6 Results

In the following, the results achieved by the IOPs will be discussed in detail and the references to the work packages formulated at the beginning will be presented.

6.1 Observations during the IOPs (packages 210 – 330)

Our first goal was to develop a suitable measurement strategy for the optimal use of the mobile measurement laboratory during the intensive campaigns in Berlin and Stuttgart. The following measurement concept was implemented during the IOPs as a basis for PALM-4U modelling.
Determination and travel of fixed routes in close coordination with the other trace substance measurement groups (Berlin: TP4, TP5 and TP2, TP14; Stuttgart: TP8, TP14).

- Investigation of the time-of-day dependence of the measured trace substance concentrations
- Investigation of the seasonality of the measured trace substance concentrations

6.1.1 Berlin

The measurement route of MobiLab in the area of Ernst-Reuter-Platz can be seen in Fig. 8. The start and end points of the route are located at the charging point of MobiLab in front of the main building of the TU Berlin. The route shown was followed by us during all 4 IOPs about 3 - 4 times daily. Depending on the traffic volume, a measurement run took about 45 to 90 minutes.

Fig. 8 shows the measured concentration distribution in the vicinity of Ernst-Reuter-Platz during IOP-II on 31 July 2017 in Berlin (start 10:30 UTC - 11:20 UTC). The observed NO_2 mixing ratio shows a strong variability between maximum values on the main roads (Hardenbergstraße) and urban background values as observed on the banks of the Spree (Am Spreebord). Especially high values for NO_2 were measured in the inner city area for Budapester Straße and the highly frequented heavily built-up area of Kurfürstendamm. In contrast, on the multi-lane roads with similar traffic density (Straße des 17.Juni), comparable concentration peaks were observed only at intersections with traffic light control (Fasanenstraße).

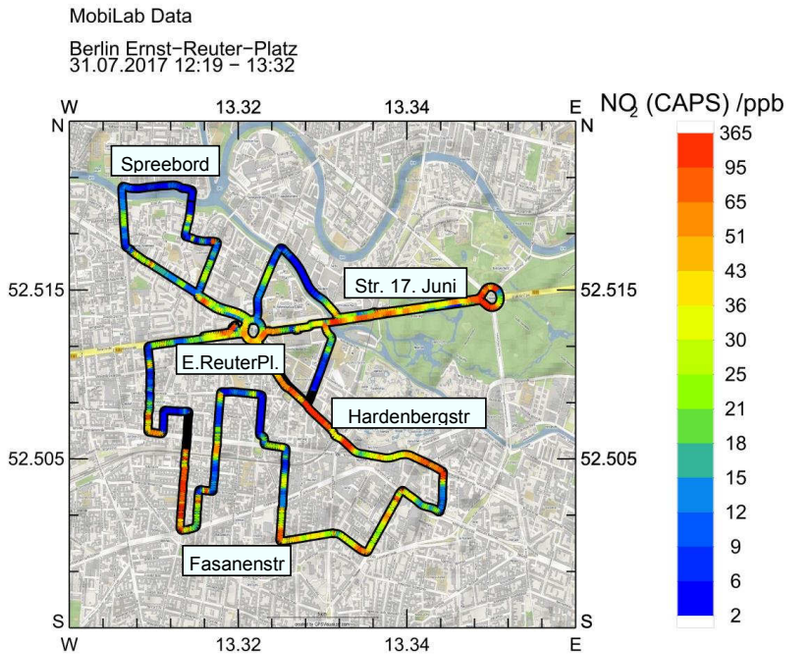

Fig. 8: Berlin measurement route of MobiLab. The plot shows measured NO_2 concentration distribution (see colorbar) in the vicinity of Ernst-Reuter-Platz during the IOP-II on 31.07.2017 in Berlin. High NO_2 mixing ratios are found on main roads and at intersections. The NO_2 local background[8] values are observed in side streets and/or residential areas.

Fig. 9 shows the temporally high-resolution recording (Time UTC: 14:17 - 15:31) of the CO_2 concentration on the Berlin route on 18.1.2017 (IOP-I). The recorded CO_2 concentrations are between 439 ppm (almost background value) and 700 ppm (peak values). The high temporal variability of the CO_2 values directly reflects the emission behavior of the surrounding traffic, since CO_2 emissions on the road correlate directly with fuel consumption.

[8] The background values for NO_2 differ substantially between winter and summer.
NO_2 winter^{BG}: > 21 ppb: NO_2 summer^{BG}: < 8 - 9 ppb.

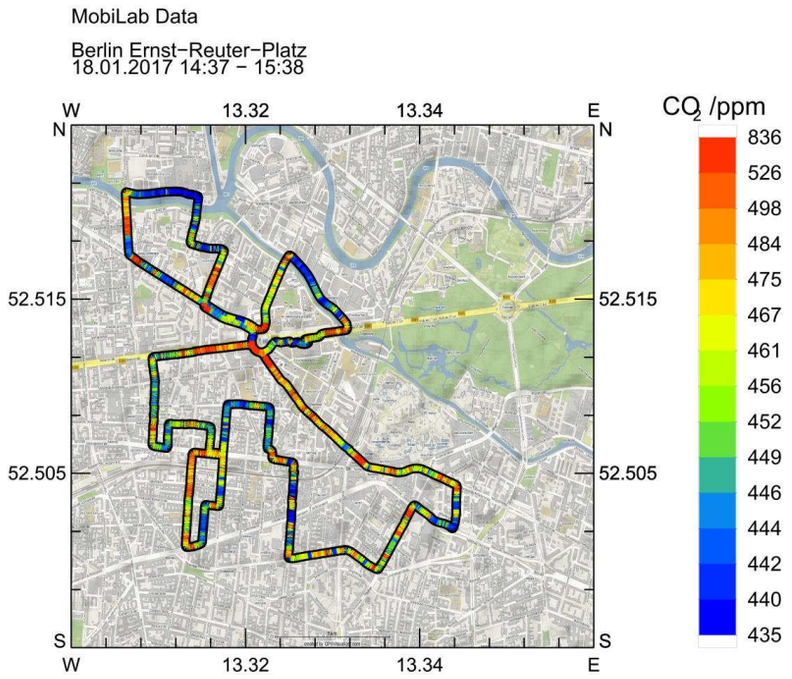

Fig. 9: Berlin measurement route of MobiLab. The measured concentration distribution of CO_2 is shown in the area around Ernst-Reuter-Platz during the IOP-I on 18.01.2017 in Berlin. Simultaneous CO_2 and NO_2 measurements are an efficient method to differentiate between direct NO_2 emissions from traffic and the NO_2 contribution generated by NO titration with O_3. It will be a task of the validations of the associated PALM-4U models to investigate the quality with which these processes are represented by the models.

In the investigations on seasonality (summer; Fig. 10 and winter; Fig. 11), the occurring background concentrations of NO_x are of particular interest. On the one hand, the background concentrations introduced on the windward side increase the values occurring in the inner city, especially in winter. On the other hand, it becomes clear that a modelling with PALM-4U requires the input of real initial values by a regional model, since only in this way the additive effect of the windward background concentrations can be adequately considered. The measured NO_2 concentration under winter conditions (20 Jan. 2017, 9:00-12:30, IOP-I) is shown in Fig. 11. The winter NO_2 values in the run-up to the city of Berlin were more than one order of magnitude higher than the summer background values. Conceivable reasons are the previous build-up of high NO_x concentrations during a low exchange high pressure situation combined with the slower degradation of NO_x by reaction with OH in winter.

In addition, the slower photochemical decomposition of NO_2 in winter due to lower radiation intensity leads to an increased NO_2/NO ratio.

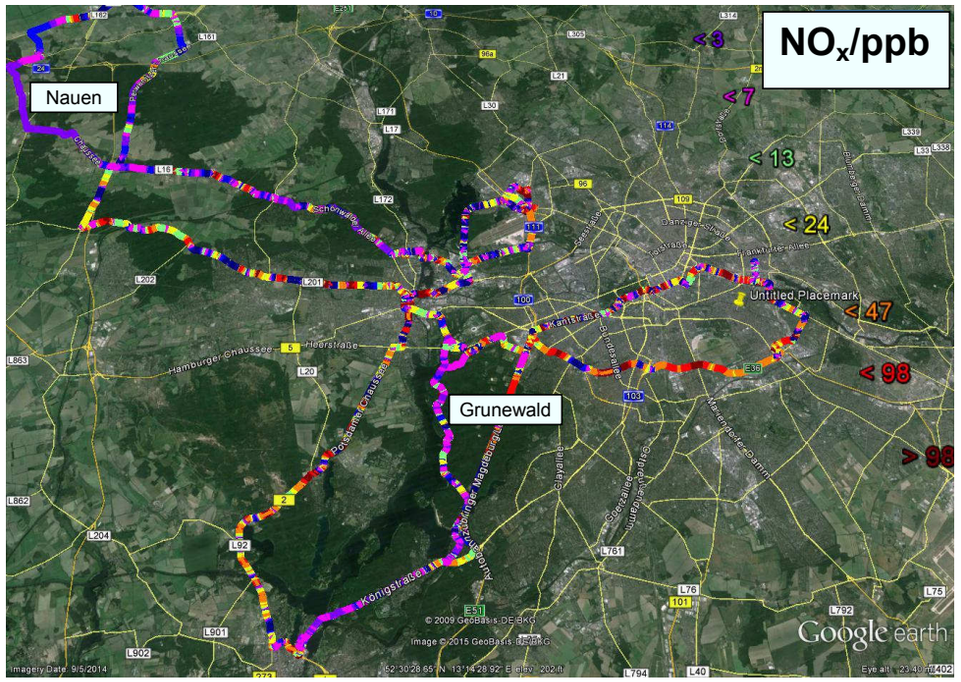

Fig. 10: Measurements of summer NO_x background concentrations (August) in the windward Hinterland of Berlin. Lowest NO_x concentrations are observed on low-traffic country side roads in the area of Nauen. The lowest NO_x concentrations on the Havelchaussee in the foreland of Grunewald are only slightly higher at 5 to 7 ppb. Under these conditions, the photostationary state during the day ensures that the NO_x is divided into a proportion distribution of about 25% NO and 75% NO_2.

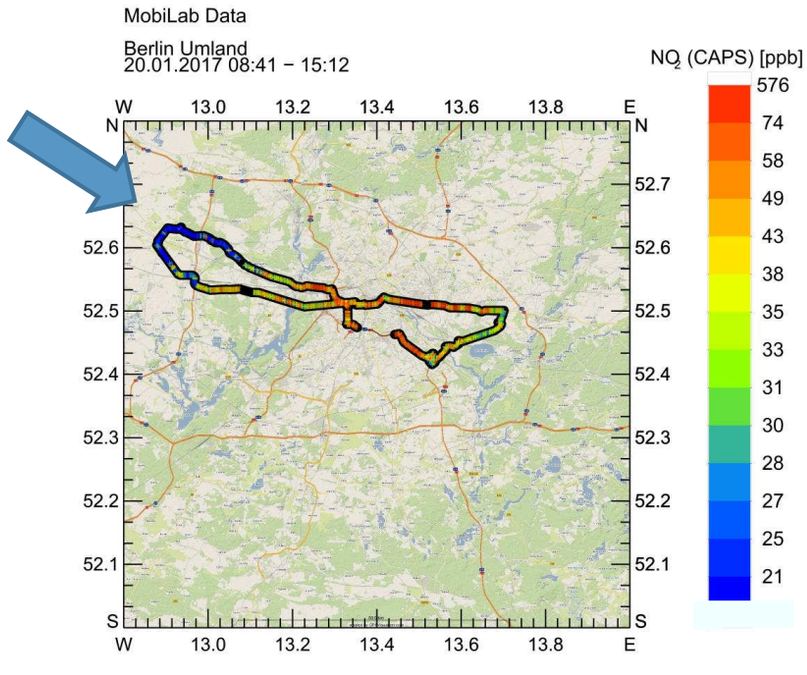

Fig. 11: Results of the NO_2 measurements (see colour scale) during the crossing of the city of Berlin in east-west direction and investigations in the windward and leeward areas of Berlin under winter conditions and northwest wind direction (see wind arrow). Lowest NO_2-concentrations in wintertime windward area (Nauen) were 21 ppb, which is approximately one magnitude higher than the respective summertime values. The measurements with MobiLab presented here took place on a weekday during IOP-I (20 January 2017 between 9:00 and 12:30 UTC).

6.1.2 Stuttgart

A periodic measuring route was definded for the Stuttgart intensive in cooperation with TP8. Starting point and end point was at the Marienplatz. The route led north via the B14 beyond the Neckartor. Afterwards, the eastern and western side of the B14 were surveyed. The loop west of the B14 led through the residential area located on Uhlandshöhe, while the left loop first crossed the main station forecourt and then passed the Europaviertel. The left loop joined the B14 at Neckartor and led back to Marienplatz.

Fig. 12 shows the concentration curve of the trace gases NO_2 during the IOP-III on 13.02.2018. It is clearly evident that road traffic is a direct source of emissions

of NO_x: High traffic density, e.g. at the Neckartor, is accompanied by peak values of NO_2. In contrast, the residential area on the west side of the B14 (Uhlandshöhe) shows much lower values for NO_2.

Fig. 13 shows the spatial distribution of NO_x concentration at the foot of Uhlandshöhe, looking northwards towards the Neckartor. The minimum distance between Kernerplatz and the B14 in the east is only 100 m. Even at this short distance, the influence of the closely neighbouring and heavily trafficked B14 is hardly noticeable.

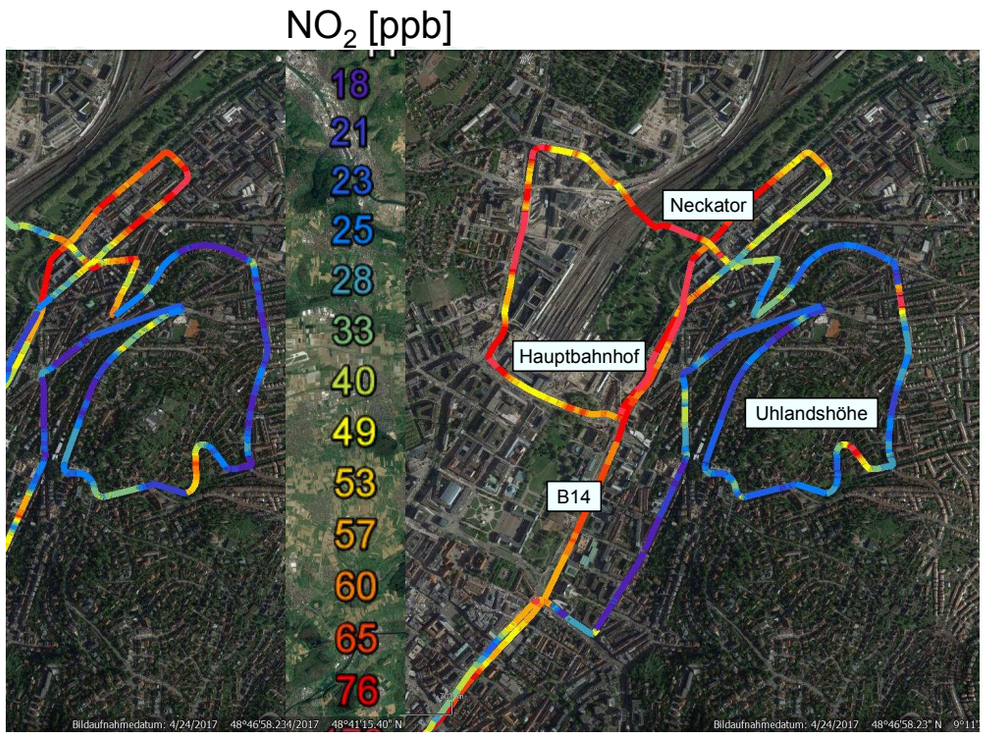

Fig. 12: The mixing ratio of NO_2 around the Neckartor in Stuttgart (IOP-III, 13.02.2018) on the standard route of MobiLab.

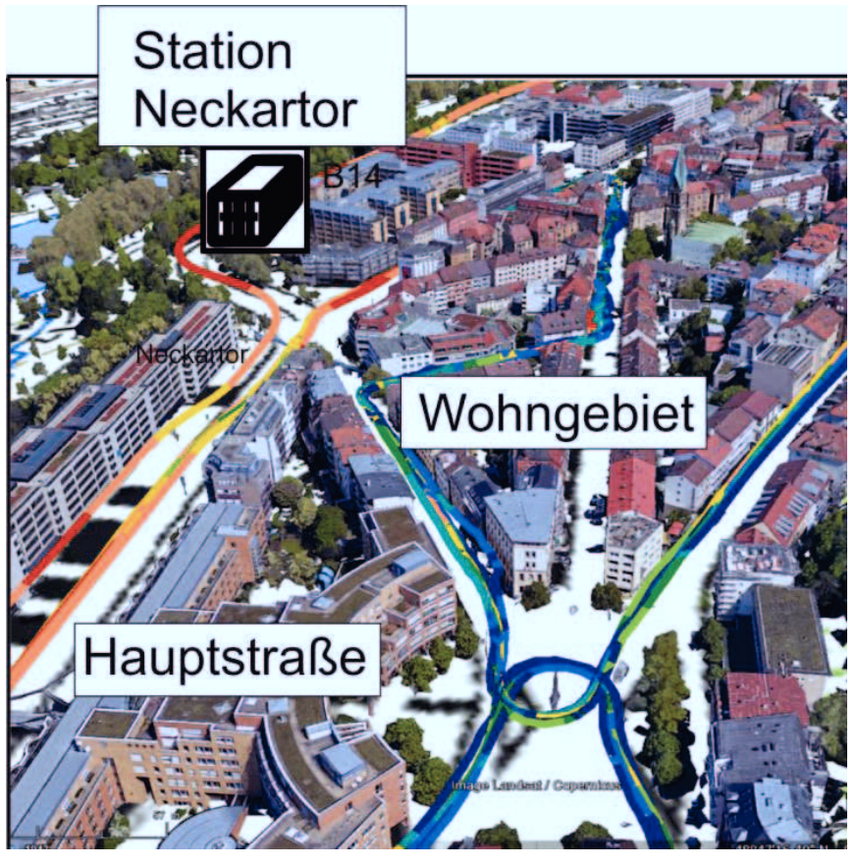

Fig. 13: Kernerplatz in Stuttgart with a view to the north towards the Neckartor. Spatial variability of NO_2 concentration (minimum distance B14 - Kernerplatz: approx. 100 m). Colour scale for NO_2 as in Fig. 12.

The diurnal course of the NO_2 concentration on the Stuttgart standard route is shown in Fig. 14. High mixing ratios were observed during the rush hour, when a low inversion layer above the Stuttgart basin prevented the free exchange of air and traffic emissions were already high. Breaking up the inversion during the day led to a significant reduction of NO_2 concentrations in areas with low traffic. This behaviour was particularly evident at the Uhlandshöhe, where NO_2 concentrations decreased significantly during the day. On the other side of the valley basin and along the bottom of the valley, however, traffic density remained high throughout the day, so that no comparable decrease was observed here.

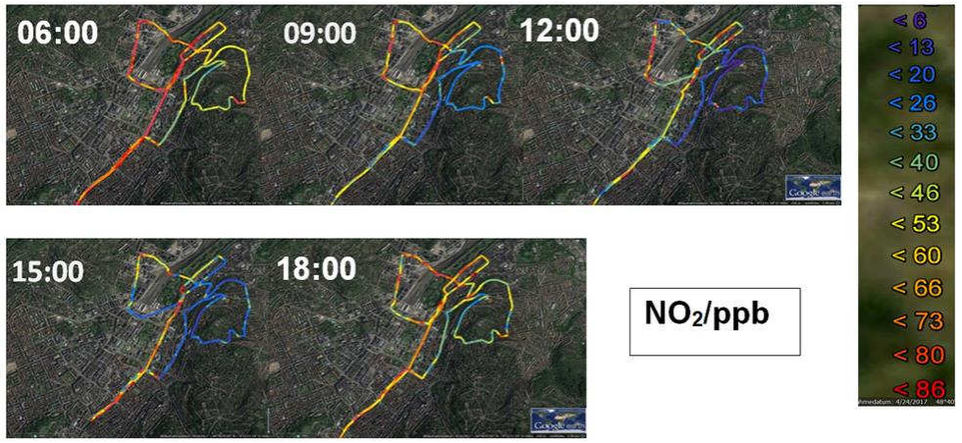

Fig. 14: Diurnal course of the NO_2 concentration during the IOP-III (13.02.2018) in Stuttgart.

During the Stuttgart IOPs, comprehensive studies of the city and surrounding area were also carried out. Fig. 15 a) and b) show the NO_2 concentrations during a measurement run in IOP-I (20.02.2017). While Fig. 15 a) contains the full temporal resolution of the measured NO_2 concentrations (especially the peak concentrations caused by the surrounding traffic), Fig. 15 b) uses a 2-minute 5-percentile low-pass filtering. In [Urban, 2010] it was shown that this method is suitable to eliminate the unavoidable traffic peaks from the data set. Thus, the measurements can be applied to the prevailing background concentrations and a direct comparison can be made with the modelled data from PALM-4U (or the regional drive data).

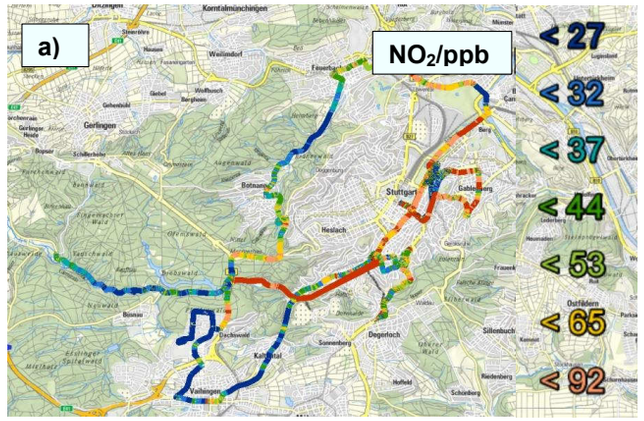

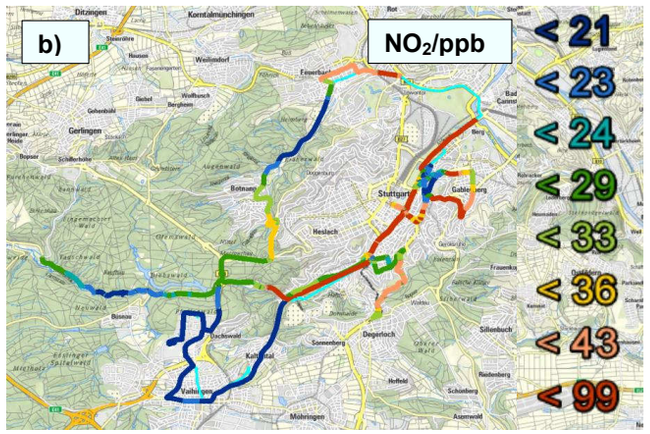

Fig. 15: a) NO_2 concentrations during a measurement run during IOP-I (20.02.2017) in the western surroundings of Stuttgart. b) 2-minute 5-percentile low-pass filtering [Urban, 2010] of the NO_2 data of this measurement run to eliminate traffic peaks.

During IOP-IV, we conducted a series of flux divergence experiments to evaluate the emission, transport, and chemistry module of PALM-4U.

Fig. 16 shows the course of a measurement run in the greater Stuttgart area. As an example for the trace substance concentration curves, the prevailing upwind and leeward concentrations of NO_2 on 09.07.2018 (7:00 - 9:30 UTC) are shown here.

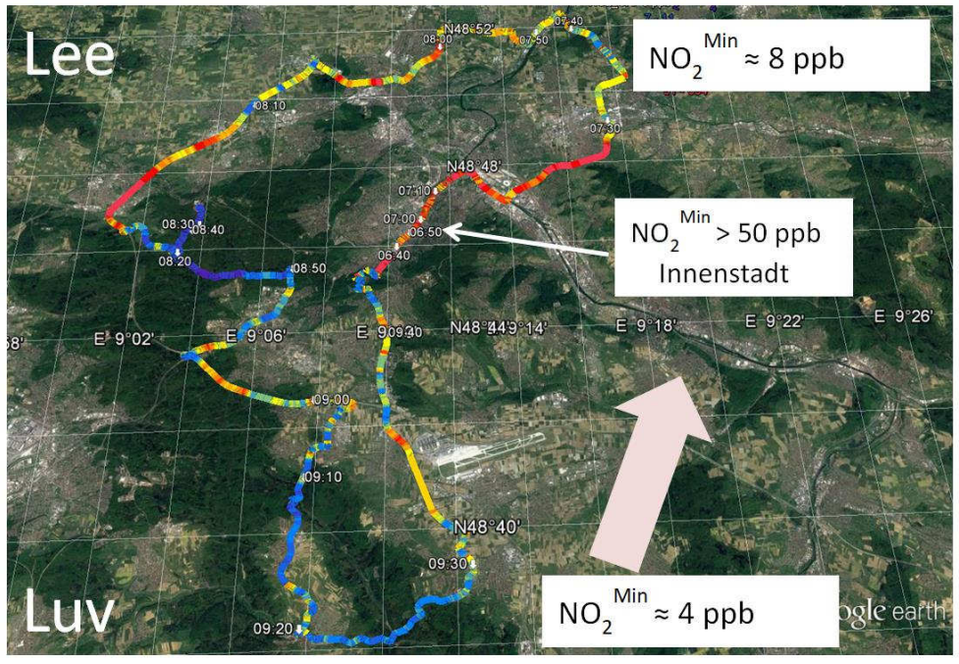

Fig. 16: NO_2 concentrations during a measurement run during IOP-IV (09.07.2018, 7:00 - 9:30 UTC) in surroundings of Stuttgart. The summer background concentrations of NO_2 in this period were only about 20% of the NO_2 background values observed during IOP-I (winter conditions).

The summer background concentrations in the windward area of Stuttgart at of 4 ppb NO_2 were more than a factor of five lower than the corresponding winter background concentrations. The NO_x emissions of Stuttgart led to a noticeable increase in NO_2 concentrations (approx. 4 ppb upwind of the city to about 8 ppb downwind of the city).

6.1.3 NO_x Contribution of a City

The observed NO_x contribution of the city, calculated from the difference between windward and leeward concentrations in this experiment accounts for approximately 5 - 6 ppb NO_x with 4 ppb NO_2 and according to the proportion distribution of the photostationary state 1 - 2 ppb NO is within the expected range. The nitrogen oxide contribution of traffic in urban areas is 60 - 80% [Karl et al., 2017], which is considerably higher than the average share of 34% for Germany [UBA, 2015] and underlines the role of road traffic as the main NO_x emitter in urban areas.

In later part of 1990s, a comparison between experimentally determined NO_x emission rates of a city and the results of an emission calculation model was carried out in the BMBF-project EVA within the Tropospheric Research Programme (TFS) in the surroundings of the city of Augsburg [Slemr et al, 2002]. Typical NO_x emission peaks in the Lee area of the city were in the range of 8 - 10 ppb NO_x [Klemp et al, 2002; Möllmann-Coers et al, 2002]. The distance between the city centre and the measurement line in the Lee side was about 5 - 6 km in both cases [Mannschreck et al., 2002], so that comparable meteorological conditions can be assumed in a first approximation. If we now assume a reduction of urban NO_x emissions by a factor of two over the last two decades for the transport sector as the main inner-city NO_x emitter [Ehlers et al., 2016; Steinemann and Zumsteg, 2010], the observed increase of approx. 4 ppb in the Lee area of the city of Augsburg appears extremely plausible.

6.1.4 Assessment of contribution of traffic emissions (work-package 320)

Within the framework of the further development of instruments for reliable differentiation between the local background of trace substances and direct emissions, various concepts have been successfully tested for road traffic as an emission source:

i) An increased N_2O to NO_x ratio as an indicator of the extent to which an air mass is affected by traffic

The $DeNO_x$ process (3-way catalytic converter, and SCR catalytic converter) in exhaust of vehicles lead to considerable amounts of N_2O emissons because of side

reactions. $\Delta(N_2O)$ to $\Delta(NO_x)$ ratio[9] is a characteristic measure of the intensity of the traffic impact on an air mass. The maximum value of $\Delta(N_2O)$ / $\Delta(NO_x)$ was 0.025 [ppb/ppb] (see section 6.2.1).

ii) A high NO to NO_2 ratio as an indicator of the extent to which an air mass is affected by traffic

The nitrogen oxide emissions of the internal combustion process take place almost exclusively in the form of NO. Later, a smaller part of the original NO transforms into NO_2 in commonly used oxidation-catalysist by reaction with the excess oxygen present in the diesel exhaust. Due to high NO emissions, such air masses near the source can be characterized by high NO/NO_2 ratios (see for example Fig 19, tunnel studies).

In contrast, the photostationary equilibrium (PSS) between NO, NO_2, and O_3 during the day time leads to an NO/NO_2 ratio with values well below 1 [ppb/ppb]. In the absence of nearby emissions, the emitted NO from distant roads is converted to NO_2 by the transported O_3 (from outside the city) on a time scale of 1-2 minutes, resulting in a typical NO/NO_2 ratio of about 1/3 after a transport time of a few minutes. Low NO/NO_2 ratios in combination with simultaneous O_3 concentrations of ~50 – 60 ppb (background level) are a clear indication of air masses of urban background areas.

iii) Composition of the VOCs mix as an indicator of the extent of traffic impact

The role of VOCs is important in the formation of O_3. The impact of traffic on the VOCs mixture is discussed in detail in section 6.3.

iv) The O_x-concept ($O_x = O_3 + NO_2$) as a method for determining the direct NO_2 emission fraction

On the time scale of a few minutes, the atmospheric loss processes are almost negligible for the sum of O_3, and NO_2. If we disregard photochemical O_3 production in

[9] $\Delta(N_2O) = (N_2O - N_2O_{\text{Background}})$; $\Delta(NO_x) = (NO_x - NO_{x\ \text{Background}})$

the first approximation, the photostationary equilibrium ensures the exchange of concentration of the two components on the time scale of a few minutes during the day. Two conclusions can be drawn:

- If all NO_x emissions were in the form of NO only, O_x in the windward and leeward regions of a strong NO_x source (e.g. a road) would be a conservation variable [Guicherit, 1988] i.e., O_x would remain constant before and after the NO_x source.
- Direct NO_2 emissions cause an increase in O_x values in the O_x balance due to the additional NO_2 addition (e.g., application of the O_x concept to Augsburg, [Mannschreck, 2001]). On the other hand, the increase of O_x in front of and behind the NO_x source can be directly attributed to the share of direct NO_2 emissions in NO_x.

In fact, direct emissions of NO_2 from road transport play a major role in exceeding the permissible limit of 40 µg/m³ (annual average). If NO_x emissions from transport consisted exclusively of NO, then NO_2 peaks could at best only reach the level of background O_3 concentration entering the city[10]. Only direct NO_2 emissions cause the annual average for NO_2 in street canyons to rise significantly above the background O_3 value of approx. 60 – 70 µg/m³.

This procedure represents the second approach for the determination of direct NO_2 emissions[11] in addition to the road tunnel investigations also carried out by us.

The relationships described above can be visualized using a large number of data sets (https://stickoxid-rechner.de/)[12] [Rohrer and Schultz, 2018]. The following relationships are valid for all measuring locations:

---

[10] This simplified presentation does not consider the effects of the relatively rare summer peak ozone concentrations, especially since the effect of such ozone peaks is absolutely irrelevant for the annual NO_2 average.

[11] In contrast to NO, the NO_2 concentration has been subject to strict regulation by the legislator since 2010 for health reasons: the annual average for NO_2 must not exceed 40 µg/m³ of air.

[12] The web tool "Stickoxid-Rechner" was developed in the Research Centre Jülich. The developers are F. Rohrer (IEK-8, FZJ) and M. Schultz (Jülich Supercomputing Centre, FZJ).

- The exhaust gas of combustion engines contains primarily NO and a smaller contribution of NO_2, generated by the partial conversion of NO to NO_2 in the oxidation catalytic converter of diesel vehicles.
- The essential part of the NO_2 is only produced by the chemical reaction ($NO + O_3$) in the air.
- In general, the relationship between traffic density and NO_2 is non-linear and depends on the traffic composition.
- However, if the O_3 is depleted from the titration, i.e. NO [ppb] > O_3 [ppb], the remaining slope $\Delta(NO_2) / \Delta(NO_x)$ is the share of direct NO_2 emissions in NO_x.

Comment: For a reliable modelling of traffic emissions from the knowledge of traffic census, not only the total NO_x emissions are relevant, but also the share of direct NO_2 emissions. This becomes immediately obvious when considering the occurrence of NO_2 values at high NO_x. If one disregard in the first approximation NO_2 inputs from the surrounding area, the measured NO_2 value should not exceed that of the background O_3, if there were no direct NO_2 emissions near the source. Only the contribution of direct NO_2 emissions leads to a continuously increasing NO_2 value with growing NO_x.

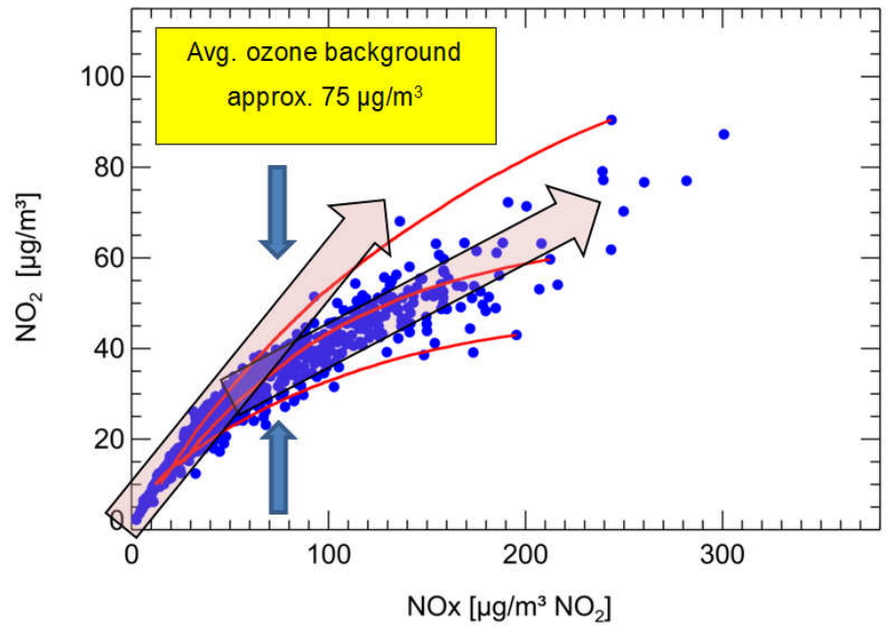

Fig. 17: Annual mean values for NO_2 and NO_x of almost all federal and state controlled measuring stations in Germany. In addition, the ozone background annual average [Schmidtke and Schmidt, 2019] is shown. For this data set (O_3 = 75 µg m^{-3}), the proportion of direct NO_2 emissions at $\Delta(NO_2)$ / $\Delta(NO_x)$ is (0.2 ± 0.02) NO_2 of the emitted NO_x.

6.2 Monitoring traffic emissions (workpackage 430)

6.2.1 NO_x emission of the current vehicle fleet by means of tunnel studies

A major emitter of gaseous and particulate trace substances in urban environments is road traffic. The Handbook Emission Factors of Road Transport (HBEFA) [v4.1, Aug. 2019] is used as a data base of traffic-transmitted emissions in urban environments for model studies with PALM-4U. An important aspect for the quality of PALM-4U model studies is therefore the reliable description of the emission behaviour of the current vehicle fleet. For this purpose trace gas measurements in road tunnels were carried out with MobiLab. The source attribution of tunnel measurements is particularly easy, since the pollutants here clearly originate from road traffic. Characteristic parameters are the trace substance/CO_2 ratios of a current road traffic fleet, as they represent a measure of trace substance emission normalised to fuel consumption. Furthermore, the determined trace substance/CO_2 ratio allows a direct comparison of different tunnel studies, independent of the number of vehicles passing through the tunnel.

6.2.1.1 Tiergarten-Tunnel Berlin

Fig. 18 describes the temporal behaviour of different trace gases during the crossing of the Berlin Tiergarten tunnel on 21 January 2017 (IOP-I). The period of passage through the Tiergarten tunnel between 10:29 and 10:33 UTC is indicated by the two dotted lines. All trace substances (except O_3) increase parallel to the measured CO_2 concentration. Comparing the measured concentrations of trace gases in front of and behind the tunnel with the concentrations in the tunnel, it can be seen that the additional (health) burden on the tunnel users in the Tiergarten tunnel is rather moderate compared to the situation in the Stuttgart Heslacher Tunnel (see Fig. 19).

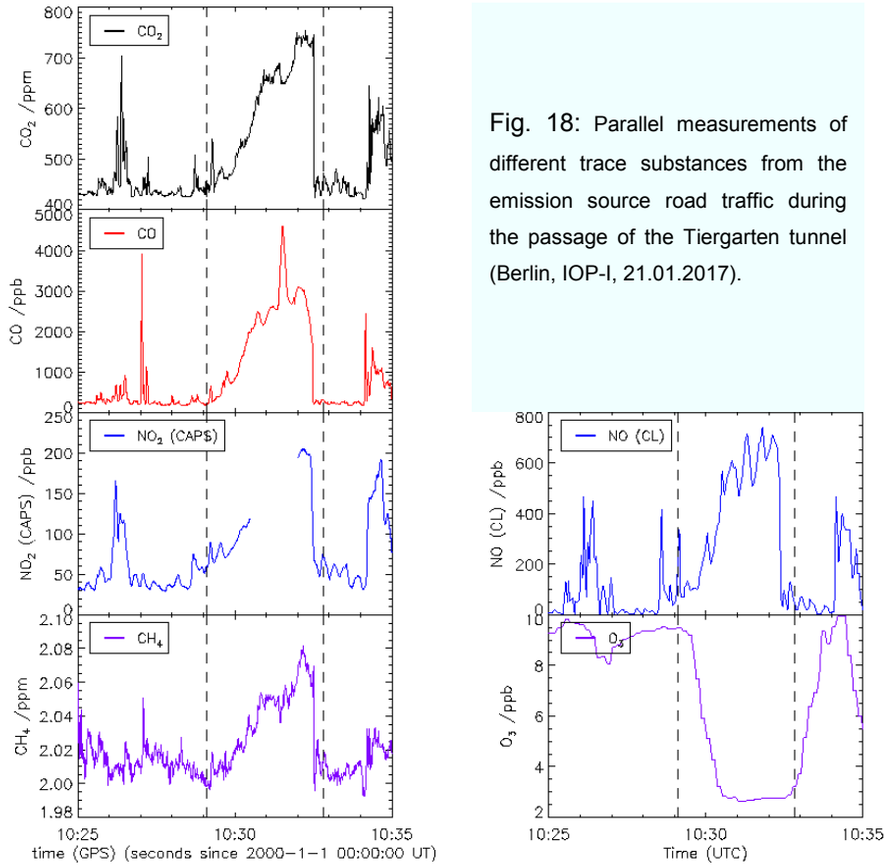

Fig. 18: Parallel measurements of different trace substances from the emission source road traffic during the passage of the Tiergarten tunnel (Berlin, IOP-I, 21.01.2017).

- In contrast to all other trace gases shown, the concentration of ozone decreases to 2 ppb as a result of titration with the NO abundant in the tunnel.

- Urban traffic is only an insignificant methane emitter with the emission ratio of

$$\Delta CH_4 / \Delta CO_2 \approx 0.0005 \text{ [ppm/ppm]}.$$

- The NO_2 to NO_x emission ratio in the Tiergarten tunnel was

$$\Delta NO_2 / \Delta NO_x \approx 175/900 \text{ [ppb/ppb]} = (0.21 \pm 0.04^{13}) \; NO_2/NO_x.$$

[13] Error estimation from the scattering width of the NO_2 and NO pass in the Tiergartentunnel

6.2.1.2 Heslacher Tunnel Stuttgart

One focus of the investigations during the Stuttgart IOPs was tunnel studies in the Heslacher tunnel. Fig. 19 shows the results of a series of passes through the Heslacher tunnel during IOP-II. The aim was to characterise the emission behaviour of the current vehicle fleet. The tunnel is particularly suitable for this purpose:

- It connects the Stuttgart motorway junction with the B-14, which runs directly through Stuttgart and therefore has an exceptionally high traffic volume (approx. 50000 vehicles/weekday including 2500 trucks).
- It has a sufficient length (2300 m) so that atmospheric trace substances (in this case O_3) introduced by vehicle-induced turbulence have no noticeable effect on the measured NO_x concentrations.
- The changing engine-load situations (constant speed conditions outside rush hours and stop-and-go conditions during rush hours) allow the investigation of different emission conditions of the current vehicle fleet. For a detailed comparison with HBEFA results in a planned paper this should be taken into account.
- The proximity of the tunnel to the campaign site at Marienplatz allows a high frequency of tunnel passages via MobiLab.

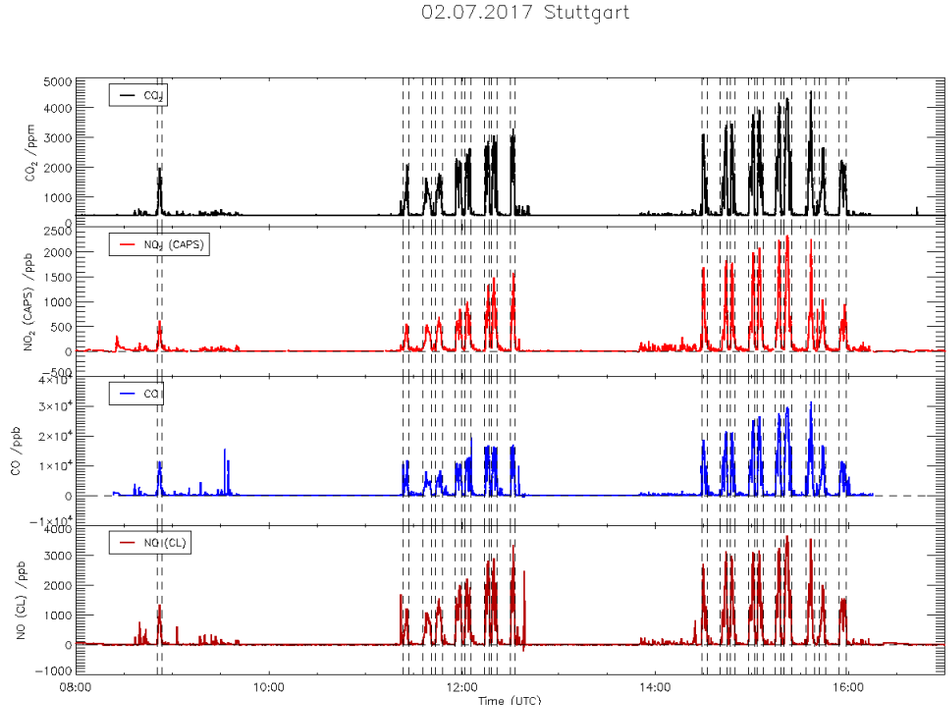

Fig. 19: Measured concentration trends of CO_2, NO_2, NO and CO during the passages of the Stuttgart Heslacher tunnel (IOP-II, 02.07.2017). The dotted lines mark the respective entry and exit times of the mobile measuring laboratory.

The comparison of the concentration peaks for NO, NO_2 and CO_2 from Fig. 18 with Fig. 19 reflects the different pollution situations. In particular, the measurement runs between 15:00 and 16:00 UTC fall directly into the afternoon rush hour and are therefore associated with particularly high traffic density. Up to a factor of ten higher CO_2 concentrations were observed in Stuttgart Heslacher tunnel compared to the Berlin Tiergarten Tunnel.

Linear correlations were performed to normalise the trace gases to the CO_2 concentrations. As an example, Fig. 20 shows the correlation fit between CO and CO_2 for the crossing of the Heslacher tunnel from 15:14 -15:18.

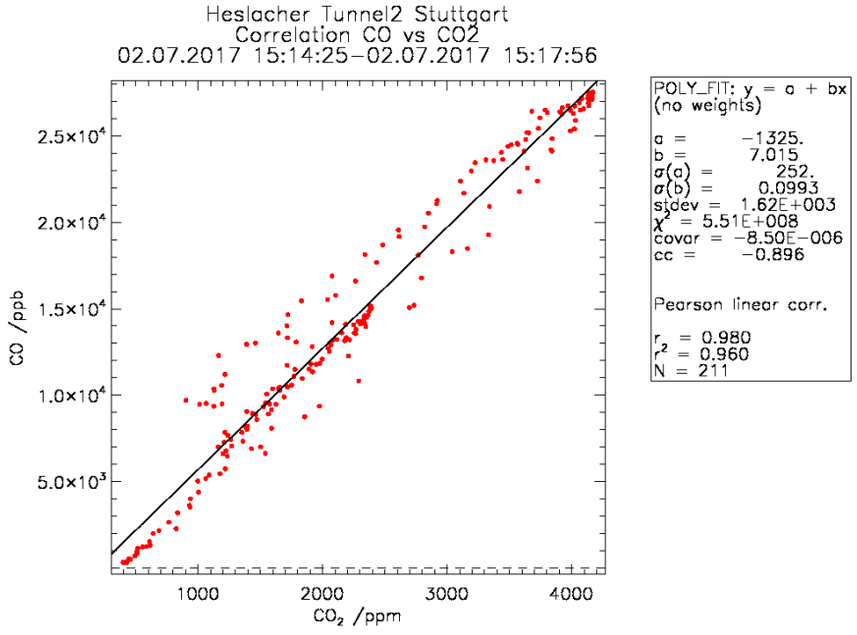

Fig. 20: Example of a linear correlation fit between CO and the simultaneously measured CO_2 concentrations in the Heslacher Tunnel (Stuttgart, IOP-II, 02.07.2017 15:14 - 15:18 UTC). The following applies: CO [ppm] = 7.015 × 10^{-3} CO_2 [ppm], R^2 = 0.96.

Table 6.1: Comparison of the trace gas concentrations (SPi) from the Berlin Tiergarten Tunnel (winter conditions, Temp = -2° to 1°C) normalized for fuel consumption (CO_2) with the results of the Heslacher Tunnel in Stuttgart (summer conditions, Temp = 24 to 29 °C).

Trace gase (SP_i)	**Tiergarten Tunnel Berlin IOP- I, Winter 2017 SP_i / CO_2 [ppb/ppm]**	**Heslacher Tunnel Stuttgart IOP- II, Summer 2017 SP_i / CO_2 [ppb/ppm]**
CO	9.5 ± 1.0	7.35 ± 0.8
NO	2.2 ± 0.2	0.85 ± 0.07
NO_2	0.61 ± 0.05	0.48 ± 0.04
NO_2-fraction NO_2/NO_x	0.21 ± 0.04	0.36 ± 0.05

Table 6.1 provides a comparison based on mean values (CO, NO, and NO_2) for tunnel passages in Berlin (Fig. 18) and Stuttgart (Fig. 19). In addition, the resulting NO_2 shares in NO_x are given. It can also be seen from the comparison that the outside temperature has a significant influence on the NO_x emissions of the vehicle fleet.

- Both measurement days fall on weekend days (21. 01. 2017 is a Saturday; 02.07.2017 is a Sunday). This ensures that for both measurement days, car traffic dominates the emission situation in the tunnel.
- The CO mixing ratios standardised to CO_2 are the same for both seasons within a range of 15 %. It can therefore be concluded that, under both winter and summer outdoor temperature conditions, the catalytic converters of both gasoline vehicles (3-way catalytic converter) and diesel vehicles (oxidation catalytic converter) in the vehicle fleet investigated have sufficient temperatures to efficiently reduce CO[14].

However, there is a considerable difference in NO_x emissions standardized to CO_2:

- In the tunnels, the NO_2/NO_x ratio measured in summer is about 60% higher than in winter.
- Also, NO_x emissions are observed to be more than a factor 2 higher at low outside temperatures compared to summer conditions.

  The cause of this situation may be the effects of the various exhaust gas cleaning technologies for diesel vehicles[15]. Higher temperatures in summer heat the oxidation catalytic converters of diesel vehicles on average to higher temperatures than in winter. The result is a higher degree of conversion of NO to NO_2 in the oxidation catalysts due to the temperature-dependent NO to NO_2 equilibrium. Higher NO_x emissions in winter are likely to be caused primarily by

[14] Under cold-start conditions, gasoline vehicles would have the largest contribution to emissions (e.g., [Klemp et al., 2012]). Their CO/CO_2 emission ratio would be around 0.05→0.07 [ppm/ppm] under cold start conditions. However, a CO/CO_2 ratio of significantly less than 0.01 [ppm/ppm] is actually found in the tunnel.

[15] Diesel vehicles account for 70 - 80 % of NO_x emissions from motor vehicle traffic [see Klemp et al., 2012; Wiechmann-Fiebig, UBA 2017].

SCR catalysts that are not sufficiently tempered (because they are not functional). With regard to NO_2 emissions, at the time of the investigations both effects roughly compensated each other in the seasonal mean. For the future development, however, it is foreseeable that with the improved SCR catalytic converter systems (EURO-6-Temp) and a higher market penetration of EURO-6 diesel, NO_x and thus also direct NO_2 emissions will decrease significantly.

The influence of the outside temperature on the nitrogen oxide emissions of the current vehicle fleet was investigated during different IOPs for different vehicle compositions (Fig. 21). The NO_x/CO_2 ratio in the Heslacher Tunnel is 1.5 - 2 times higher in winter than in summer. This result is in very good agreement with the comparison of the tunnel results from the Tiergarten tunnel (IOP-I, winter 2017) with those of the Heslacher tunnel (IOP-II, summer 2017).

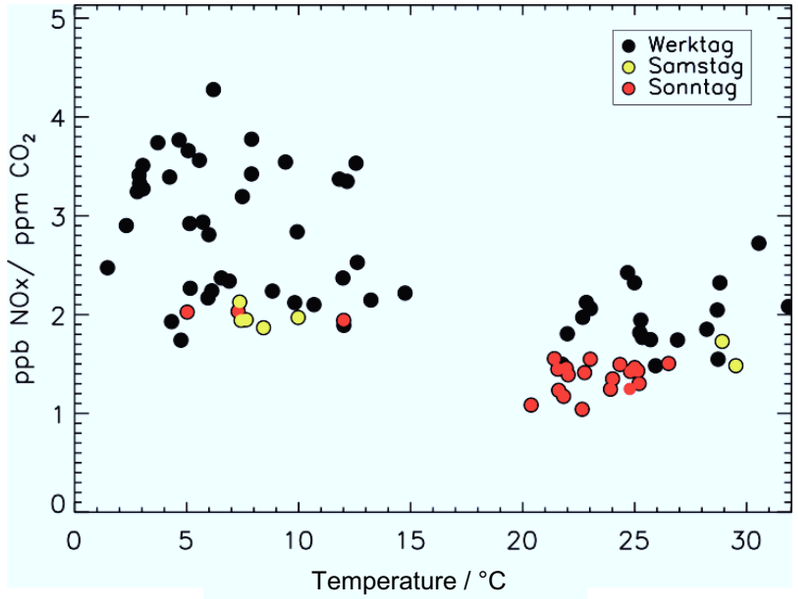

Fig. 21: NO_x/CO_2 ratio as a function of the outside temperature in the Heslacher Tunnel (Stuttgart). Passages of the Heslacher Tunnel during the Stuttgart IOPs for different weekdays and weekends [Wegener et al., 02.07.2019, Mannheim].

It could be shown [Wegener et al., 02.07.2019, Mannheim] that NO_x emissions standardized to CO_2 emissions are increased by more than 40% on weekdays compared to weekends, regardless of the season. The comparison with traffic data identifies the causes. At weekends, the proportion of light and heavy commercial vehicles falls from around 7% on weekdays to around 3% (Fig. 22). If halving the proportion of commercial vehicles leads to a reduction in NO_x emissions to more than 40%, then a commercial vehicle proportion of 7% (as is typical on weekdays) contributes more than 50% to the total NO_x emissions of the measured vehicle fleet.

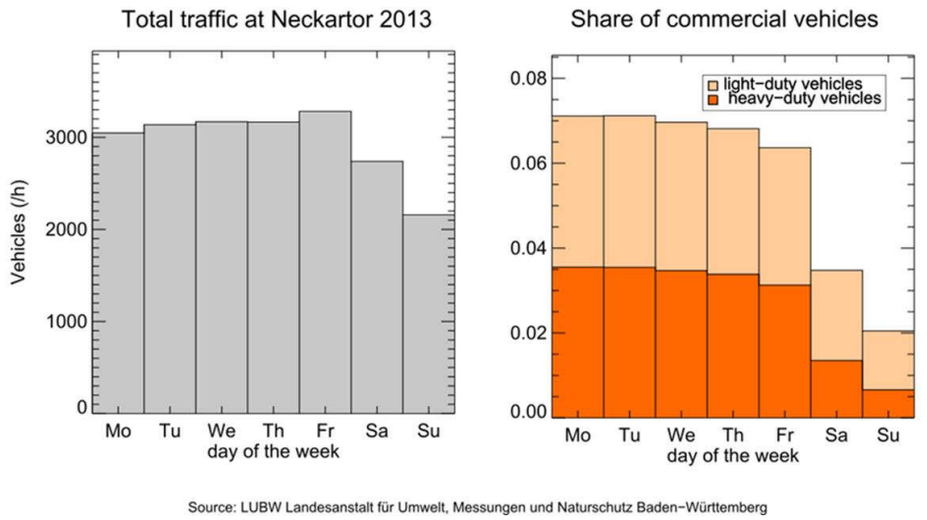

Source: LUBW Landesanstalt für Umwelt, Messungen und Naturschutz Baden−Württemberg

Fig. 22: Traffic data from the Neckartor monitoring station as an estimate of the number and proportion of commercial vehicles in the fleet composition of the Heslacher Tunnel (Stuttgart) [LUBW, Referat 31: Luftreinhaltung, Umwelttechnik, 2013].

Fig. 23 describes the measured concentration-time curves of other trace gases emitted by road traffic in the Heslacher tunnel (Nov. 2016).

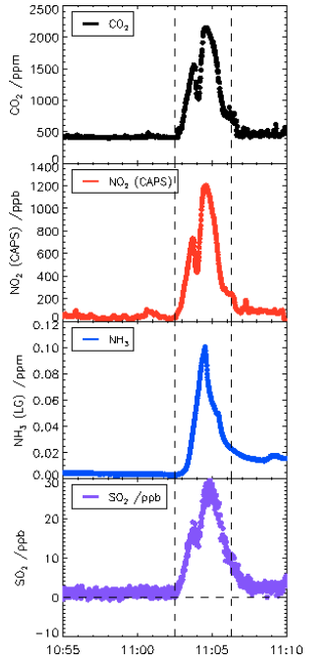

Fig. 23: Time series for CO_2, NO_2, NH_3, and SO_2 during a passage of the Stuttgart Heslach tunnel. For the vehicle fleet in the tunnel, the following trace substance to CO_2 ratios were specified for this tunnel passage:

With CO_2 : Measured CO_2 concentrations
and $(CO_2)^0$ = 405 ppm (CO_2-background-winter).

The following applies to the CO_2 tunnel contribution:

$$(CO_2)^{Tunnel} = CO_2 - (CO_2)^0$$

$NO_2/(CO_2)^{Tunnel}$ [ppb/ppm] : (0.65 ± 0.05)

$NH_3/(CO_2)^{Tunnel}$ [ppb/ppm] : (0.06 ± 0.005)

The NO_2/CO_2 ratio measured in the tunnel describes the directly emitted NO_2 share of the normalised NO_x emission of a vehicle fleet. Outside of tunnels, meteorological and chemical processes change concentrations and the ratio between NO and NO_2 immediately after emission: 1) the exhaust gases are diluted after emission, 2) the emitted NO reacts quickly with the existing O_3 to form NO_2. In total, the NO_2 contribution produced by so-called O_3 titration is added to the originally emitted NO_2 share of NO_x. Away from the sources, the importance of the second NO_2 generation process increases compared to the first (see comments; Fig. 17).

In a later phase of the project, the mobile measuring laboratory was equipped with a sensitive N_2O analysis from the institute's own funds in order to investigate the current emission behaviour of climate-relevant trace gases[16] from inner-city areas (and in a later phase to provide it as an additional species for the emission module of PALM-4U).

[16] Laughing gas (N_2O) is a greenhouse gas that has an around 300 times larger impact on global warming compared to carbon dioxide (CO_2). The main sources of N_2O are nitrogenous fertilisers used in agriculture and animal husbandry, activities involving chemical industry, and combustion processes.

6.2.2 N_2O-Emissions

Already during the first runs with MobiLab during IOP-III it was demonstrated that road traffic[17] contributes substantially to N_2O emissions. The simultaneous measurement of N_2O and NO_2 are shown in Fig. 24 for the standard driving route in Stuttgart. Both trace gases show clear correlations with traffic density. Highest contributions are found for both species along the B14. In the less densely trafficked residential areas near Uhlandshöhe, however, the increase compared to the respective background concentrations is rather small.

However, a quantitative determination of the emission ratio of the traffic-borne contributions of N_2O and NO_2 from road measurements is difficult, since the NO_2/NO_x ratio near the source is highly variable (see also Fig. 17). Furthermore, the comparison must be based on NO_x, since the extent of titration of NO with O_3 to NO_2 varies with time and place. Nevertheless, Fig. 17 provides a rough estimate of the NO_2/NO_x ratio near the source. As a first approximation, NO_2 ≈ is 0.5 * NO_x and is obtained from Fig. 24:

$$\{N_2O/NO_x\}^{\text{Avg. Fig. 24}} \approx (0.04 \pm 0.015)\ [\text{ppb/ppb}].$$

The current UBA emissions register provides an extrapolated emissions[18] ratio of

$$\{N_2O/NO_x\}^{\text{UBA Extrap. 2018}} \approx (0.0146)\ [\text{ppb/ppb}].$$

[17] In an older work [Lörzer, 2002], investigations in the Wuppertal Kiesberg tunnel were carried out and the emission ratio between N_2O and NO_x was calculated. Lörzer found an emission ratio for N_2O/NO_x of 0.077 (g/km)/ 0.76 (g/km). The emission ratio between N_2O and CO_2 was also determined. Lörzer found an emission ratio for N_2O/CO_2 of (0.051 ± 0.021) [ppb/ppm].

[18] The current emissions (extrapolated to 2018) of N_2O from road traffic are 5690 tonnes [UBA, Nationale Trendtabellen 1990 – 2016 (14.02.2018)]. The corresponding value for NO_x (calculated as NO_2) for 2018 is 422240 tonnes.

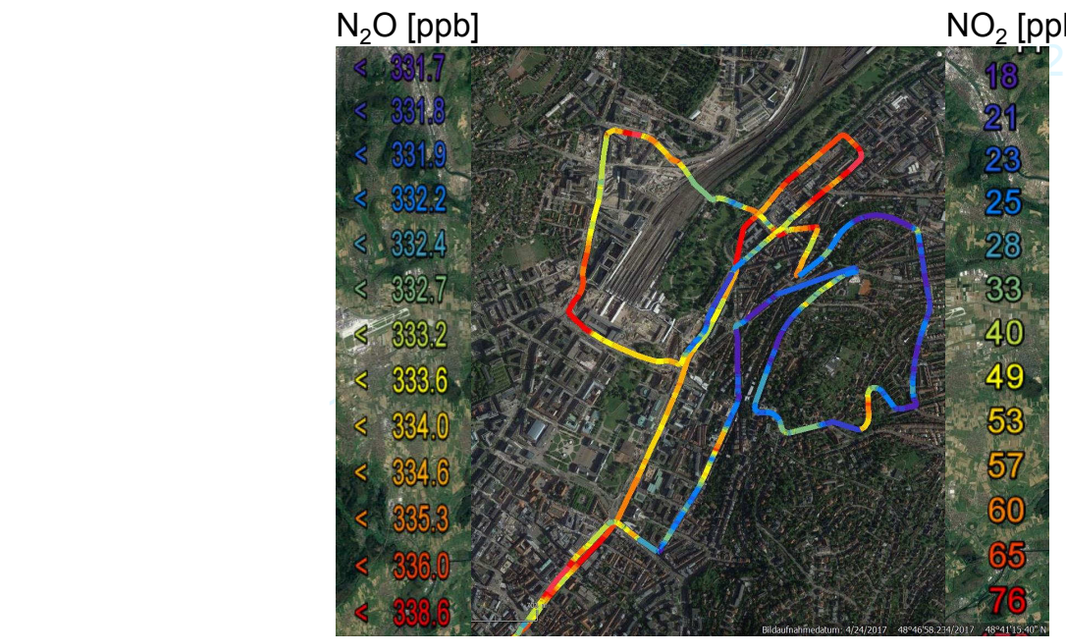

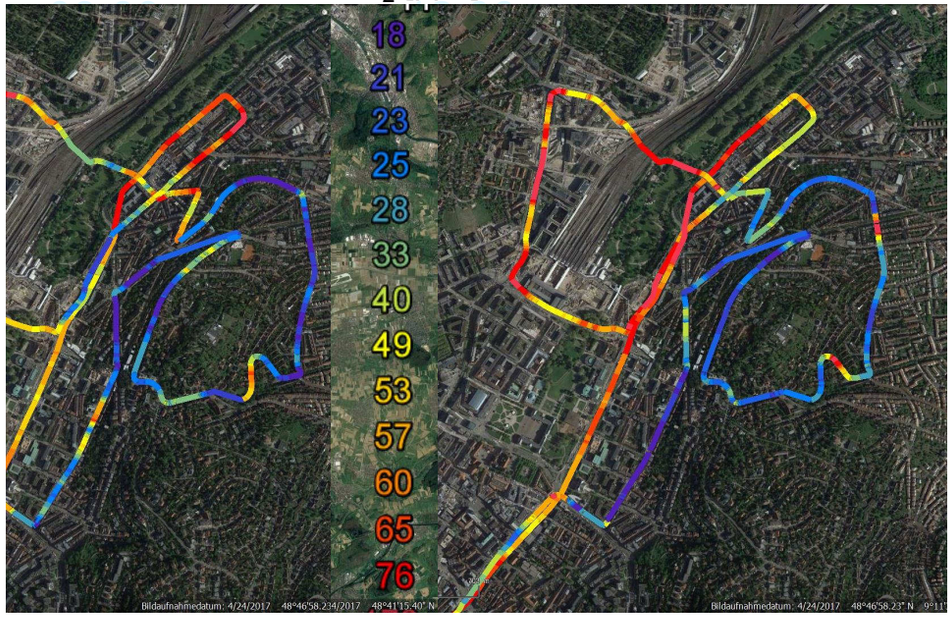

Fig. 24: Simultaneous recording of N_2O and NO_2 on the standard route around the Neckartor in Stuttgart (IOP-III, 13.02.2018).

There is indeed a certain trend towards higher N_2O/NO_x ratios from the MobiLab measurements compared to the emission scenario. However, the uncertainty of the experimental boundary conditions is much too high (unclear shares of other emission sources, share of NO_2 in NO_x) to be able to derive quantitative statements from this comparison. In fact, we had a much more precise set of instruments at our disposal for the verification of the current emission inventories of road traffic, where both photochemical conversion and the influence of other emission sources are almost[19] completely eliminated, as is the case with tunnel studies.

Figure 25 shows the results of our investigations in the Stuttgart Heslachtunnel (IOP-3, Febr. 2018) for parallel N_2O- and NO_x-measurements. The relative deviation (1σ) of the calculated mean N_2O/NO_x value was about 33 %.

$$\{N_2O/NO_x\}^{\text{Avg. Fig 25.}} = (0.0228 \pm 0.0076)\ [\text{ppb/ppb}].$$

The UBA scenario [UBA, Nationale Trendtabellen 1990 – 2016 (Status: 14.02.2018)] results in an N_2O/NO_x ratio for the year 2018:

$$\{N_2O/NO_x\}^{\text{UBA Extrap. 2018}} \approx 0.01475\ [\text{ppb/ppb}].$$

Thus the ratio between N_2O/NO_x determined by us is around the factor

$$\frac{\{N_2O/NO_x\}^{\text{Avg. Fig 25}}}{\{N_2O/NO_x\}^{\text{UBA Extrap. 2018}}} = (1.55 \pm 0.54)$$

[19] The role of non-tunnel specific trace gas inputs has already been mentioned. Fig. 18 shows the leakage of O_3 into the tunnel caused by the vehicle-induced turbulence. This O_3 does not have a noticeable influence on the NO/NO_2 ratio (at least locally) in presence of very high NO_x concentrations in the Heslacher tunnel. A noticeable NO_2-photolysis by light emission from lamps in the tunnel can also be excluded because the irradiance is also much weaker (less light source) in the tunnel compared to an outdoor condition. Otherwise, a noticeable photolysis would have been directly recognizable by an increase in O_3 in the tunnel.

higher than shown by the UBA emissions scenario.

It should be noted that the experimentally determined ratio of N_2O/NO_x shows a trend towards higher ratios than the corresponding ratio from the UBA scenario. However, the stated value of the 1-sigma standard deviation makes it clear that the deviation found in the N_2O/NO_x ratios is not significant.

In order to clarify whether a major reason for the high variability of the N_2O/NO_x ratios is due to the highly variable NO_x emissions[20] of the vehicles, the fuel consumption (i.e. the CO_2 mixing ratio) was used as the normalisation factor.

N_2O/CO_2 ratios found in the Heslacher tunnel as a function of the external temperature (before the tunnel) are shown in Fig 26. The methodology for determining the N_2O/CO_2 ratios shown has already been presented (see Fig. 20). Unfortunately, corresponding tunnel measurements could so far only be carried out for a very limited temperature range (2° - 8° C) because a defect in the N_2O measuring system prevented its use during IOP-IV. Although the determined N_2O/CO_2 ratios varied by more than a factor of two, a 1-σ standard deviation of 18 % for the N_2O/CO_2 mean value was found due to the relatively high number of tunnel passages (n = 42):

$$\{N_2O/CO_2\}^{\text{Avg. Fig. 26}} = (0.057 \pm 0.01)\ [\text{ppb/ppm}].$$

The corresponding ratio from the UBA scenario [UBA, 2018] is

$$\{N_2O/CO_2\}^{\text{UBA Extrap. 2018}} = 0.038\ [\text{ppb/ppm}].$$

Thus the ratio between N_2O/CO_2 determined by us is around the factor

$$\frac{\{N_2O/CO_2\}^{\text{Avg. Fig. 26}}}{\{N_2O/CO_2\}^{\text{UBA Extrap. 2018}}} = (1.51 \pm 0.27)$$

higher than the UBA emissions scenario[21].

---

[20] In the case of petrol vehicles, the difference in NO_x emissions between cold start and warm operating conditions is well over one order of magnitude. Even for modern diesel vehicles with SCR catalytic converters, the difference in NO_x emissions between cold start and warm operating conditions can be more than a factor of five.

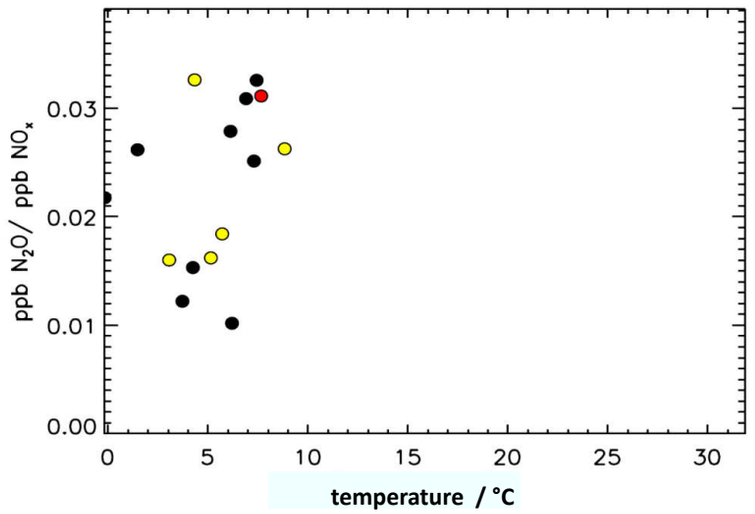

Fig. 25: Parallel measurements of N_2O and NO_x with MobiLab while passing through tunnel[22] (Stuttgart) during IOP-III (black: working days, yellow: Saturday, red: Sunday). A defect of the N_2O cavity-ringdown system prevented the use during IOP-IV under summer conditions[23].

---

[21] It should be noted that the fleet of vehicles in Stuttgart at the time of the measurements differs markedly from the average fleet composition for Germany at that time (the average age of the vehicles in the Stuttgart fleet composition is lower than the average German fleet composition age). Nevertheless, the result of the Stuttgart tunnel measurements supports the expected trend in the N_2O/CO_2 ratios.

[22] A comprehensive publication of all results from the Stuttgart emission comparisons is in preparation [Wegener et al., in preparation].

[23] There is some evidence that the higher proportion of functioning SCR catalytic converter systems in summer will increase the N_2O/CO_2 ratio for summer conditions. Detailed studies on this issue are firmly planned for Urban Climate phase-2.

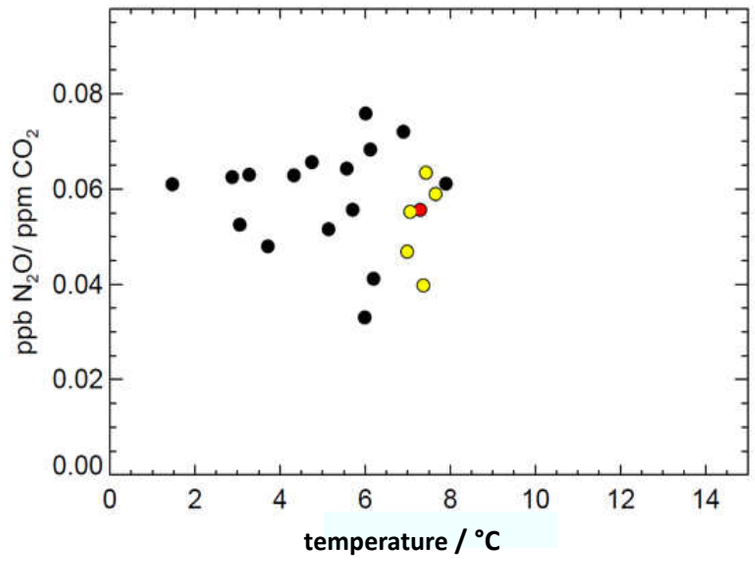

Fig. 26: Parallel measurements of N_2O and CO_2 with MobiLab while passing through tunnel (Stuttgart) during IOP-III (black: working days, yellow: Saturday, red: Sunday). A defect of the N_2O cavity-ringdown system prevented the use during IOP-IV under summer conditions.

Both results show the same trend. The N_2O ratios measured in the Heslacher tunnel (related to CO_2, and NO_x) are higher in both cases than in the current emission scenario. The result of the comparison, normalized for CO_2, indicates significant differences between the measurement and the emission model. The ratio normalized for NO_x shows the same trend, but the margin of error is significantly larger in the case of NO_x normalization. A possible new source of additional N_2O emissions is SCR catalytic converter technology, which has only been introduced in diesel vehicles in recent years. There are indications in the literature that considerable amounts of N_2O are produced when NH_3 or urea is used in SCR catalytic converters [Grosso et al., 2009][24]. Therefore, a further increase of traffic-related N_2O emissions

[24] Within the framework of a parallel project in our working group (Virtual Institute Electricity to Gas and Heat: Emission behaviour of conventional and alternative fuels by means of on-board measurements), it is planned to carry out detailed investigations into the exhaust gas behaviour (including N_2O emissions) of diesel vehicles with SCR catalytic converter.

is likely to be expected in the future due to the foreseeable widespread introduction of SCR catalytic converters.

6.2.3 NH_3-emissions from chasing experiments

In some cases, the emission behaviour of individual emitters is very complex and difficult to determine, particularly if the real emission behaviour in traffic can only be inadequately represented by test bench measurements, as is the case with trucks or buses, for example [Ehlers et al., 2017]. Optical measuring methods, where the light path is directed across a street [Carslaw et al., 2013] are particularly suitable for this purpose, as they can directly measure the emission behaviour of individual vehicles in traffic. Such data sets are principally useful because they can be used to derive statements on the representativeness of emission measurements or to detect the emergence of new types of trace emissions.

The chasing-method, in which the MobiLab directly follows the emission source to be measured and simultaneously determines its trace substance to CO_2 ratio, also provides information on individual emission factors of individual vehicles. For a clear interpretation of the results, the signal must be clearly separable from the background (by its high signal strength and/or low traffic density). In the case of the results of the chasing-investigations on modern EURO 6 buses in Stuttgart, shown in Fig. 27, both conditions were fulfilled in good approximation.

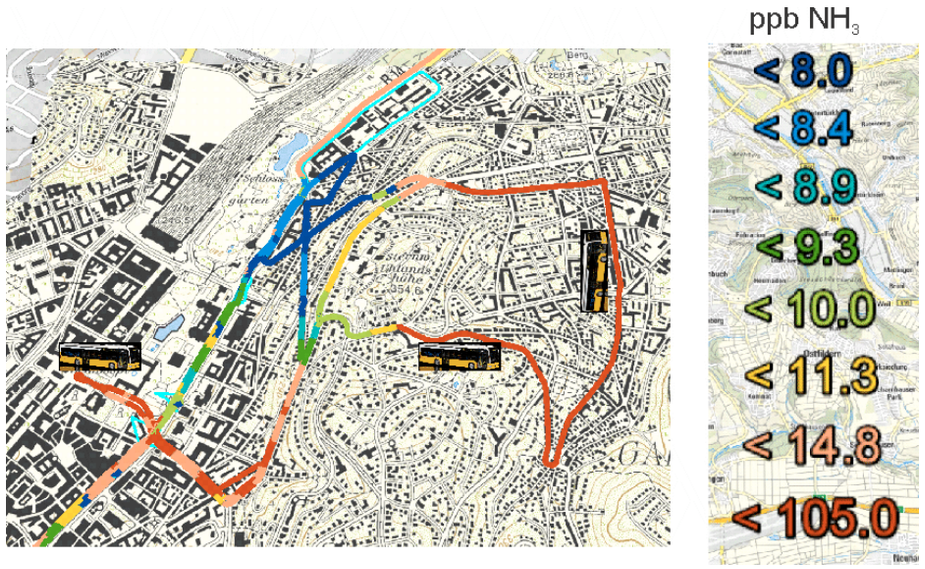

Fig. 27: Chasing investigation behind a EURO-6 bus of the Stuttgart city bus company (line 42) with starting point at the Stadtschloss. The strongly increasing power output of the diesel engine during "climbing the Uhlandshöhe" led at the same time to overdosing of the ammonia of the SCR catalytic converter system, so that significant NH_3 concentrations were found in the exhaust gas of this bus (for the exact concentration curve see Fig. 28).

The temporal concentration levels observed during a chasing experiment are shown in Fig. 28. While no significant NH_3 emissions from the bus are observable in the area of the Schlossgarten, the measured NH_3 concentration suddenly rose sharply up to 1 ppm when the Bus had to climb Uhlandshoehe. Based on the observed NH_3 to CO_2 ratio, a clear source differentiation can be made for both cases (i.e. tunnel vs. bus-chase). In the tunnel, NH_3-to-CO_2 ratios in the range of 0.06 [ppb/ppm] (Fig. 23) were caused by side reactions during the conversion of the NO_x on the 3-way precious metal catalysts. While, the NH_3-to-CO_2 ratios of 1 [ppb/ppm] observed here can be clearly assigned to the NH_3 slip of the SCR catalyst of this EURO 6 bus. The task of future investigations will be to quantify this new NH_3 source and to evaluate its significance in comparison to other NH_3 sources (e.g. those from the agricultural sector).

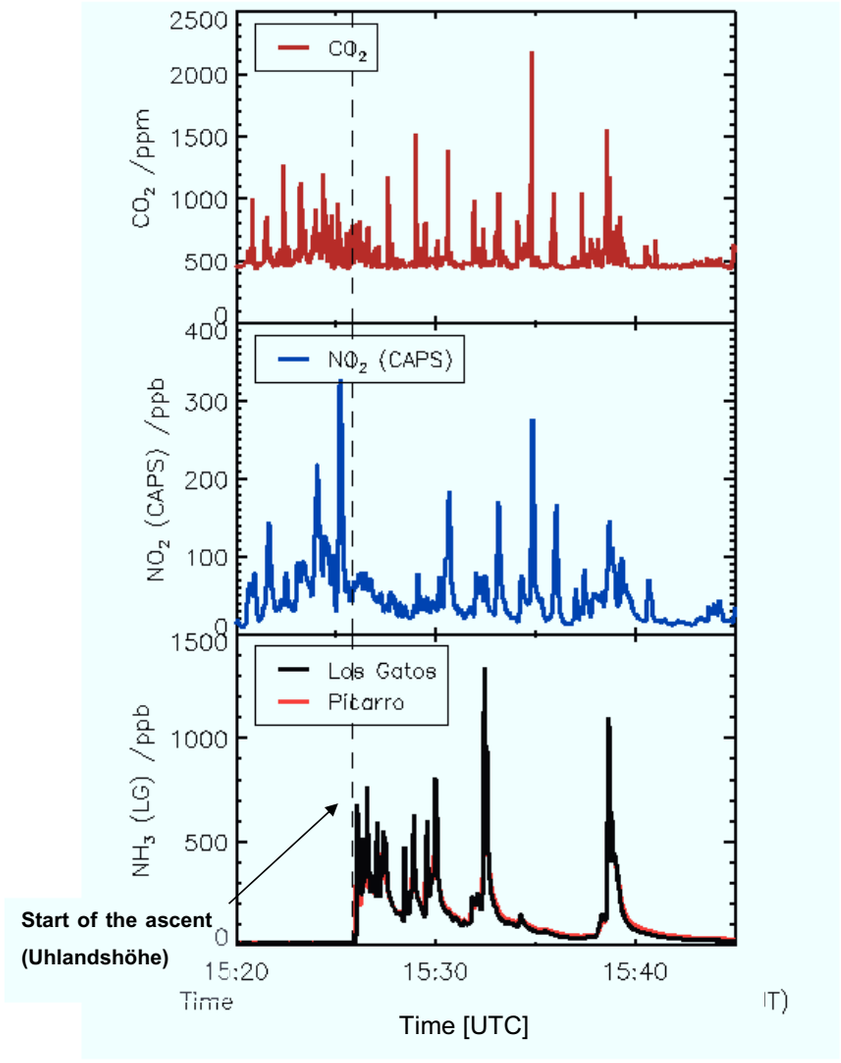

Fig. 28: Temporal concentration course of the "chasing" experiment of the bus of line 42: Sudden rise of the NH_3 concentration during climbing the Uhlandshoehe, measured with two different NH_3 measuring systems (Los Gatos (TDL system) and Picarro (cavity ringdown detection). The NH_3 to CO_2 ratio of about 1 [ppb/ppm] observed here can be clearly attributed to the NH_3 slip of the SCR catalytic converter of this EURO 6 bus.

Table 6.1: Comparison of the two different NH_3 sources of traffic

NH_3 from transport fleet	**NH_3 from EURO-6 Diesel**
Source: Mainly gasoline with 3-way catalytic converter	Source: SCR catalyst slip from EURO-6 Diesel
Emission Ratio [ppb/ppm CO_2] **NO : 2 – 2.5** **NO_2 : 0.6 – 0.8** **NH_3 : 0.05 – 0.1**	Emission Ratio [ppb/ppm CO_2] **NO ≈ 3** **NO_2 ≈ 0.1** **NH_3 ≈ 1**
NH_3 / NO_x-ratios ≈ 2 to 3 % of NO_x [ppb/ppb]	NH_3 / NO_x-ratios Up to 20 % of NO_x [ppb/ppb]

To assess the significance of such NH_3 high emitters for urban air quality, it is important to get an idea of their frequency and duration. On the standard route in Berlin in winter 2017 around Ernst-Reuter-Platz, the influence of both NH_3 sources were observed and distinguished under evening inversion conditions. Fig. 29 a) and b) show the simultaneous measurement of NO_2 and NH_3 during the MobiLab measurement run on 17.01.2017 16:15 - 17:20 UTC. Two different NH_3 peak structures could be distinguished under evening inversion conditions and in calm weather: Many individual NH_3 peaks with a typical height of 2 to 4 ppb were observed, whose peak NH_3 to NO_2 ratios to correspond to the emission ratios found in the tunnel studies. In addition, two significantly stronger NH_3 peaks of about 30 ppb were observed from vehicles, whose high NO_2 emissions characterized them as to Euro 6 diesels with malfunctions in urea dosage.

It can be stated that for a reliable PALM-4U modeling of urban NO_2 emission levels, there is a need to continuously monitor the consequence of changes in emission regulations (by law) and related air-chemistry effects.

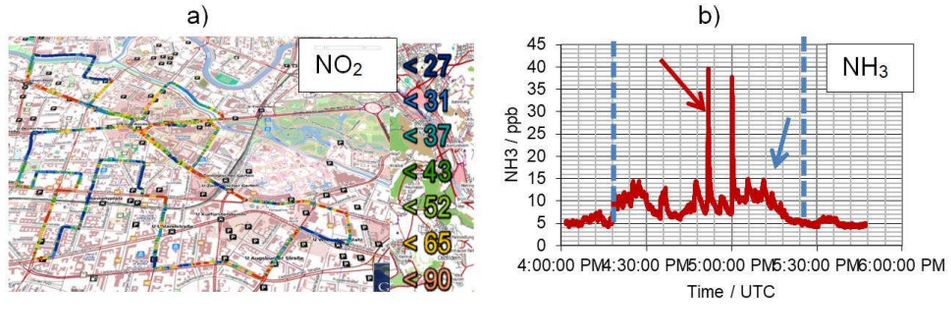

Fig. 29: Simultaneous measurements of NO_2 and NH_3 during the MobiLab measurement run on 17.01.2017 16:15 - 17:20 UTC. a) NO_2 time history [ppb] on the Berlin standard route. b) NH_3 concentration time series for the same MobiLab measurement run. Two different NH_3 peak structures can be distinguished under evening inversion conditions. Many individual NH_3 peaks with a typical height of 2-4 ppb are identifiable, whose peak height ratio to NO_2 corresponds to the emission ratios found in the tunnel studies. In addition, two significantly stronger NH_3 peaks of about 30 ppb can be observed (red arrow), which have similar mixing ratios to the NO_2 measured in parallel.

6.3 VOCs as presurcors for ozone production

6.3.1 Modeling summer photo-oxidant formation with MCM-3.3

It was shown that the dominant source of VOCs is still petrol vehicles with temporarily reduced catalyst efficiency (so-called cold start conditions) [Ehlers et al., 2016]. On the other hand, diesel vehicles are the main source of NO_x from traffic. Our long-term studies from the vicinity of traffic hot-spots using stationary and mobile measurements show that the VOCs/NO_x [ppb]/[ppb] ratio decreased by a factor of 7.5 between 1994 and 2014. This experimentally determined decrease is significantly greater than the decrease of a factor of 2.5 predicted by the Federal Environment Agency [Umweltbundesamt, 2015]. Using box model studies, we were able to show [Ehlers et al., 2016] that the disproportionate decrease in VOCs compared to NO_x is mainly responsible for the observed reduction in summer ozone formation.

Irrespective of this, the results obtained in the urban climate project support us in continuing our long-term investigations of NO_x and VOCs emissions from road traffic. The data sets obtained within the framework of the urban climate project can

additionally be used for a continuation of our long-term measurement data set of VOCs and NO_x in urban environments, so that we can supplement the long-term data set [Ehlers et al., 2016], which has been running from 1994 to 2014, with the latest data sets and document current developments.

A main objective of the work for work package 410 was the modeling of summer photochemical O_3 formation in Berlin (noon, and clear sky conditions) using a detailed box model (MCM-3.3). For this approach, the VOCs data (C_2 - C_{11}), radiation parameters, and observed VOCs/NO_x ratio from IOP-II and IOP-IV were used.

The results of these investigations are part of the validations of the chemistry module of PALM-4U, in which the photochemical photo-oxidant formation is modelled in varying degrees of detail, depending on the computational capacities. A crucial part of the corresponding validations will be to compare the results of summer photochemical oxidant formation for the different modules independently of transport processes on real emission mixes with a detailed box model. For this purpose, a number of VOCs and NO_x point measurements have already been carried out, so that the relevant air chemical processes in different evolutionary stages can be studied and compared with the reference model (MCM-3.3). A major goal of the planned experimental investigations in the second phase of the urban climate project will be to comprehensively test the combined capabilities of the PALM-4U model with respect to transport and chemistry in an urban-rural transport study (see preliminary investigations in the Stuttgart area, IOP-IV, Fig. 16).

In the framework of the urban climate project, we took canister samples during all four IOPs in Berlin and Stuttgart and analysed them for their individual VOCs compositions in Jülich. The comparison of different canister samples with pure source VOCs-profiles allowed us to draw conclusions about the source of the VOCs.
In the following the gas chromatographic system used will be presented and the results of VOCs measurements, on roads and in tunnels, will be described. At first, an overview of the VOCs mixing ratios found for different loading conditions will be given. In a second part, the relationship of the emitted VOCs and NO_x concentrations to the air-chemically formed secondary pollutants as well as the self-purification processes of the atmosphere, which are also controlled by air chemistry, will be presented.

6.3.2 The reactivity concept

In the atmosphere almost 90 % of VOCs react with atmospheric OH radical. The atmospheric processing of an air mass can therefore be described in good approximation by the total reactivity of Rvoc with OH. The composition of the VOCs mixture found therefore allows a transformation of the concentration of VOC_i into its respective reactivity R_{voci} with respect to OH. The OH reactivity describes the rate of a VOC_i to react with OH radicals. The summation over all R_{voci} then provides a total reactivity R_{VOC} of VOCs mixture with respect to OH.

$$R_{VOC} = \sum k_{OH+VOC_i} \times [VOC_i]$$

The reactivity parameter is extremely useful because it allows the local O_3 production for VOCs mixes of different composition to be described using a single parameter (see [Klemp et al., 2012]). In atmospheric processing, the reaction paths given by the OH concentration compete with each other. Only on the reaction path R_{VOC}, additional ozone is formed in the atmosphere. The reaction path R_{NO2} converts the NO_x present in the form of NO_2 to HNO_3, which is subsequently removed from the atmosphere by rain-out and surface deposition. The ratio of the reactivities R_{VOC}/R_{NO2} controls the relative importance of the two processes in trace substance degradation. In Fig. 30, these processes are shown in a simplified scheme of the degradation of VOCs and NO_x in the troposphere.

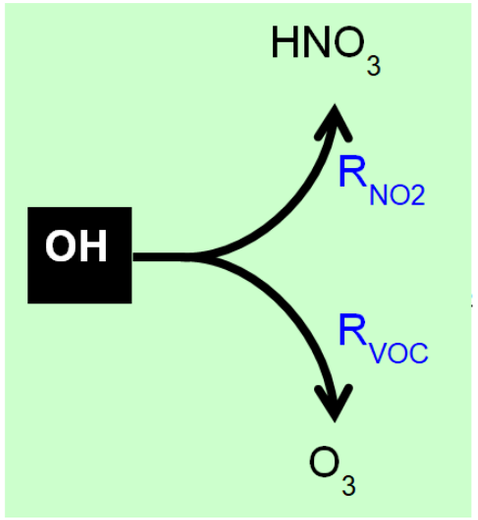

$$R_{NO_2} = k_{OH+NO_2} \times [NO_2]$$

$$R_{VOC} = \sum k_{OH+VOC_i} \times [VOC_i]$$

Fig. 30: Simplified scheme of the reaction paths of OH radicals in the degradation of NO_x and VOCs. The reaction path R_{VOC} leads to net O_3 formation in the atmosphere while the reaction path R_{NO2} represents the radical removal process.

The local O_3 production is determined by the total OH radical turnover of all VOCs. As already mentioned, mixtures of VOCs of different composition can be described with a single parameter called reactivity R_{VOC}. Therefore, the following section will compare different VOCs mixtures on the basis of their reactivity fractions.

As can be seen from Fig. 33, the reactivity distributions of the alkenes and aromatics in particular differed between anthropogenically dominated inner city samples and samples from the urban background. The share of the anthropogenic alkenes in the ‘fresh’ inner city mix of 42 % decreased to 17 % in the urban background. A similar behaviour was observed for the aromatics. Their share decreased from 17 % to 7 %. In general, a reduced share of short-lived anthropogenic VOCs (alkenes, aromatics) was observed in the background mix due to their photochemical degradation. The highly reactive BVOCs (BVOCs: VOCs of biogenic origin) were prominent close to their sources. Berlin has a particularly high proportion of BVOCs-emitting vegetation, especially in the urban background areas.

6.3.3 Invariance of the VOC profile from traffic

Fig. 31 (from: [Ehlers et al., 2016]) compares reactivity-weighted VOCs profiles in the form of so-called Rorschach plots. Here, a recent VOC profile of from summer 2014 [Bonn et al., 2016] is compared with a profile of our measurements in Munich from 1997. The most significant change in the current traffic profiles is the occurrence of previously non-existent alcohols in the traffic-dominated VOCs profiles (resulting from the 5 or 10% admixture of bioethanol to petrol since 2011).

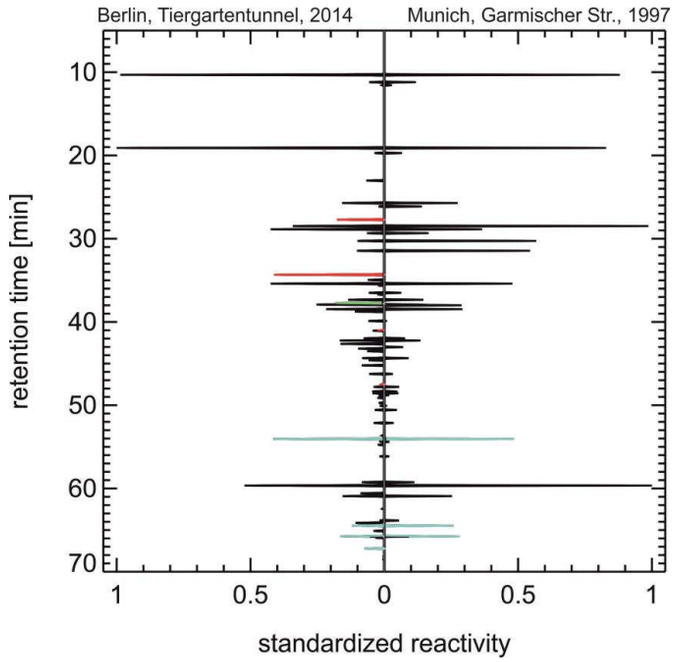

Fig. 31: Reactivity weighted VOCs profiles (so-called "Rorschach" plots) from a measurement campaign with MobiLab in summer 2014 [Bonn et al., 2016; von Schneidemesser et al., 2018] and from measurements in the inner city area of Munich in Feb. 1997 [Kern et al., 1998]. The reactivity shares of alcohols (methanol, ethanol, and propanol), isoprene, and some aromatics (toluene, trimethylbenzenes) are highlighted in red, green, and mint green colours, respectively.

Also, a rather recent gasoline engine exhaust chromatogram from 2015 (cold start conditions) and a more than 20-year-old emission chromatogram from 1997 on Garmischer Straße in Munich were compared in Fig. 32 (also from: [Ehlers et al., 2016]). The similarity of the exhaust gas chromatogram with the 1997 VOCs

emission profile is somewhat less than in the case of the two emission profiles in Fig. 31. Because the averaging effect due to the superposition of the many individual sources is omitted in Fig. 32. However, the release of alcohols can also be clearly identified from the cold-start emissions of the gasoline engine. The VOCs pattern of traffic, which has remained largely constant over decades, is still dominated by the same class of emitters i.e. Petrol vehicles with (not yet) working catalytic converters (catalytic converters in the so-called cold start state)[25].

[25] This is also the actual reason for the found high constancy of the VOCs composition in road tunnels (see Fig. 34). A more detailed explanation of this factual connection will be given on the basis of own test bench investigations on Diesel and Petrol vehicles in different operating conditions [Klemp et al., 2012].

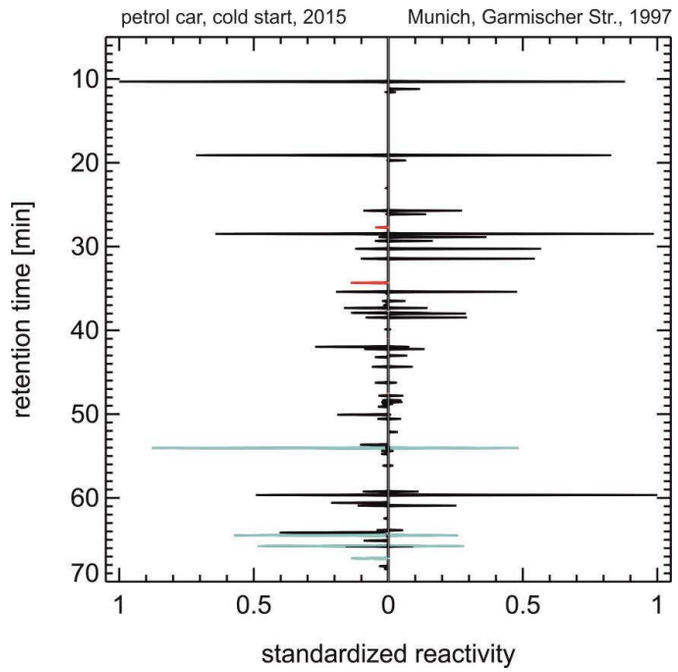

Fig. 32: Reactivity weighted VOCs profiles ("Rorschach" plots) of a petrol engine in a cold start from 2015 in comparison to the inner city area of Munich from Feb. 1997 [Kern et al., 1998]. The reactivity shares of alcohols (methanol, ethanol, and propanol), isoprene, and some aromatics (toluene, trimethylbenzenes) is presented in red, green, and mint green colours, respectively.

The dominant role of traffic as main source of VOC is underlined comparing the Berlin inner city VOCs mix (Fig. 33) with a VOCs mix from the Heslacher Tunnel, Stuttgart, August 2017, Fig. 34. The source allocation of tunnel measurements is particularly easy, since the pollutants here clearly originate from the emission source traffic. The agreement between the Berlin inner city VOCs mix and the Stuttgart tunnel measurements (almost pure exhaust VOCs mix) is remarkably good.

Fig. 34 demonstrates the invariance of the VOCs composition of the almost[26] pure traffic mix. Apart from minor differences in the reactivity fractions, identical fractions distributions were measured for both the Stuttgart and the Berlin tunnel in

[26] Tunnels also contain ouside air. The pure traffic mix can be obtained by subtracting the background values after and behind the tunnel. The impact of outside air can be seen by the share of BVOCs reactivity to the total reactivity of both tunnels.

summer. In principle, this behaviour is an indication of the resilience of the statements derived from the tunnel data due to the high number of emitters.

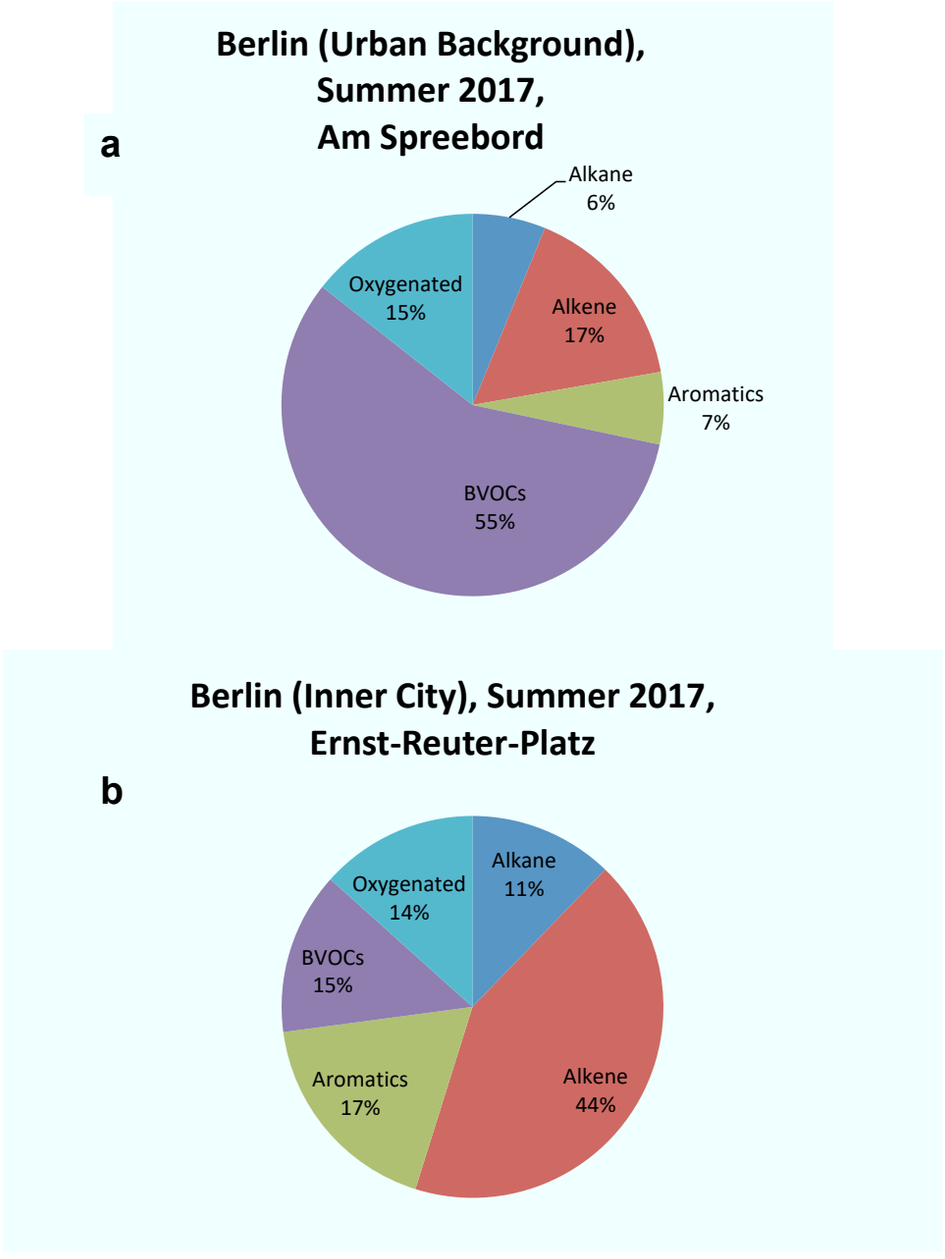

Fig. 33: Reactivity shares for five different VOCs subgroups; medians for two different emission scenarios are shown: **(a)** Berlin (urban background) and **(b)** Berlin (inner city), both originating from IOP-2, Berlin, August 2017.

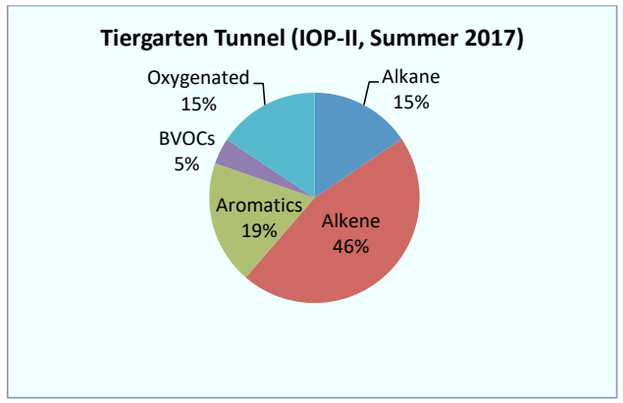

Fig. 34: Reactivity shares for five different VOCs subgroups; the medians for the Berlin Tiergarten tunnel (IOP-II, summer 2017) and the Stuttgart Heslacher tunnel (IOP-II, summer 2017) are shown.

<u>Insertion:</u> Local O_3 formation rate as a function of R_{VOC} und R_{NO2} using a zero-dimensional model

The formation of photooxidants can be estimated for different R_{VOC}/NO_x ratios by using a detailed reaction mechanism (MCM, **M**aster **C**hemical **M**echanism [Jenkin et al., 1997]. The main advantage of this approach is that the measured input parameters (NO_2, VOCs mix, and radiation data) can be used as constrain to study the photochemical O_3 formation at a specific region. Fig. 35 shows the result of variation calculations with MCM-3.3, in which the resulting O_3 production rates for different start conditions are shown as a so-called isopleth plot.

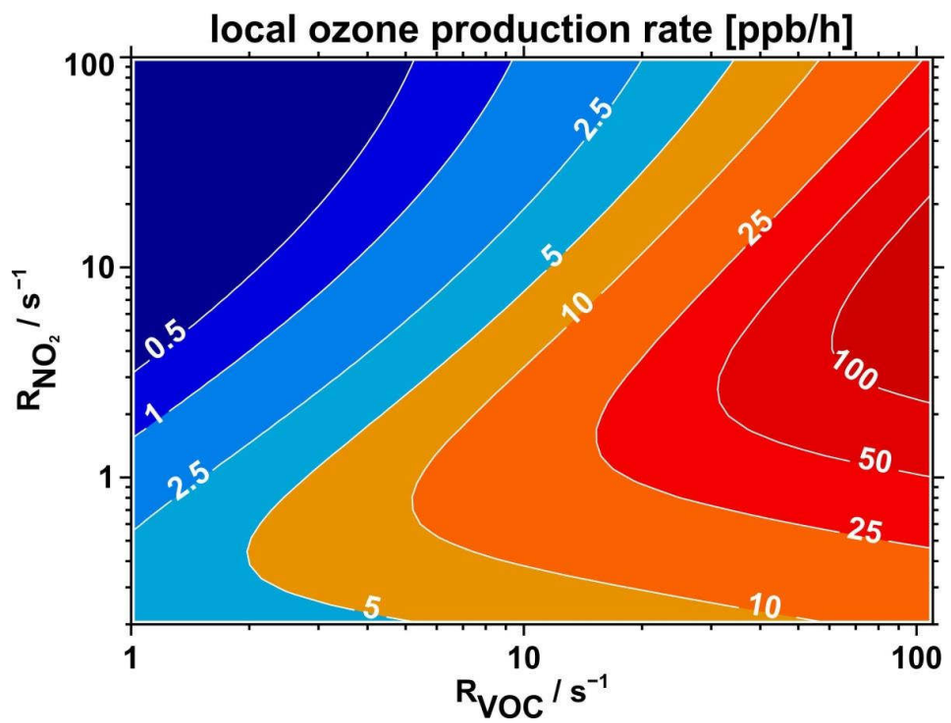

Fig. 35: Result of varied calculations with MCM-3.3 (details: see Klemp et al. 2012]), in which the resulting O_3 production rates for different starting conditions of VOCs and NO_2 along reactivities are shown as a so-called $P(O_3)$-isopleth plot. General conditions are: Latitude: 52.5° northern latitude, radiation conditions: 21.06., local noon 12:00. A rapid conversion between NO and NO_2 occurs at noon via the photostationary state on the time scale of 1 - 2 minutes.

The upper left area of the EKMA diagram is characterized by small VOCs/NO_x ratios, as typically found in urban areas of Central Europe. A reduction of the VOCs leads to a reduction of the calculated O_3 production. In contrast, a reduction of the NO_x concentration leads to an increase in the calculated O_3 production. The reason for this is that at high NO_x concentrations the reaction of NO_2 with OH competes with the reduction of VOCs by OH. The reduction of the NO_x concentration leads to an increase in O_3 production as a result of the increased degradation of the VOCs. In general, positive slopes of the $P(O_3)$-isopleths indicate the presence of VOCs limitation in the isopleth plot.

Large VOCs/NO_x ratios are present in the lower right area of the isopleth plot. This air-chemistry scenario is typical for rural regions far from the source, because during the transport of an air mass the NO_x are removed from the atmosphere by OH radicals faster on average than the VOCs. In the range of negative slopes of the $P(O_3)$-isopleths, the reduction of NO_x leads to a reduction of O_3 formation. Therefore, this part of the diagram is called NO_x-limited range. In contrast, a change in VOCs concentration has only a minor effect on O_3 formation. This is because the O_3 formation rate is limited by the amount of NO_x available. In this range, the system does not contain enough NO_x to recycle OH radical efficiently by the radical (HO_2) reaction with NO.

6.3.4 Local O_3 formation of current trace gas mixes in the Berlin area

In recent years, our working group has conducted a series of summer measurement campaigns in the vicinity of the city of Berlin (BÄRLIN2014 in Aug. 2014, IOP-II in 2017, and IOP-IV in 2018). The isopleth plot in Fig. 36 shows O_3 formation at the beginning of summer at the time of the highest sun elevation (21. 06.) as a function of the precursor reactivities R_{NO2} and R_{VOC} (including R_{CO} and R_{CH4}). The results of a series of canister samples from IOP-IV (July 2018) and their positioning on the $P(O_3)$-isopleth plot according to their VOCs and NO_2 reactivities (red dots with white border) are shown in Fig. 35. Also, an overview of measurement locations and times is given in Table 6. 3. The processing and dilution curve with the predicted 2014 trend is taken from our publication [Ehlers et al., 2016, figure 25]. The trend of the year 2014 describes the general behaviour of an air mass during processing in the course of transport from the city to biogenically dominated areas. The results of the Berlin summer measurement campaign 2018 (IOP-IV) are grouping quite well around the marked trend pattern for 2014 for both high and low reactivities (Fig. 36). Additionally, the mean values of the reactivities from four exposure scenarios from summer 2017 (IOP-II) as well as two single measurements (Table 6.3) from August 2014 are shown (Fig. 36). They are also grouped around the plotted trend and thus underline the stable temporal trend of the trajectory.

Table 6.2.: List of comparative measurements from 2017 and 2014: In addition to the results of individual measurements from one episode of IOP-IV (July 2018) shows the mean values of the NO, NO_2, VOC, CO, and CH_4 measurements for the associated VOCs reactivities of four different pollution scenarios (mean inner city, mean Tiergarten tunnel, mean "before the city west", mean "before the city east") from the Berlin IOP-II (July 2017). Additionally, results of two background characterizations from BÄRLIN-2014 [Bonn et al., 2016; by von Schneidemesser et al., 2018] are shown for comparison.

Berlin Campaigns	**NO** [ppb]	**NO_2** [ppb]	**NO_2*[27]** [s^{-1}]	**VOC** [s^{-1}]	**CH_4 + CO** [s^{-1}]
Inner-city 2017	102	53	34.4	8.04	2.3
Tiergarten tunnel 2017	180	77	73	11.6	6.4
"before the city west"[28] 2017	1	4	0.9	2.76	0.75
"before the city east"[29] 2017	0.5	2	0.55	4.65	0.7
"outside the town"[30] 2014	0.5	1.7	0.55	3.87	0.76
"Outside the town"[31] 2014	0.7	2.0	0.67	5.78	0.79

[27] When calculating the respective relevant NO_2 reactivity (NO_2*), the photostationary state was assumed to be set with a ratio of $NO_2/NO \approx 3 / 1$.
[28] Schöneiche, eastern inflow conditions
[29] Grunewald, Pfaueninsel, August 2017, western inflow conditions
[30] Alt Landsberg, August 2014, eastern inflow conditions
[31] Pfaueninsel, August 2014, western inflow conditions

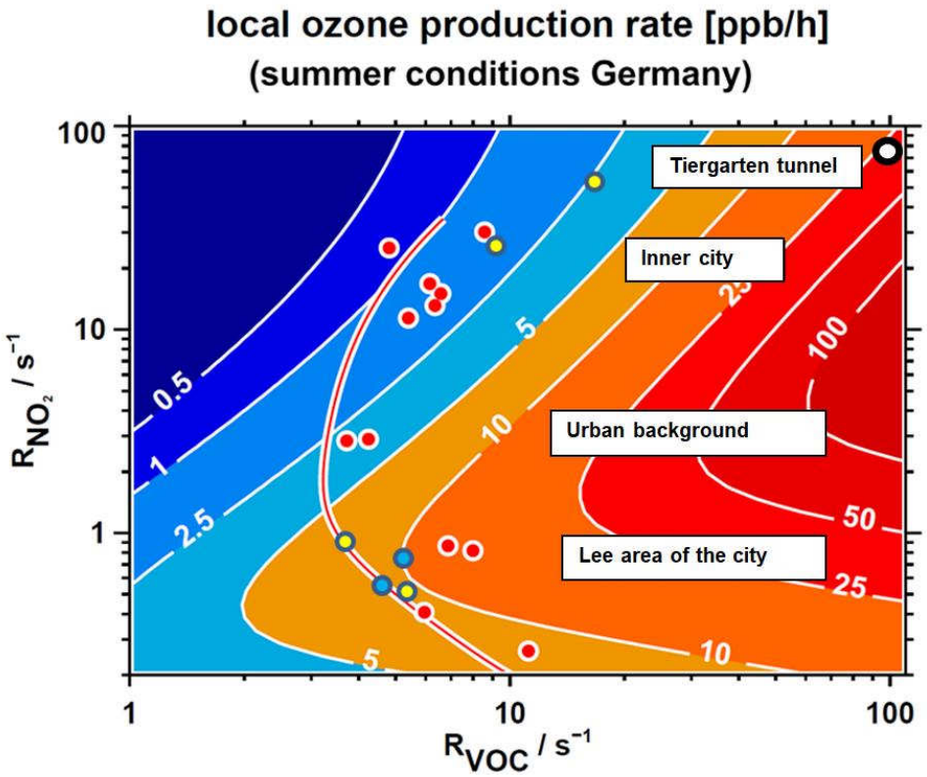

Fig. 36: Berlin summer measurement campaign 2018 in the isopleth plot is presented by red circles with white border. In addition, the mean values of the reactivities from four exposure scenarios (see Table 6.3) from the Berlin measurements during the IOP-II in summer 2017 are shown in yellow circles with black border. Furthermore, the results of two background measurements (August 2014) with MobiLab from the eastern and western Berlin Hinterland are shown [Bonn et al., 2016] in light blue circles with dark blue boarder. The white circle with black border describes the location of the mean city centre ratio R_{NO2}/R_{VOC} for the year 1994. The red trend line [Ehlers et al., 2016] describes the principle behaviour of an air mass during processing in the course of transport from the city to biogenically dominated areas. All Berlin results are grouped quite well around the trajectory predicted by [Ehlers et al., 2016]. Also for the range of low NO_2 values the trend given in [Ehlers et al., 2016] is supported by the measurements.

The following conclusions can be drawn from this comparison of the current urban climate data sets (IOP-IV, July 2018) with the long-term trend studies based on older data sets from [Ehlers et al., 2016]:

- The starting ratio of R_{VOC}/R_{NO2} (represented by the starting point of the drawn line in Fig. 36) can be reproduced in good approximation by the urban climate project measurements. This can be interpreted as confirmation of the trend given in [Ehlers et al., 2016].
- The canister samples collected during the project urban climate from less polluted environments confirm the course of the 2014 processing/dilution curve.
- From the progression of the 2014 processing/dilution curve shown in [Ehlers et al., 2016] it can be seen that the current photochemical O_3 formation in the source regions is decreasing compared to the situation 20 years ago (see the location of the mean inner-city R_{NO2}/R_{VOC} ratio from our measurements "mid-1990s with white circle with black border, reference year 1994) and is shifting more and more to the background areas.

Our new investigations from Berlin in the summer of 2018, as well as from 2014, show a decline in OH reactivities in the source regions for VOCs and NO_2 of varying intensity. During the reference year 1994, the ratio (R_{VOC}/R_{NO2}) was 1.4. Today, we find a ratio R_{VOC}/R_{NO2} of about 0.3. The decrease for NO_2 is much smaller (about a factor of 2) compared to the decrease in VOCs (more than a factor of 10). This is the real reason for the drastically reduced O_3 formation near the source regions. The current R_{VOC}/R_{NO2} ratios in the vicinity of the sources are not high enough to ensure that under VOC-limited conditions efficient O_3 formation takes place. This will only change when biogenic sources replenish the VOCs budget in the summer, without NO_x being supplied at the same time.

However, the following point should also be kept in mind. The exclusive focus on anthropogenic NO_x reduction tends to lead to an increase in O_3 formation as the associated trajectory on its way from urban to rural areas now passes through isopleth regions with higher O_3 production. A balanced reduction strategy with bilateral reductions of VOCs and NO_x must be effective in preventing this unwanted effect.

6.3.5 Seasonal dependency of biogenic contributions to the VOC mix

For the Berlin canister samples of IOP-III (Feb. 2018) and IOP-IV (July 2018), mean reactivities were calculated for the three different scenarios from Fig. 36 (inner city, urban background and windward range of the city; see Table 6.3). In addition, the biogenic contributions to the mean reactivity of the VOCs mixes were determined for the three scenarios for summer and winter conditions.

Table 6.3: Mean concentrations and mean reactivities of Berlin VOCs measurements from one episode of IOP-III and IOP-IV for the three different scenarios (inner city, urban background and Luv area of the city) are provided. Also biogenic fractions (isoprene and monoterpenes) of the observed VOCs mixes are given. Winter isoprene shares reflect the (small) anthropogenic share of isoprene emissions in urban environments (see for example [Wagner and Kuttler, 2014]).

Season	Total concentration [ppb]	Reactivity R [s^{-1}]	Av. Rate const.[32] ‹k_{OH}› [$cm^3 s^{-1} 10^{12}$]	Biogenic R [s^{-1}]	Share Biogenic [%]
Summer					
Inner city	27.4	4.9	7.4	0.8	15
Urban background	27.9	3.0	4.6	0.4	13
Luv area of the city	21.7	7.2	13.9	3.7	51
Winter					
Inner city	43.5	8.0	7.5	0.32	4
Urban background	33.2	3.0	3.7	0.08	3
Luv area of the city	21.5	2.3	4.3	0.04	2

We found the highest biogenic shares in summer with over 50 % of VOCs reactivity in the Luv area of the city of Berlin, while the observed share in the other cases (inner city and urban background) was within the range of 13 – 15 %. It is also

[32] According to [Schmitz et al., 1997] averaged rate constants were calculated as follows:

$$< k_{OH} > = \frac{\sum k_{OH}^{i} * [VOC]_i}{\sum [VOC]_i}$$

noteworthy that the VOCs samples collected in summer at the windward side of Berlin showed higher reactivities R compared those from the inner city.

Under winter conditions the biogenic fraction was largely absent. The mean VOC concentrations in the inner city in winter were about 50 % higher than in summer concentrations, but the average weighted reaction rates with OH of the winter and summer inner city mixes were almost the same. Upcoming simulations with PALM-4U will investigate whether meteorological reasons or changes in emission behaviour (e.g. heating contributions) were mainly responsible for the observed concentration increase winter. The observed small remaining biogenic contributions in winter could be at least partly due to emissions of volatile chemical products (e.g. cleaning agents, personal care products, etc.) [McDonald et al., 2018].

6.4 Further usability of the results

With the exception of programme package 420, Forschungszentrum Juelich was able to meet all the project objectives listed in Table 3.1 completely and on schedule. We have collected a representative data set[33] of urban emissions of gaseous and particulate trace substances for the study cities of Berlin and Stuttgart. Participation in all 4 IOPs enabled us to establish climatology of these trace substance concentrations, so that a comprehensive data set for the evaluation of PALM-4U is now available.

The temporally and spatially highly resolved data set comprises a variety of gaseous and particulate trace substances of air quality and climatological relevance. A considerable proportion of these trace substances are not covered by the standard measuring technology of the State Environmental Agencies. Special attention was paid to the development of standard routes (see Fig. 14), which were frequently traversed during the IOPs with our mobile measuring laboratory MobiLab. In addition, the windward background concentrations of the considered trace substances were determined, so that the inner-city contribution of these substances can be separated from the regional background for the upcoming model comparisons with PALM-4U.

The investigations showed significant differences between summer and winter conditions. These differences are caused both by meteorological processes (e.g.

[33] A publication of the results is in preparation.

change of the inversion layer height) and by different orographic conditions, so that a large number of different validation cases for PALM-4U can be provided. In addition, the aspect of faster daytime photochemical processes (photostationary state) was investigated meteorologically and their influence on the NO-to-NO_2 ratio was described. These data sets will also be subject of the validation processes of existing chemistry modules of PALM-4U.

In addition, we performed extensive VOCs measurements on reactive organic gases. For this purpose VOCs canister samples were taken and analysed for their content of C_2 - C_{11} hydrocarbons and oxidized substances. Preparations were made for a comprehensive comparison of the different chemistry modules[34]. It is planned to compare the results of the different chemistry modules with those of an explicit chemistry mechanism (MCM-3.3, approx. 15000 reactions).

The data set generated in this project is of considerable relevance beyond the actual project objectives:

- Trace gas measurements in tunnels near the source reflect the emission conditions of the current vehicle fleet. By normalizing to the CO_2-increase measured simultaneously with high time resolution in the tunnel, the quality of existing emission models of road traffic can be verified experimentally[35].
- The application of the reactivity concept provides the direct comparison between different emission mixes with regard to O_3 formation. Based on the reactivity concept, comparisons were made between current and past emission scenario using calculation model (MCM 3.3). The reactivity (R_{VOC}/R_{NO2}) ratio allows for the direct comparison of the respective O_3 formation rates of the different mixes with each other based on the results of a photochemical box model.
- As a further direct application of this concept, the contribution of BVOCs to O_3 formation can be estimated directly by comparing the position of the site (R_{VOC}/R_{NO2}) on the isopleth surface (see Fig. 36) with and without biogenic R_{VOC} reactivity contributions and the respective resulting O_3 formation. These

[34] The implementation of air chemistry modules increases the computing times of PALM-4U considerably, chemistry modules of varying complexity can be integrated into the code as required.

[35] It has been shown that in the past considerable deviations between predicted and experimentally observed VOCs/NO_x ratios have been found [Ehlers et al., 2016].

findings can be used in the planning of future forest and urban planting concepts, where the extent of BVOCs emissions should be a criterion for the selection of tree species.

- The current emission data sets obtained during the urban climate project (TP6) can be used for extensive chemical and transport modelling, so that reliable statements on the atmospheric residence time of the introduced trace substances can also be derived.
- Within the framework of the urban climate project, extensive measurements of NH_3 were carried out. The emission ratio of NH_3/CO_2 in the exhaust gas of gasoline vehicles could be determined to a value of approx. 0.06 [ppb/ppm] by means of tunnel studies. For the first time it could be demonstrated by this analysis that some diesel EURO-6 vehicles (city buses equipped with SCR-NO_x exhaust gas purification) emit far higher NH_3 to CO_2 ratios of approx. 1 [ppb/ppm] under pollution conditions [Wegener et al., 2017]. We will quantify this newly occurring NH_3 input from SCR-catalyst vehicles on the basis of future long-term investigations and investigate its significance for secondary particle formation.
- Our extensive tunnel investigations have shown that the N_2O emissions attributable to road traffic emissions differ significantly between measured and predicted fractions (N_2O/NO_x and N_2O/CO_2). Both measured ratios were found to be higher (compared to inventory data of UBA) by more than a factor of 1.5. The planned investigations[36] will focus on the N_2O emission contribution of the EURO-6-SCR-catalyst for the transport sector in the future.
- It is planned to make the temporally and spatially high-resolution data sets generated within the urban climate project also accessible for the assessment of health effects[37] in the areas impacted by traffic related pollution.

---

[36] It is planned to investigate this question within the framework of the NRW Virtual Institute "Electricity to Gas and Heat", where our working group will record the emission compositions of conventional and alternative fuels by on-road measurements.

[37] Contacts already exist within a joint HGF project "SMARAGD" with the Helmholtz Centre for Infection Research.

7 Appendix

7.1 Current VOCs road-traffic-mixture

Table 7.1: VOCs mixing ratios and associated OH reactivities during IOP-II in summer 2017. The measured VOCs mix is related to almost pure road traffic (Heslacher Tunnel, Stuttgart).

Heslacher Tunnel IOP-II, Summer 2017	ppt	s^{-1}
Alkane		
ethane	14449.4	0.088
propane	5786.0	0.155
isobutane	7103.3	0.363
butane	18261.3	1.059
2-methylbutane	42004.5	3.726
pentane	10964.5	1.064
2,2-dimethylbutane	4873.0	0.268
cyclopentane / 2,3-dimethylbutane	3843.9	0.470
2-methylpentane	8163.0	1.046
3-methylpentane	4294.2	0.550
hexane	4739.3	0.636
methylcyclopentane	0.0	0.000
2,4-dimethylpentane	1265.6	0.149
cyclohexane	735.9	0.132
2-methylhexane	3291.4	0.556
2,3-dimethylpentane	3679.2	0.647
3-methylhexane	2687.6	0.473
cis-1,3-dimethylcyclopentane	905.4	0.152
2,2,4-trimethylpentane	4428.3	0.364
heptane	1555.2	0.271
cis-1,2-dimethylcyclopentane	142.4	0.024
methylcyclohexane	933.6	0.222
2,5-dimethylhexane	558.6	0.114
2,4-dimethylhexane	949.6	0.200
ethylcyclopentane	288.4	0.051
1-cis,2-trans,4-trimethylcyclopentane	173.5	0.028
2,3,4-trimethylpentane	3673.7	0.597
2-methylheptane	1277.3	0.260
4-methylheptane	502.4	0.106
3-methylheptane	969.4	0.204
trans-1,4-dimethylcyclohexane	702.7	0.205
1,1-dimethylcyclohexane	0.0	0.000

cis-3-ethylmethylcyclopentane	0.0	0.000
trans-3-ethylmethylcyclopentane	0.0	0.000
octane	772.0	0.168
cis-1,4-dimethylcyclohexane	170.2	0.050
cis-1,3-dimethylcyclohexane	262.7	0.077
isopropylcyclohexane	104.9	0.000
ethylcyclohexane	214.3	0.063
4-methyloctane	1199.9	0.295
nonane	897.3	0.220
2,6-dimethyloctane	290.0	0.081
n-butylcyclopentane	936.5	0.232
3,6-dimethyloctane	0.0	0.000
5-methylnonane	195.5	0.055
decane	1490.2	0.408
dodecane	0.0	0.000
undecane	2694.0	0.862
Dodecane	703.0	0.242
		16.933
Alkene		
ethene	79394.5	16.665
ethyne	47762.7	0.917
propene	13543.0	8.772
propyne	999.6	0.176
isobutene/1-butene	6135.0	4.747
1,3-butadiene	768.1	1.276
trans-butene	3411.2	5.376
cis-butene	3184.9	4.424
1,2-butadiene	54.9	0.035
3-methyl-1-butene	0.0	0.000
1-pentene	1590.0	1.214
2-methyl-1-butene	3455.7	5.191
trans-pentene	2847.1	4.698
cis-pentene	1431.0	2.291
2-methyl-2-butene	3834.0	8.206
1,3-pentadiene	0.0	0.000
cyclopentadiene	0.0	0.000
cyclopentene	980.8	1.618
1-hexene	0.0	0.000
2-methyl-1-pentene	778.7	1.208
trans-2-hexene	427.4	0.701
cis-2-hexene	197.9	0.292
1,3-hexadiene	489.9	1.327
cyclohexene	174.8	0.293
1-heptene	0.0	0.000
2,3-dimethyl-2-pentene	127.8	0.315

octene	0.0	0.000
1-methylcyclohexene	0.0	0.000
1-nonene	0.0	0.000
cyclooctatetraene	0.0	0.000
1-Propenylbenzene	0.0	0.000
4-ethenyl-1,2-dimethylbenzene	0.0	0.000
1-ethenyl-3-ethylbenzene	0.0	0.000
		69.741
Biogenic VOCs		
isoprene	30.2	0.074
α-pinene	115.4	0.149
pinane	0.0	0.000
sabinene	0.0	0.000
β-pinene	0.0	0.000
myrcene	310.7	2.561
d2-carene	38.9	0.077
α-phellandrene	36.0	0.000
d3-carene	249.0	0.540
alpha-terpinene	0.0	0.000
limonene	402.0	1.635
eucalyptol (1,8-cineole)	0.0	0.000
z-*β*-ocimene	0.0	0.000
2,3-dihydroinden	549.1	0.257
e-*β*-ocimene	292.8	1.817
terpinolene	0.0	0.000
		7.110
Oxygenated		
acetaldehyde	25102.4	9.248
methanol	0.0	0.000
ethanol	125429.9	9.909
acetonitrile	0.0	0.000
acetone	24069.7	0.103
propanal	0.0	0.000
propan-2-ol	1734.5	0.217
methyl-acetate	0.0	0.000
1-propanol	184.7	0.026
metacrolein	32.4	0.023
methyl vinylketone	235.5	0.117
butanal	382.2	0.224
butanone	3192.7	0.087
2-Butanol	0.0	0.000
ethyl tert-butyl ether	4437.3	0.970
1-butanol	745.3	0.156
pentanal	0.0	0.000
hexanal	323.5	0.239

butyl-acetate	28856.3	1.192
2,3-dimethyl-2-butanol	0.0	0.000
2e-hexenal	0.0	0.000
heptanal	144.7	0.107
benzaldehydene	387.8	0.120
octanal	110.8	0.086
		22.823
Aromatics		
benzene	8133.0	0.243
toluene	21428.8	2.972
ethylbenzene	14001.7	2.414
m/p-xylene	20807.0	11.785
styrene	501.3	0.716
o-xylene	8049.5	2.775
isopropylbenzene	204.8	0.032
propylbenzene	2107.9	0.301
3-ethyltoluene	3093.3	1.417
4-ethyltoluene	1387.1	0.403
mesitylene	1216.6	1.708
2-ethyltoluene	1089.1	0.319
tert-butylbenzene / 1,2,4-trimethylbenzene	4947.9	0.548
m-cymene	0.0	0.000
o-cymene	0.0	0.000
1,2,3-trimethylbenzene	1266.1	1.029
1,3-diethylbenzene	415.6	0.146
3-methylpropylbenzene	713.0	0.000
1,4-diethylbenzene	1207.6	0.241
butylbenzene	186.5	0.040
2-methylpropylbenzene	899.7	0.000
1,3-dimethyl-4-ethylbenzene	445.3	0.185
1,2-dimethyl-4-ethylbenzene	132.9	0.055
1,3-dimethyl-2-ethylbenzene	855.6	0.000
2-phenylpentane	171.4	0.042
1,2,4,5-tetramethylbenzene	304.3	0.154
1,2,3,4-tetramethylbenzene	401,2	0.203
1,2,3,5-tetramethylbenzene	696,9	0.739
naphthalene	1142,2	0.650
		29.117
Sum Reaktivity/ s^{-1}		145.725

Alkane	11.6%
Alkene	47.9%
Biogenic	4.9%
Oxygenated	15.7%
Aromatics	20.0%

7.2 Comparison of VOC composition of a diesel vehicle with the current Heslacher tunnel mix

Fig. 37 shows the comparison of the calculated reactivities of C_2 - C_{11} VOCs measured on the exhaust gas under cold start conditions of MobiLab's diesel vehicle (EURO-6 with SCR catalytic converter and particulate filter, built in 2016) with the exhaust gas mix in the Stuttgart Heslachtunnel (see Table 7.1). It is obvious that the composition of the average exhaust gas mix of the Heslacher tunnel is fundamentally different from the exhaust gas mix of a diesel vehicle in cold start. This shows that the VOCs emissions of diesel vehicles play only a minor role in the road traffic-related VOCs emissions. The dominant emitters are gasoline vehicles with insufficiently heated 3-way catalytic converters [see e.g., Klemp et al, 2012].

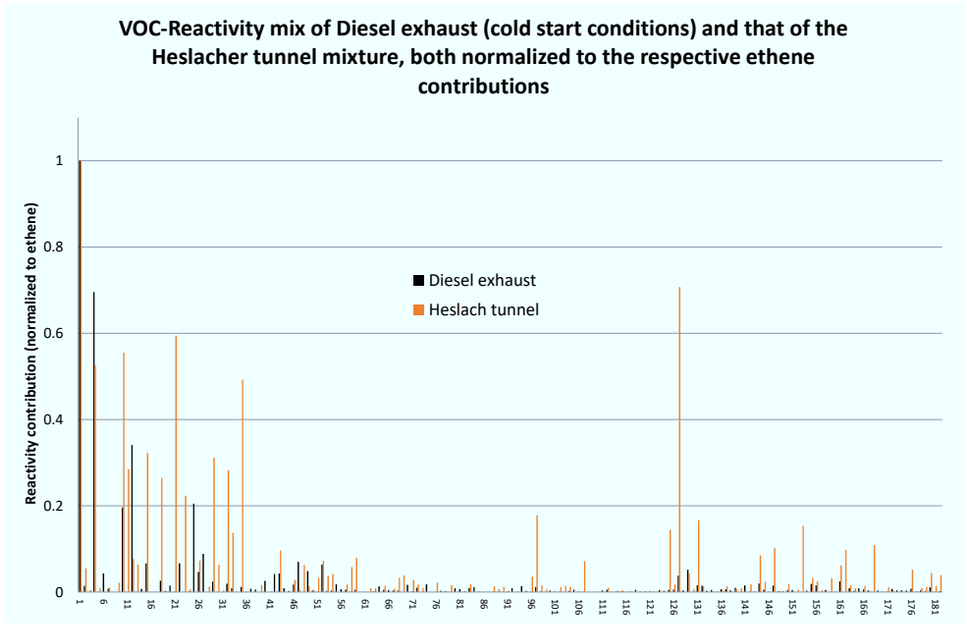

Fig. 37: Comparison of the calculated reactivities of the C_2 - C_{11} VOCs measured on the exhaust gas under cold start conditions of MobiLab's diesel vehicle (EURO-6 with SCR catalytic converter and particulate filter, built in 2016) with the exhaust gas mix in the Stuttgart Heslachtunnel (see Table 7.1). The scales of both reactivity plots were normalized to equal ethylene contents.

1: ethene; 2: ethyne; 3: ethane; 4: propene; 5: propane, 6: cyclopropene; 7: propyne; 8: methyl nitrite; 9: isobutane; 10: acetaldehyde; 11 Sum of 1-butene and isobutene; 12: 1,3-butadiene; 13: butane; 14: 1-butene-3-yne; 15: trans-butene, 16: 1-butyne; 17: methylethyl-ether; 18: cis-butene; 19: 1,2-butadiene; 20: 3-methyl-1-butene; 21: ethanol; 22: acrolein; 23: isopentane; 24: acetone; 25: 1,4-pentadiene; 26: 1-pentene; 27: furan; 28: 2-propanol; 29: 2-methyl-1-butene; 30: pentane; 31: trans-pentene; 32: isoprene; 33: cis-pentene; 34: methyl nitrate; 35: 2-methyl-2-butene; 36: methyl acetate; 37: trans-1,3-pentadiene; 38: nitromethane; 39: 2,2-dimethylbutane; 40: methyl-propanal; 41: propanol; 42: metacrolein; 43: cyclopentene; 44: 4-methyl-1-pentene; 45: 3-methyl-1-pentene; 46: 2,3-dimethylbutane; 47: methyl vinyl ketone; 48: 2-methylpentane; 49: butanal; 50: methyl ethyl ketone; 51: 3-methyl-pentane; 52: 2-methyl-1-pentene; 53: hexane; 54: trans-2-hexene; 55: 2-methylfuran; 56: 3-methylcyclopentene; 57: cis-2-hexene; 58: ethyl tertbutyl ether; 59: trans-1-3-hexadiene; 60: methylcyclopentane; 61: 2-butenal; 62: 2,4-dimethylpentane; 63: butanol; 64: cis-2-methyl-3-hexene; 65: benzene; 66: 2-methyltetrahydrofuran; 67: cyclohexane; 68: 2-methylhexane; 69: 2,3-dimethylpentane; 70: pentanal; 71: 3-methylhexane; 72: cyclohexene; 73: cis-1,3-dimethylcyclopentane; 74: 1-heptene; 75: trans-1,3-dimethylcyclopentane; 76: 2,2,4-trimethylpentane; 77: methyl 3-butenoate; 78: 2-methyl-2-hexen; 79; heptane; 80: 3,5-dimethylcyclohexene; 81: trans-2-heptene; 82: cis-2-heptene; 83: 2,3-dimethyl-2-pentene; 84: 3-ethylcyclopentene; 85: 1-ethylcyclopentene; 86: cyclopentanone; 87: cis-1,2-dimethylcyclopentane; 88: methylcyclohexane; 89: 2,5-dimethylhexane; 90: 2,4-dimethylhexane; 91: ethylcyclopentane; 92: 4-methylcyclohexene; 93: 1,cis-2,trans-4-trimethylcyclopentane; 94: cis-2-octene; 95: cis-3-octene; 96: 2,3,4-trimethylpentane; 97: toluene; 98: 2-methylheptane; 99: 4-methylheptane; 100: 2-ethyl-1-hexene; 101: 1-methylcyclohexene; 102: 3-methylheptane; 103: hexanal; 104: trans 1,4-dimethylcyclohexane: 105: 1-octene; 106: 1,1-dimethylcyclohexane; 107: butyl-acetate; 108: trans-4-octene; 109: cis-1-ethyl-3-methylcyclopentane; 110: trans-1-ethyl-3-methylcyclopentane; 111: trans-3-octene; 112: octane; 113: trans-2-octene; 114: cis-1,4-dimethylcyclohexane; 115: cis-1,3-dimethylcyclohexane; 116: isopropylcyclopentane; 117: 1-propylcyclopentene; 118: 1,2-dimethylcyclohexene; 119: (E)-2-Hexen-1-al; 120: trans 3,5-dimethylcyclohexene; 121: 2-methyloctane; 122: cis-3,5-dimethylcyclohexene; 123: ethylcyclohexane; 124: 1,1,3-trimethylcyclohexane; 125: ethylbenzene; 126: 4-methyloctane; 127: meta and para xylene; 128: 3-methyloctane; 129: styrene; 130: heptanal 131: o-xylene; 132: nonane; 133: 1-ethyl-2-methylcyclohexane; 134: 1-ethyl-4-methylcyclohexabe; 135: isopropylbenzene; 136: 2,6-dimethyloctane; 137: butylcyclopentane; 138: 1-propenylbenzene; 139: benzaldehydene; 140: α-pinene; 141: cyclooctatetraene; 142: propylbenzene; 143: 3,6-dimethyloctane; 144: 3-ethyltoluen; 145: 4-ethyltoluene; 146: trans-pinane; 147: mesitylene; 148: 1-propenylbenzene; 149: 1,1,2,3-tetramethylcyclohexane; 150: 2-ethyltoluene; 151: 1-decene; 152: octanal; 153: myrcene; 154: tert-butylbenzene; 155: 1,2,4-trimethylbenzene; 156: decane; 157: δ2-carene; 158: 1,3-methyl-isopropylbenzene; 159: δ3-carene; 160: 1,2-methyl-isopropylbenzene; 161: 1,2,3-trimethylbenzene; 162: limonene; 163: indane; 164: 1,3-diethylbenzene; 165: 1,3-methyl-propylbenzene; 166: 1-4-diethylbenzene; 167: butylbenzene; 168: (E)-β-ocimene; 169: 1,2-methyl-propylbenzene; 170: 1,2-diethylbenzene; 171: 1,3-dimethyl-4-ethylbenzene; 172: 1,2-dimethyl-4-ethylbenzene; 173: 1,3-dimethyl-2-ethylbenzene; 174: 1,3-dimethyl-2-ethylbenzene; 175: 1-ethenyl-3-ethylbenzene; 176: undecane; 177: (1-methylbutyl)-benzene; 178: 1,2,4,5-tetramethylbenzene; 179: 1,2,3,4-tetramethylbenzene; 180: 1,2,3,5-tetramethylbenzene; 181: dodecane; 182: naphthalene.

7.3 Results of TP6 reference measurements for the validation periods of PALM-4U in Berlin and Stuttgart

7.3.1 Berlin (VALR01 , VALR02, VALR06)

During VALR01 (see Table 3.2 for the designation), the mobile measuring laboratory of FZJ carried out a whole series of measurement runs on the Berlin reference route. Fig. 38 a) – m) shows an example of the results of the second measurement run from 17 January 2017 9:10 - 10:25 UTC of the measurement run. Fig. 39 a) - h) shows some results for VALR02 (third measurements run from 17. 07. 2018 11:18 - 12:43 UTC.

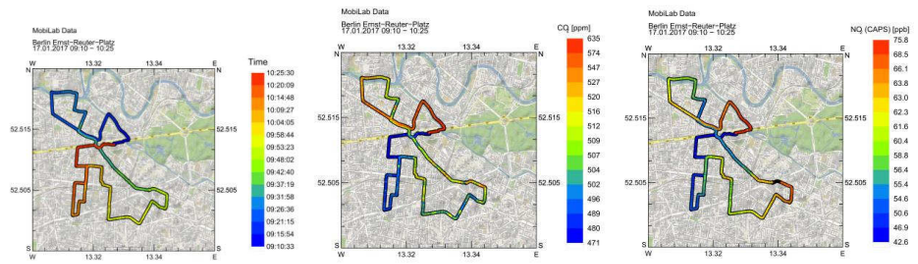

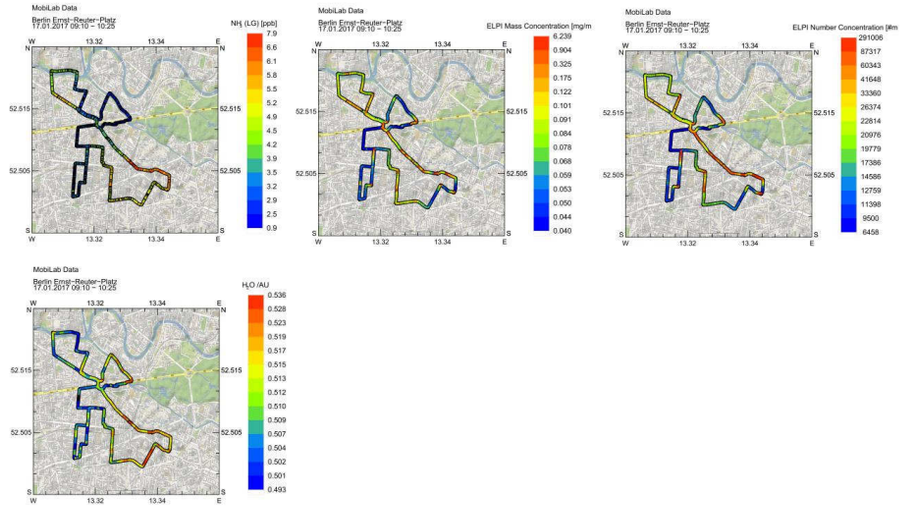

Fig. 38 a) - m): VALR01: TP6 Selection of measuring run 17. 01. 2017 9:10 - 10:25. a) Time and location of the measurement run, b) CO_2 concentration [ppm], c) NO_2 concentration [ppb], d) CO concentration [ppb], e) NO concentration [ppb], f) O_3 concentration [ppb], g) CH_4 concentration [ppm], h) SO_2 concentration [ppb], i) NH_3 concentration (Picarro) [ppb], j) NH_3 concentration (LosGatos) [ppb], k) ELPI particle mass [mg/m^3], l) ELPI particle number [#/cm^3], m) H_2O concentration [AU].

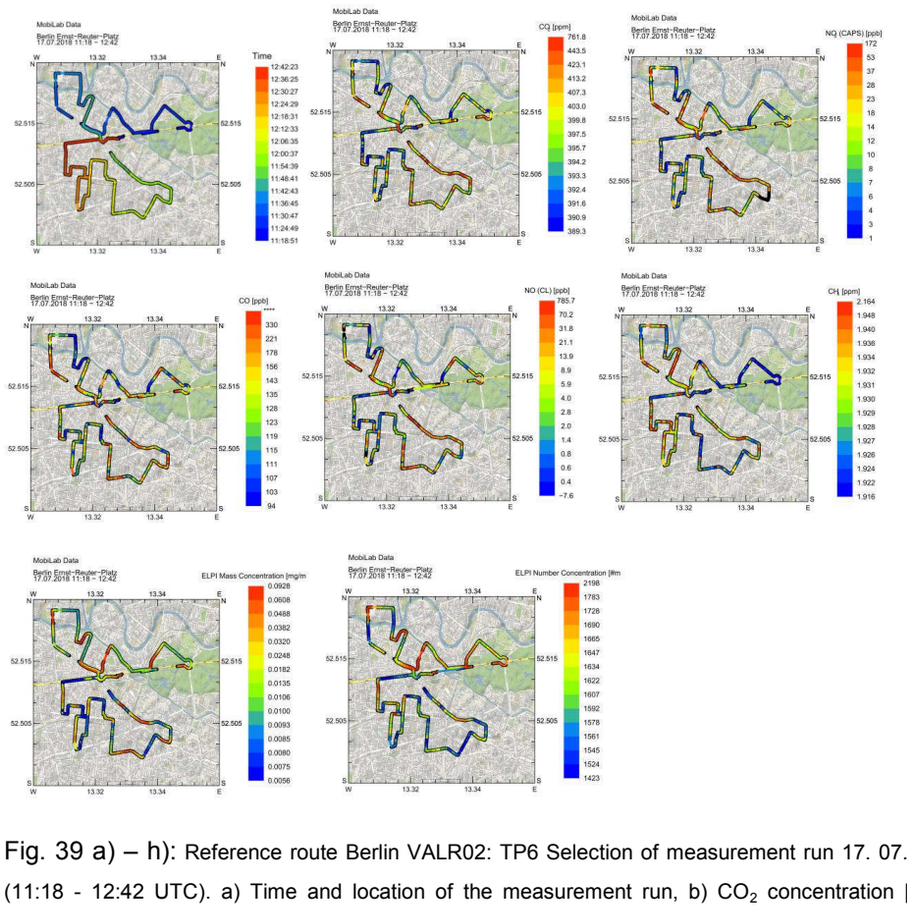

Fig. 39 a) – h): Reference route Berlin VALR02: TP6 Selection of measurement run 17. 07. 2018 (11:18 - 12:42 UTC). a) Time and location of the measurement run, b) CO_2 concentration [ppm], c) NO_2 concentration [ppb], d) CO concentration [ppb], e) NO concentration [ppb], f) CH_4 concentration [ppm], g) ELPI particle mass [mg/m^3], h) ELPI particle number [$\#/cm^3$].

Fig. 40 a) – m) shows the results of a measurement run with MobiLab during IOP-II in summer 2017. VALR06 covers the period from 30.07.2017 06:00 UTC to 01.08.2017 06:00 UTC. Shown is a drive with MobiLab during the morning rush hour (06:55 - 8:10 UTC).

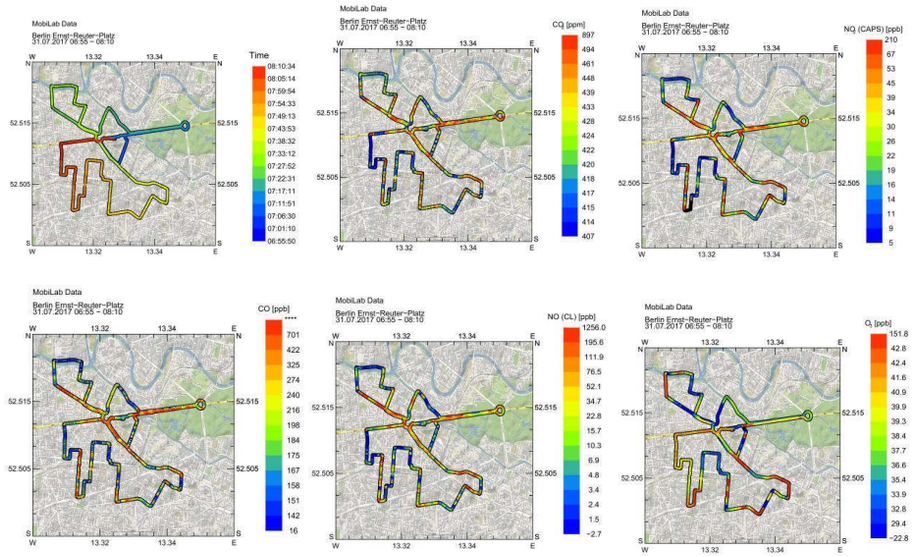

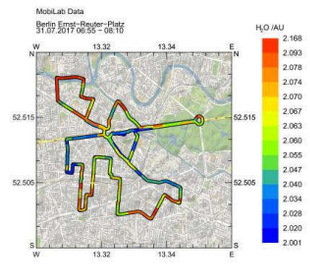

Fig. 40 a) – m): VALR06: TP6 Selection of measuring run 30.07.2017 06:55 → 8:10 UTC. a) Time and location of the measurement run, b) CO_2 concentration [ppm], c) NO_2 concentration [ppb], d) CO concentration [ppb], e) NO concentration [ppb], f) O_3 concentration [ppb], g) CH_4 concentration [ppm], h) SO_2 concentration [ppb], i) NH_3 concentration (Picarro) [ppb], j) NH_3 concentration (LosGatos) [ppb], k) ELPI particle mass [mg/m^3], l) ELPI particle number [#/cm^3], m) H_2O concentration [AU].

7.3.2 Stuttgart (VALR03 , VALR04)

The mobile measuring laboratory of FZJ carried out two different measuring runs during VALR03 ("Stuttgart and its western suburbs" and "Stuttgart city centre"). In the following, the results of the measurement round ("Stuttgart and its western surroundings") will be presented in more detail (see Fig. 41). The route begins at the MobiLab station at Marienplatz in Stuttgart and then directly through the Heslacher tunnel. Aftewards the route goes down to the valley of Feuerbach and leads along the busy B14 through the city centre of Stuttgart back to Marienplatz. The route for 14.02.2017 (7:54 - 9:58 UTC) and the measured concentration profiles are shown in Fig. 41.

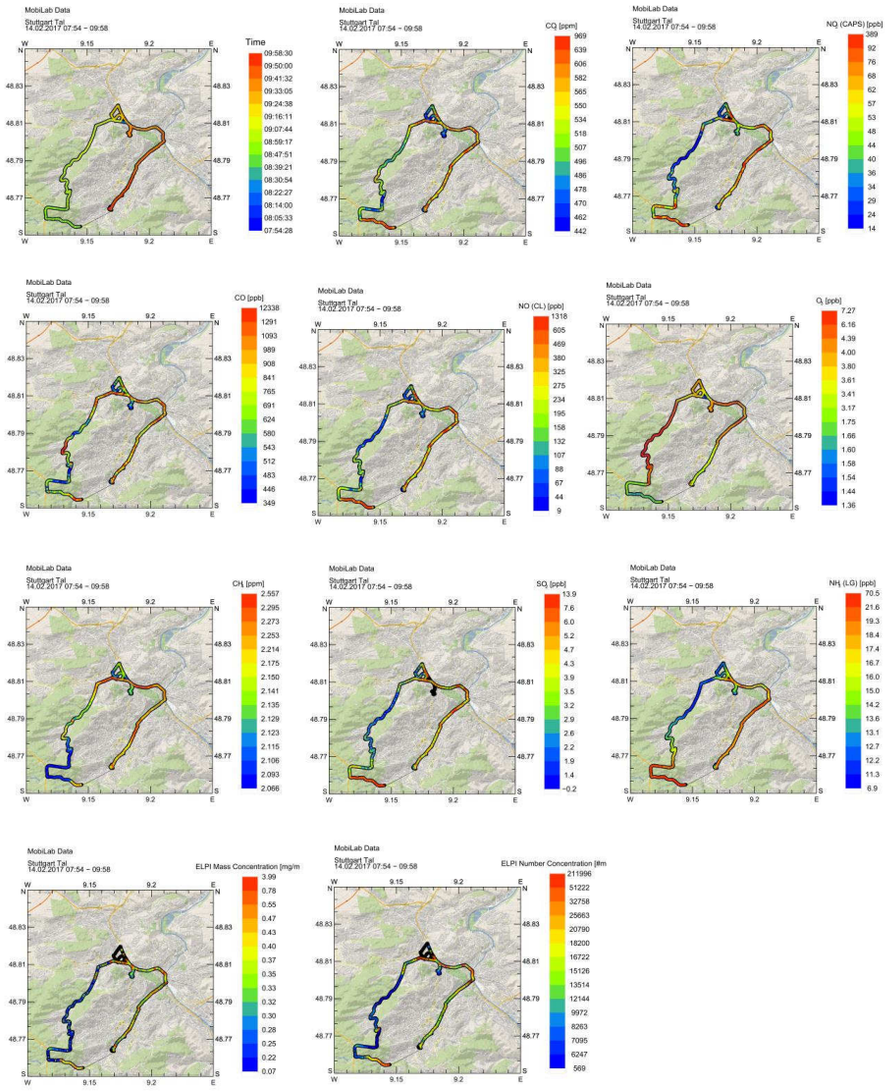

Fig. 41 a) – h): Reference route "Stuttgart and its western surroundings" VALR03: TP6 Selection of measurement run (14.02.2017 7:54 - 9:58 UTC). a) Time and location of the measurement run, b) CO_2 concentration [ppm], c) NO_2 concentration [ppb], d) CO concentration [ppb], e) NO concentration [ppb], f) O_3 concentration [ppb], g) CH_4 concentration [ppm], h) SO_2 concentration [ppb], i) NH_3 concentration [ppb], j) ELPI particle mass [mg/m^3], k) ELPI particle number [$\#/cm^3$].

During IOP-IV, for the validation comparisons for VALR04, in addition to driving the usual Stuttgart city centre reference route, a "city-surrounding investigation route" was selected (see Fig. 42 a - h), which is particularly suitable for testing the quality of the air chemistry module and the interaction of "chemistry and transport" in the PALM-4U model for summer conditions.

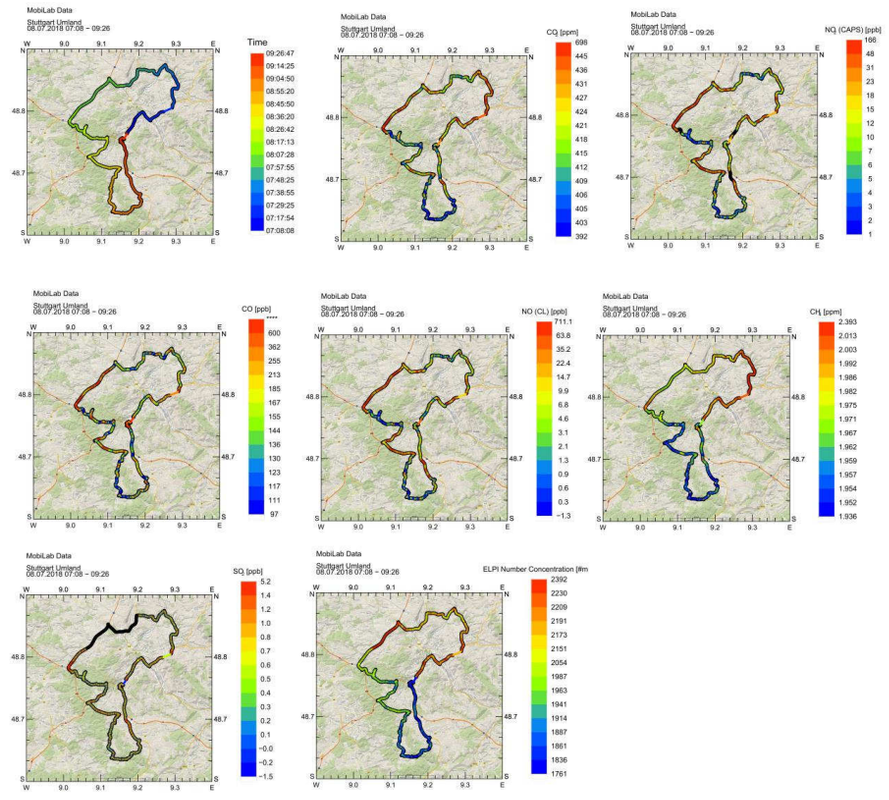

Fig. 42 a) – h): Reference route "Stuttgart and its western surroundings" VALR04: TP6 Selection of measurement run (08.07.2018 07:08 – 09:26 UTC), a) Time and location of the measurement run, b) CO_2 concentration [ppm], c) NO_2 concentration [ppb], d) CO concentration [ppb], e) NO concentration [ppb], f) O_3 concentration [ppb], g) SO_2 concentration [ppb], h) ELPI particle count [#/cm^3].

8 Literature

[Apel et al., 2008] Apel, E.C., Brauers, T., Koppmann, R., Bandowe, B., Boßmeyer, J., Holzke, C., Tillmann, R., Wahner, A., Wegener, R., Brunner, A., Jocher, M., Ruuskanen, T., Spirig, C., Steigner, D., Steinbrecher, R., Gomez Alvarez, E., Müller, K., Burrows, J.P., Schade, G., Solomon, S.J., Ladstätter-Weißenmayer, A., Simmonds, P., Young, D., Hopkins, J.R., Lewis, A.C., Legreid, G., Reimann, S., Hansel, A., Wisthaler, A., Blake, R.S., Ellis, A.M., Monks, P.S., and K.P. Wyche. „Intercomparison of oxygenated volatile organic compound measurements at the SAPHIR atmosphere simulation chamber“, *Journal of Geophysical Research D: Atmospheres*, (2008) 113: D20307.

[Bonn et al., 2016] Bonn, B., E. von Schneidemesser, D. Andrich, J. Quedenau, H. Gerwig, A. Ludecke, J. Kura, A. Pietsch, C. Ehlers, D. Klemp, C. Kofahl, R. Nothard, A. Kerschbaumer, W. Junkermann, R. Grote, T. Pohl, K. Weber, B. Lode, P. Schonberger, G. Churkina, T. M. Butler, and M. G. Lawrence. 2016. „BAERLIN2014 - the influence of land surface types on and the horizontal heterogeneity of air pollutant levels in Berlin“, *Atmospheric Chemistry and Physics*, (2016) 16: 7785-811.

[Bonn et al., 2018] Bonn, B., von Schneidemesser, E., Butler, T., Churkina, G.,Ehlers, C., Grote, R., Klemp, D., Nothard, R., Schäfer, K. , von Stülpnagel, A., Kerschbaumer A., Yousefpour, R., Fountoukis, C., Lawrence, M. „ Impact of vegetative emissions on urban ozone and biogenic secondary organic aerosol: Box model study for Berlin“, Journal of Cleaner Production 176 (2018) 827- 841.

[Bukowieki et al., 2002] Bukowieki, N., Dommen, J., Prevot, A. S. H., Richter, R., Weingartner, E., Baltensberger., U., „A mobile pollutant measurement laboratory-measuring gas phase and aerosol ambient concentrations with high special and temporal resolution”, *Atmos. Environ.*, (2002), 36, 5569.

[Carslaw, Rhys-Tyler, 2013] Carslaw, D. C., Rhys-Tyler, G., “New insights from comprehensive on-road measurements of NO_x, NO_2 and NH_3 from vehicle emission remote sensing in London, UK“, *Atmos. Environ.,* (2013) 81 , 339 – 347, 2013.

[Ehlers, 2013] Ehlers, C. „Mobile Messungen – Messung und Bewertung von Verkehrsemissionen“, Dissertation, Universität zu Köln, (2013), pp. 139.

[Ehlers et al., 2014] Ehlers, C., Elbern, H., Klemp, D., Rohrer, F., Wahner, A., „Comparison of measured data and model results during PEGASOS 2012“, Poster presented at EGU conference, 27. 05. - 2. 06. 2014 Vienna (2014).

[Ehlers et al., 2016] Ehlers, C., Klemp, D., Rohrer, F., Mihelcic. D., Wegener, R., Kiendler-Scharr, A., Wahner, A.: „Twenty years of ambient observations of nitrogen oxides and specified hydrocarbons in air masses dominated by traffic emissions in Germany”, *Faraday Discuss*., (2016), 189, 407.

[Ehlers et al., 2017] Ehlers, C., Klemp, D., Kofahl, C:, Fröhlich, H., Möllmann-Coers, M., und Wahner, A.: „Untersuchungen zur Luftqualität in Bad Homburg“, *Reihe Energie und Umwelt, Verlag des Forschungszentrums Jülich,* (2017), ISBN 978-3-95806-199-6, pp. 96.

[Fuchs et al., 2013] Fuchs, H., A. Hofzumahaus, F. Rohrer, B. Bohn, T. Brauers, H. P. Dorn, R. Haeseler, F. Holland, M. Kaminski, X. Li, K. Lu, S. Nehr, R. Tillmann, R. Wegener, and A. Wahner. „Experimental evidence for efficient hydroxyl radical regeneration in isoprene oxidation“, *Nature Geoscience*, (2013) 6: 1023-26.

[Fuchs et al., 2017] Fuchs, H., A. Novelli, M. Rolletter, A. Hofzumahaus, E. Y. Pfannerstill, S. Kessel, A. Edtbauer, J. Williams, V. Michoud, S. Dusanter, N. Locoge, N. Zannoni, V. Gros, F. Truong, R. Sarda-Esteve, D. R. Cryer, C. A. Brumby, L. K. Whalley, D. Stone, P. W. Seakins, D. E. Heard, C. Schoemaecker, M. Blocquet, S. Coudert, S. Batut, C. Fittschen, A. B. Thames, W. H. Brune, C. Ernest, H. Harder, J. B. A. Muller, T. Elste, D. Kubistin, S. Andres, B. Bohn, T. Hohaus, F. Holland, X. Li, F. Rohrer, A. Kiendler-Scharr, R. Tillmann, R. Wegener, Z. Yu, Q. Zou, and A. Wahner. „Comparison of OH reactivity measurements in the atmospheric simulation chamber SAPHIR“, *Atmos. Meas. Tech.*, (2017) 10: 4023-53.

[Fuchs et al., 2010] Fuchs, H., S.M. Ball, B. Bohn, T. Brauers, R.C. Cohen, H.-P. Dorn, W.P. Dubé, J.L. Fry, R. Häseler, U. Heitmann, R.L. Jones, J. Kleffmann, T.F. Mentel, P. Müsgen, F. Rohrer, A.W. Rollings, A.A. Ruth, A. Kiendler-Scharr, E. Schlosser, A.J.L. Shillings, R. Tillmann, R.M. Varma, D.S. Venables, F. Villena Tapia, A. Wahner, R. Wegener, P.J. Wolldridge, and S.S. Brown. „Intercomparison of measurements of NO_2 concentrations in the

atmosphere simulation chamber SAPHIR during the NO_3-Comp campaign“, *Atmospheric Measurement Techniques*, (2010) 3: 21-37.

[Grosso and Rigamonti, 2009] Grosso, E., Rigamonti, L.: “Experimental assessment of N_2O emissions from waste incineration: the role of NO_x control technology”. Politecnico di Milano. (2009) Mailand. http://www.iswa.org/uploads/tx_iswaknowledgebase/3-311pa-per_long.pdf.

[Guicherit, 1988] Guicherit, R., „Ozone on a urban and regional scale with special reference to the situation in the Netherlands“. *NATO ASC. Series C. Dordrecht*, (1988) The Netherlands, D. Reichel Publishers, 49-62.

[Hoerger et al., 2015] Hoerger, C. C., A. Claude, C. Plass-Duelmer, S. Reimann, E. Eckart, R. Steinbrecher, J. Aalto, J. Arduini, N. Bonnaire, J. N. Cape, A. Colomb, R. Connolly, J. Diskova, P. Dumitrean, C. Ehlers, V. Gros, H. Hakola, M. Hill, J. R. Hopkins, J. Jäger, R. Junek, M. K. Kajos, D. Klemp, M. Leuchner, A. C. Lewis, N. Locoge, M. Maione, D. Martin, K. Michl, E. Nemitz, S. O'Doherty, P. Pérez Ballesta, T. M. Ruuskanen, S. Sauvage, N. Schmidbauer, T. G. Spain, E. Straube, M. Vana, M. K. Vollmer, R. Wegener, and A. Wenger. „ACTRIS non-methane hydrocarbon intercomparison experiment in Europe to support WMO GAW and EMEP observation networks“, *Atmos. Meas. Tech.*, (2015) 8: 2715-36.

[Jenkin et al., 1997] Jenkin, M. E., S., Saunders, S., and Pilling, M. J., "The tropospheric degradation of volatile organic compounds: a protocol for mechanism development", *Atmospheric Environment* (1997), 31(1), 81.

[Kaiser et al., 2015] Kaiser, J., G. M. Wolfe, B. Bohn, S. Broch, H. Fuchs, L. N. Ganzeveld, S. Gomm, R. Häseler, A. Hofzumahaus, F. Holland, J. Jäger, X. Li, I. Lohse, K. Lu, A. S. H. Prévôt, F. Rohrer, R. Wegener, R. Wolf, T. F. Mentel, A. Kiendler-Scharr, A. Wahner, and F. N. Keutsch. „Evidence for an unidentified non-photochemical ground-level source of formaldehyde in the Po Valley with potential implications for ozone production“, *Atmos. Chem. Phys.*, (2015) 15: 1289-98.

[Kaminski et al., 2017] Kaminski, M., H. Fuchs, I. H. Acir, B. Bohn, T. Brauers, H. P. Dorn, R. Haseler, A. Hofzumahaus, X. Li, A. Lutz, S. Nehr, F. Rohrer, R. Tillmann, L. Vereecken, R. Wegener, and A. Wahner. „Investigation of the beta-pinene photooxidation by OH in the atmosphere simulation chamber SAPHIR“, *Atmospheric Chemistry and Physics*, (2017) 17: 6631-50.

[Karl et al., 2017] Karl, T., Graus, M., Striednig, M. *et al.* „Urban eddy covariance measurements reveal significant missing NO_x emissions in Central Europe“. *Sci Rep* (2017) **7,** 2536.

[Kern et al., 1998] Kern, T., Metz, N., and Kley, D., „Untersuchungen von Verkehrsabgasemissionen insbesondere im Hinblick auf die Ozonbildung“, (1998), *Abschlußbericht des Gemeinschaftsprojektes zwischen BMW AG und der Forschungszentrum Jülich GmbH*, München und Jülich.

[Klemp et al., 1997] Klemp, D., Kley, D., Kramp, F., Buers, H.-J., Pilwat, G., Flocke, F., Pätz, H.-W., Volz-Thomas, A., „Long-term measurements of light hydrocarbons (C_2 – C_5) at Schauinsland (Black Forest“, *Journal of Atmospheric Chemistry* (1997) 28 (1-3):135-171.

[Klemp et al., 2012] Klemp, D., Mihelcic, D., Mittermaier, B., „Messung und Bewertung von Verkehrsemissionen“, *Reihe Energie und Umwelt, Band 21,* ISBN 978-3-89336-546-3, Jülich, (2012), pp. 319.

[Klemp et al., 2020] Klemp, D., Wegener, R., Dubus, R., Karadurmus, L., Tan, X., „Distribution of trace gases with adverse effects on fuel cells“, *Reihe Energie und Umwelt*, Band XX, Jülich (2020), im Druck.

[Klemp et al., 2002] Klemp, D., K. Mannschreck, H. W. Patz, M. Habram, P. Matuska und F. Slemr, "Determination of anthropogenic emission ratios in the Augsburg area from concentration ratios: results from long-term measurements" *Atmospheric Environment* (2002) 36(Supplement 1): 61-80.

[Klemp et al., 2002a] Klemp, D., B. Mittermaier, H. J. Buers und T. Schmitz, "Determination of temporally highly resolved passenger car emissions of important exhaust components by means of on-board measurements under real traffic conditions" (2002) *VKM-THD Mitteilungen* 81: 41-48.

[Konrad und Volz-Thomas, 2000] Konrad, S., and Volz-Thomas, A., "Characterization of a commercial gas chromatography-flame ionization detection system for the in situ determination of C_5-C_{10} hydrocarbons in ambient air", *Journal of Chromatography A* (2000) 878(2), 215-234.

[Li et al., 2014] Li, Xin, F. Rohrer, A. Hofzumahaus, T. Brauers, R. Häseler, B. Bohn, S. Broch, H. Fuchs, S. Gomm, F. Holland, J. Jäger, J. Kaiser, F. N. Keutsch, I. Lohse, K. Lu, R. Tillmann, R. Wegener, G. M. Wolfe, T. F. Mentel, A. Kiendler-Scharr, and A. Wahner., „Missing Gas-Phase Source of HONO Inferred from Zeppelin Measurements in the Troposphere“, *Science*, (2014) 344: 292-96.

[Karl et al., 2017] Karl, T., Graus, M., Striednig, M. *et al.* Urban eddy covariance measurements reveal significant missing NO_x emissions in Central Europe. *Sci Rep* **7,** 2536 (2017).

[Landesamt für Umwelt BW, 2013] LUBW, Referat 31: *Luftreinhaltung, Umwelttechnik*, 2013.

[Lörzer, J., 2002] „Messungen ausgewählter Abgaskomponenten in einem Verkehrstunnel zur Bestimmung von Emissionsfaktoren“ Dissertation zur Erlangung des Doktorgrades(Dr. rerum naturalium) des Fachbereiches 9 – *Chemie der Bergischen Universität - Gesamthochschule Wuppertal* (2002).

[McDonald et al., 2018] McDonald, B. C., de Gouw, J. A., Gilman, J. B., Jathar, S. H., Akherati, A., Cappa, C. D., Jimenez, J. L., Lee-Taylor, J., Hayes, P. L., McKeen, S. A., Cui, Y. Y., Kim, S. W., Gentner, D. R., Isaacman-VanWertz, G., Goldstein, A. H., Harley, R. A., Frost, G. J., Roberts, J. M., Ryerson, T. B., and Trainer, M.: Volatile chemical products emerging as largest petrochemical source of urban organic emissions, Science, 359, 760-764, 10.1126/science.aaq0524, 2018.

[Mannschreck, K., 2001] Mannschreck, K., "Experimentelle Bestimmung von städtischen Emissionen anhand von Konzentrationsmessungen im Lee einer Stadt - Untersuchungen zum Beitrag verschiedener Quelltypen und Vergleich mit einem Emissionsberechnungsmodell". Dissertation *Universtät und Gesamthochschule Wuppertal und Berichte des Forschungszentrums Jülich*: Forschungszentrum Jülich, Zentralbibliothek.

[Mannschreck et al., 2002] Mannschreck, K., D. Klemp, D. Kley, R. Friedrich, J. Kühlwein, B. Wickert, P. Matuska, M. Habram und F. Slemr, "Evaluation of an emission inventory by comparisons of modelled and measured emission ratios of individual HCs, CO and NO_x" *Atmospheric Environment* (2002) 36 (Supplement 1): 81-94.

[Mihelcic et al., 1993] Mihelcic, D., D. Klemp, P. Müsgen, H. W. Patz und A. Volz-Thomas, "Simultaneous measurements of peroxy and nitrate radicals at Schauinsland” *Journal of Atmospheric Chemistry* (1993) 16(4): 313-335.

[Mittermaier et al., 2003] Mittermaier, B., D. Klemp and H. J. Buers, "Regulated and unregulated exhaust emissions from nine passenger cars" *Actes Inrets* (2003) 92: 183-190.

[Mittermaier et al., 2003a] Mittermaier, B., T. Schmitz, D. Hassel, F. J. Weber and D. Klemp, "VOC-split of gasoline and diesel passenger cars". In: R. Friedrich und S. Reis: "Emissions of air pollutants. Measurements, calculations, uncertainties: *Results from the EUROTRAC subproject GENEMIS" Berlin, Springer*, (2003), 25-32.

[Mittermaier und Klemp, 2004] Mittermaier, B., D. Klemp, “Messung wichtiger Abgaskomponenten am fahrenden Pkw im realen innerstädtischen Straßenverkehr“, *Gefahrstoffe – Reinhaltung der Luft* (2004) 64 Nr. 11/12: 487 – 493.

[Möllmann-Coers et al., 2002] Möllmann-Coers, M., D. Klemp, K. Mannschreck and F. Slemr, "Determination of anthropogenic emissions in the Augsburg area by the source-tracer-ratio method" *Atmospheric Environment* (2002) 36 (Supplement 1): 95-107.

[Pätz et al., 2000] Pätz, H. W., U. Corsmeier, K. Glaser, U. Vogt, N. Kalthoff, D. Klemp, B. Kolahgar, A. Lerner, B. Neininger, T. Schmitz, M. Schultz, J. Slemr and A. Volz-Thomas „Measurements of trace gases and photolysis frequencies during SLOPE 96 and a coase estimate of the local OH concentration from HNO_3 formation” *Journal of Geophysical Research* (2000) 105(D1): 1563-1583.

[Pijola et al., 2004] Pijola, J., Parviainen, H., Hussein, T., Valli, A., Hämeri, K.,Aaalto, P., Virtanen, A., Keskinen, J., Pakkanen, T., Mäkela, T., Hillamo, R. E., “Sniffer- a novel tool for chasing vehicles and measuring traffic pollutants”, *Atmos. Environment*, (2004), 38, 3625.

[Scherer et al., 2019] Scherer, D., Ament F., Emeis S., Fehrenbach U., Leitl B., Scherber K., Schneider C., Vogt U. (2019), „Three-dimensional observation of atmospheric processes in three German cities“. *Met. Z.*, (2019) Vol. 28, 2, 121-138, DOI: 10.1127/metz/2019/0911.

[Scherer et al., 2019a] Scherer, D., Antretter F., Bender S., Cortekar J., Emeis S., Fehrenbach U., Groß G., Halbig G., Hasse J., Maronga B., Raasch S., Scherber K., „Urban Climate Under Change $[UC]^2$ - A National Research Programme for Developing a Building-Resolving Atmospheric Model for Entire City Regions“. *Met. Z.*, (2019) Vol. 28, 2, 95-104. DOI: 10.1127/metz/2019/0913.

[Schmidtke and Schmidt, 2019] Schmidtke, J., Schmidt, K., UBA-FB 002741, „Ableitung sicherer Trendaussagen zur Entwicklung der Luftqualität in Deutschland“ (2019), Texte 47/2019.

[Schmitz et al., 1997] Schmitz, T., D. Klemp and D. Kley "Messungen der Immissionskonzentrationen verschiedener Ozonvorläufersubstanzen in Ballungsgebieten und an Autobahnen: Charakterisierung der Emissionsverhältnisse des Straßenverkehrs unter verschiedenen Verkehrssituationen durch Messungen in Quellnähe". (1997) *Berichte des Forschungszentrums Jülich: Forschungszentrum Jülich*, Zentralbibliothek.

[Schmitz et al., 2000] Schmitz, T., D. Hassel and F.-J. Weber, "Determination of VOC components in the exhaust of gasoline and diesel passenger cars" *Atmospheric Environment* (2000) 34(27): 4639-4647.

[Slemr et al, 2002] Slemr, F., G. Baumbach, P. Blank, U. Corsmeier, F. Fiedler, R. Friedrich, M. Habram, N. Kalthoff, D. Klemp, J. Kühlwein, K. Mannschreck, M. Möllmann-Coers, K. Nester, H. J. Panitz, P. Rabl, J. Slemr, U. Vogt, B. Wickert, "Evaluation of modeled spatially and temporarily highly resolved emission inventories of photosmog precursors for the city of Augsburg: The experiment EVA and its major results" (2002) *Journal of Atmospheric Chemistry* 42(1): 207-233.

[Steinemann and Zumsteg, 2010], Steinemann, U., and F. Zumsteg, „Verkehrs- und Schadstoffmessungen 2008 im Gubristtunnel (Traffic and trace gas pollutant measurements 2008 in the Gubrist tunnel)“, *report US 89 - 16 - 13*, OSTLUFT durch Amt für Abfall, Wasser, Energie und Luft des Kantons Zürich (AWEL), Zürich, Switzerland, update May 25, 2010.

[Talke et al., 2018] Talke, A., Misz, U., Konrad, G., Heinzel, A., Klemp, D., Wegener, R., “Influence of urban air on PEMFC vehicles – long term effects of air contaminants in an authentic driving cycle”, *Journal of Power Sources*, (2018) 400, 556 – 565.

[UBA, 2018] Umweltbundesamt, *Nationale Trendtabellen für die deutsche Berichterstattung atmosphärischer Emissionen seit 1990* (Stand 14. 2. 2018), Dessau, 2018.

[Urban, 2010] Urban, S., “Charakterisierung der Quellverteilung von Feinstaub und Stickoxiden in ländlichem und städtischem Gebiet“, *Dissertation, Universität Wuppertal*, (2010), pp. 210.

[von Schneidemesser et al., 2018] von Schneidemesser, E., B. Bonn, T. M. Butler, C. Ehlers, H. Gerwig, H. Hakola, H. Hellen, A. Kerschbaumer, D. Klemp, C. Kofahl, J. Kura, A. Ludecke, R. Nothard, A. Pietsch, J. Quedenau, K. Schafer, J. J. Schauer, A. Singh, A. M. Villalobos, M. Wiegner, and M. G. Lawrence. „BAERLIN2014-stationary measurements and source apportionment at an urban background station in Berlin, Germany“, *Atmospheric Chemistry and Physics*, (2018)18: 8621-45.

[Wagner and Kuttler, 2014] Wagner, P., Kuttler, W.: „Biogenic and anthropogenic isoprene in the near surface urban atmosphere - A case study in Essen, Germany”, *Science of the Total Environment*, (2014) 475, 104.

Wegener, R., T. Brauers, R. Koppmann, S. R. Bares, F. Rohrer, R. Tillmann, A. Wahner, A. Hansel, and A. Wisthaler, „Simulation chamber investigation of the reactions of ozone with short-chained alkenes“, *Journal of Geophysical Research-Atmospheres*, (2007) 112.

[Weijers et al., 2004] Weijers, E. P., Khlystov, A. Y., Kos , G. P. A., Erishmen, J. M, „Variabitity of particulate matter concentrations along roads and motorways determined by a moving measurement unit”, *Atmos. Environment*, (2004), 38, 2993.

[Westerdahl et al., 2005] Westerdahl, D., Fruin, S., Sax, T., Fine, P. M., Sioutas, C., „Mobile platform measurements of ultrafine particle an associated pollutant concentrations on freeways and residential streets in Los Angeles”, *Atmos. Environment*, (2005), 39, 3597.

[Wichmann-Fiebig, 2017] Wichmann-Fiebig, M., “Gefahr durch Stickoxide – Verursacher, Grenzwerte und Folgen”, Umweltbundesamt, Dessau 2017, https://www.stephankuehn.com/fileadmin/user_upload/20170213_01_Wichmann-Fiebig.pdf.

9 List of Figures

10 List of Tables

11 List of Abbrevations

3DO: Three-dimensional Observations

BMBF: Federal Ministry of Education and Research

CPC: Condensation Particle Counter

ELPI: Electrical Low Pressure Impactor

FZJ: Forschungszentrum Jülich GmbH

GC/MS: Gas Chromatography / Mass Spectrometry

HBEFA: Handbook Emission Factors for Road Transport

IASS: Institute for Advanced Sustainability Studies

IFK: Institut für Feuerungs- und Kraftwerkstechnik

IOP: intensive observation period

MCM: Master Chemical Mechanism

PALM: Parallelized Large-eddy simulation Model

SCR: Selective Catalytic Reduction

TP: Subproject

TUBS: Technical University Braunschweig

VOC: volatile organic compounds

Band / Volume 484
IEK-3 Report 2019
Tailor-Made Energy Conversion for Sustainable Fuels
D. Stolten, B. Emonts (Eds.) (2020), 162 pp
ISBN: 978-3-95806-451-5

Band / Volume 485
Multiskalare Modellierung integrierter Energie- und Elektrizitätssysteme
T. C. Pesch (2019), XXV, 384 pp
ISBN: 978-3-95806-452-2

Band / Volume 486
Quantitative Untersuchung des Laserablationsprozesses mittels Kombination von optischer Spektroskopie und Massenspektrometrie
J. Oelmann (2020), vii, 141 pp
ISBN: 978-3-95806-453-9

Band / Volume 487
Leistungssteigerung metallgestützter Festelektrolyt-Brennstoffzellen (MSCs) durch gezielte Optimierungen des Anoden/Elektrolytverbunds
C. Bischof (2020), X, 176 pp
ISBN: 978-3-95806-455-3

Band / Volume 488
Aluminiumoxiddispersionsverstärkte Haftvermittlermaterialien in Wärmedämmschichtsystemen
C. Vorkötter (2020), VIII, 99, XXXIII pp
ISBN: 978-3-95806-457-7

Band / Volume 489
The Balmer lines emission of fast hydrogen atoms at the plasma-solid interface in a low density plasma: challenges and applications
S. O. Dickheuer (2020), 117 pp
ISBN: 978-3-95806-458-4

Band / Volume 490
Micromechanical Characterization of Ceramic Solid Electrolytes for Electrochemical Storage Devices
J. F. Nonemacher (2020), xv, 131 pp
ISBN: 978-3-95806-461-4

Band / Volume 491
Nanoscale investigation of high temperature oxidation mechanisms of high-Cr ferritic steels
A. Vayyala (2020), xix, 105 pp
ISBN: 978-3-95806-467-6

Schriften des Forschungszentrums Jülich
Reihe Energie & Umwelt / Energy & Environment

Band / Volume 492
Electrolyte development for a SOFC operating at low temperature
J. Zhang (2020), vi, 121 pp
ISBN: 978-3-95806-471-3

Band / Volume 493
Modeling and Simulation of Polymer Electrolyte Fuel Cells
S. Zhang (2020), 4, xii, 214 pp
ISBN: 978-3-95806-472-0

Band / Volume 494
Ab initio perspective on hydrogenated amorphous silicon for thin-film and heterojunction photovoltaics
P. Czaja (2020), 107 pp
ISBN: 978-3-95806-474-4

Band / Volume 495
Measurements of Atmospheric OH and HO_2 Radicals by Laser-Induced Fluorescence on the HALO Aircraft during the OMO-ASIA 2015 Campaign
C. Künstler (2020), 156 pp
ISBN: 978-3-95806-477-5

Band / Volume 496
Tomographic observations of gravity waves with the infrared limb imager GLORIA
I. Krisch (2020), vii, 187 pp
ISBN: 978-3-95806-481-2

Band / Volume 497
Aquisition of temporally and spatially highly resolved data sets of relevant trace substances for model development and model evaluation purposes using a mobile measuring laboratory
D. Klemp, R. Wegener, R. Dubus, U. Javed (2020), 110 pp
ISBN: 978-3-95806-465-2

Weitere ***Schriften des Verlags im Forschungszentrum Jülich*** unter
http://wwwzb1.fz-juelich.de/verlagextern1/index.asp

Energie & Umwelt / Energy & Environment
Band / Volume 497
ISBN 978-3-95806-465-2

Mitglied der Helmholtz-Gemeinschaft

JÜLICH
Forschungszentrum